THE ELECTRODEPOSITION OF REFRACTORY
METALS FROM FUSED SALTS.

A THESIS
submitted for the
DEGREE OF DOCTOR OF PHILOSOPHY
in the
UNIVERSITY OF LONDON

by

RALPH SPENCER, B.Sc.

Department of Metallurgy,
Royal School of Mines,
Imperial College of Science and Technology.


November, 1970.

A B S T R A C T

This thesis describes a basically chronopotentiometric investigation into the electrode reactions of refractory metal ions in fused halide mixtures.

The electro-reduction of niobium (IV) in the lithium chloride - potassium chloride eutectic, $720^{\circ}C$ and in equimolar potassium chloride - caesium chloride $760^{\circ}C$ was interpreted in terms of the following process.

$$Nb^{4+} + e \rightarrow Nb^{3+}$$

$$Nb^{3+} + 3M \rightarrow Nb^{0} \quad (M = \text{alkali metal})$$
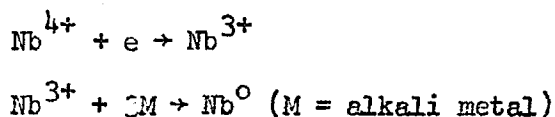
The anodic dissolution of niobium (III) was irreversible, the exchange current density was 1.7×10^{-4} Amp, cm^{-2}.

The electroreduction of molybdenum (III) in sodium chloride 20 mole% - potassium chloride 80 mole % involved the slow dissociation of a multinuclear complex, probably dinuclear.

$$Mo^{6+}_2 \ (\text{complex}) \xrightarrow{\text{slow}} 2Mo^{3+}$$

$$Mo^{3+} + 3e \rightarrow Mo^{0}.$$
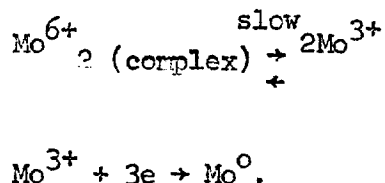
The diffusion coefficient was estimated to be 6×10^{-6} cm^2, sec^{-1}. The addition of fluoride ions reduced the stability of the molybdenum (III) complex.

Similar results were obtained for molybdenum (III) dissolved in lithium chloride-potassium chloride eutectic at $550^{\circ}C$. The diffusion coefficient was found to be $5 \times 10^{-6} cm,^2 sec^{-1}$

The addition of fluoride ions reduced the stability of the multinuclear species.

The electro-reduction of platinum (II) ions in lithium chloride - potassium eutectic at $480^{\circ}C$ was found to be partially irreversible. Adsorption (10^{-10}-10^{-9} moles cm^{-2}) intervened in the electro-reduction process. The adsorption was reduced by the addition of fluoride ions. The quasi-reversibility of the reduction process could be attributed to the slow dissociation of a multinuclear platinum (II) species. The diffusion coefficient for platinum (II) was estimated to be in the order of 2×10^{-5} cm^2 sec^{-1}.

The electro-reduction of tantalum (V) in sodium fluoride 40 mole % - potassium fluoride 60 mole % at $730^{\circ}C$ was found to occur in two steps.
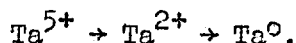
$$Ta^{5+} \rightarrow Ta^{2+} \rightarrow Ta^{0}.$$

The first step was reversible with a soluble product. The second step occurred by two processes, that is primary electro-reduction and secondary reduction by deposited alkali metals. The diffusion coefficient for tantalum (V) was estimated to be $(5.09 \pm 0.54) \times 10^{-5}$ cm^2, sec^{-1}.

"The true method of experience first lights the candle,
and then by means of the candle shows the way; commencing as
it does with experience duly ordered and digested, not
bungling or erratic, and from it educing axioms, and from
established axioms again new experiments ...."

FRANCIS BACON, "Novum Organum", (1620).

TABLE OF CONTENTS

Chapter 1: General Introduction

Chapter 2: Theoretical aspects.

Chapter 3: Structural aspects

Chapter 4: Electrochemical aspects.

CHAPTER I

GENERAL INTRODUCTION

1.1. Foreword

Apart from a high melting point, there is no agreed upon

definition for what constitutes a refractory metal. Since the

interest in refractory metals arises largely from high temperature

structural applications, it is convenient to consider metals

with a melting point greater than that of iron, $1535^{\circ}C$, to be

refractory. This definition includes groups IVA, VA and VIA

of the periodic table, the six platinum metals and rhenium.

Out of these metals, those in groups IVA, VA and VIA, owing

to their relative abundance, are the only ones, which have any

great importance as structural materials.

In addition to their mechanical properties, which make

these metals potential high temperature structural materials,

some of them possess unique combinations of chemical and

physical properties. Hence these metals have gained a very

important position in modern technology. It is not the

intention to consider these aspects any further, and detailed

discussions of the properties of these metals are treated

elsewhere. The mechanical, thermal and oxidation properties

of groups VA and VIA metals have been described by Tietz and

Wilson (1). The properties of group IVA metals are summarised

in Hampel (2).

1.2. Production of refractory metals.

These metals tend to be very difficult to obtain in the

free state in any reasonable purity, and are extremely sensitive

to embrittlement by traces of interstitial impurities such as

oxygen, hydrogen, carbon and nitrogen. This leads to complex

and expensive processes for their isolation.

Three general approaches have been made in regard to the extraction of these metals; (a) thermal reduction; (b) thermal dissociation; (c) electrolytic deposition. The thermal reduction processes, for example, the Kroll process (3) or the Goldschmidt process (4), are expensive and batch wise processes. The thermal dissociation of the halide vapour on a hot wire, that is the van Arkel-de Boer process (4), can produce extremely pure metal, but it is very costly. Electrolytic methods for the extraction of these metals offer the prospects of inexpensive materials and a continuous or semi-continuous process, in which a high state of purity should be obtainable. Electro-deposition processes also afford potential methods for fabricating articles from refractory metals (5). The properties of these deposits should be better than those obtained from powder metallurgical methods (10).

Apart from chromium there are no reports of groups IVA, VA or VIA metals giving electro-deposits, from aqueous or organic media, containing the metal as the major ingredient. All these metals on the other hand have been electrodeposited, in a powder or dendritic form, from their halides dissolved in molten halide melts (6). Coherent molybdenum deposits have been obtained from potassium hexachloromolybdate (K_3MoCl_6) dissolved in lithium chloride-potassium chloride eutectic (7-9). Tungsten has given coherent electrodeposits from tungstic oxide (WO_3) dissolved in a melt consisting of one part lithium sodium metaborate ($LiNaB_2O_4$) and six parts lithium sodium tungstate ($Li\,Na\,WO_4$) (11). All the metals from groups IVA VA and VIA apart from titanium, can be coherently electrodeposited from their pure fluorides dissolved in pure alkali fluoride melts (22). The addition of other halides or oxides was found to have a

deleterious effect on the deposits. All the above processes
are reviewed in much greater detail by Senderoff (6).

1.3. Electrodeposition processes.

Electrodeposition processes can be divided up into four
basic processes, electro-winning, electro-refining, electro-plating
and electro-forming. In electro-winning the compound of the
metal to be deposited is dissolved in the electrolyte. The
electro-refining process uses an anode of the impure metal as
the cell feed. The last two processes use a pure metal anode as
the cell feed. In the case of the first two processes, the
state of the cathode deposit is not critical, as long as the
metal is in a recoverable form.. The other two processes
require a continuous coherent metal deposit.

The metal deposits, obtained by electrochemical reduction,
are of three main forms, that is dendritic, powder and coherent
deposits. The condition of the deposit formed is very
dependent on the kinetics of the overall electrode reaction.

Barton and Bockris (13) have shown, that for a fast overall
electrode reaction , that is diffusion controlled, if the radius
of a substrate electrode sphere becomes less than the diffusion
layer thickness, "δ", the latter becomes replaced in the
equation,

$$i = \frac{(nF)^2}{RT} \frac{D\ C_\infty}{\delta}\ \eta \qquad (1.1)$$

by the radius of the substate sphere. Hence for the same current

density "i", the diffusion overvoltage "η" at such a spherical
surface would be less than that at a planar surface. It is
apparent from these results that a diffusion controlled
process would probably lead to dendritic rather than coherent
deposits.

For a very slow overall electrode process, the overvoltage
associated with the deposition, could be sufficiently high to
allow the reduction of the solvent cations, for example
alkali metals deposited from alkali halide melts. Under these
conditions the solute metal ions would be reduced by the alkali
metal deposited, giving secondary deposition.

$$M^+ + e \rightarrow M^0 \quad (M^+ = \text{solvent cation})$$
$$R^{n+} + nM^0 \rightarrow R^0 + nM^+ \quad (R^{n+} = \text{solute cation})$$
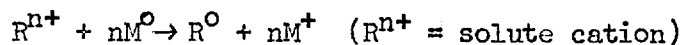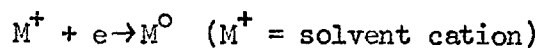
Powder deposits would result from these conditions.

The intermediate case would be, where the overall electrode
reaction is slow, but not slow enough to give rise to secondary
deposition. Such a situation should produce continuous coherent
deposits. It is therefore apparent that in order to design a
successful electrodeposition process, it is essential to
understand the kinetics and mechanism involved in the overall
electrode reduction process.

1.4. Fused salts

Fused salts can be split up into three main categories,
(a) simple ionic salts such as molten halides and halide
mixtures; (b) simple oxy-anion melts, for example molten sulphates
and nitrates;
(c) complex polymeric melts, for example phosphates and silicates.

It is the first category, simple ionic melts, which is of interest in this study.

There are a number of reviews and monographs available on the chemistry of fused salts (14-20). A number of discussions are available on high temperature techniques in fused salts (21-23). The electro-chemistry of fused salts has been reviewed by Reddy (24), Delimarskii and Markov (25), Graves, Hills and Inman (26), Inman, Graves and Sethi (27). The applicable aspects of the chemistry and electrochemistry of refractory metal ions in fused salts will be discussed in detail in later chapters.

1.5. Electro chemical Techniques

A number of techniques have been developed for the study of electrochemical processes. Chronopotentiometry proves to be a very suitable technique for the study of these processes in fused salts which involve relatively high temperatures. The technique requires only very simple electrode systems, and since the quantity of coulombs passed, during a pulse is very small, solid as well as liquid electrodes may be used. The technique can be used for the quantitative examination of multiple reduction steps, slow chemical steps, absorption and irreversible charge transfer processes. The theoretical treatment for these different processes is less complex than for other electroanalytical techniques. The theoretical aspects of the technique used will be discussed in a later chapter.

CHAPTER 2

THEORETICAL ASPECTS

2.1. Chronopotentiometry

2.1.1. Introduction

The term chronopotentiometry applies to the technique of
voltammetry at controlled current. The electrolysis is carried
out under the following conditions: (a) the solution is not stirred;
(b) the current is carried by a large excess of indifferent electrolyte
in order that migration can be neglected; (c) conditions of semi infinite
linear diffusion exist. A number of different current-time functions
have been considered for the controlled current (28-31). For this
study, chronopotentiometry will be considered to be voltammetry at
constant current.

The technique dates back historically to Weber (32) and Sand (33),
but the emphasis of this early work was placed on the verification of
Fick's diffusion laws. The important experimental perameter in
chropotentiometry, the transition time "τ", was introduced by Butler
and Armstrong (34,35). It is the time interval after the onset of
constant current electrolysis when the concentration, at the electrode
surface, of the species which is undergoing electron transfer, just
reaches zero, and is indicated by a sharp increase in the electrode
potential. A typical chronopotentiogram is shown in Fig. 2.1.
From point A to point B, the potential changes rapidly, and the
current is used almost exclusively to charge the double layer. Point
B corresponds to the potential at which electrolysis becomes
appreciable. The potential change from B to C is dependent on
the nature of the overall electrode reaction. After C the

Fig.2.1

E, micro electrode potential

Transition time τ
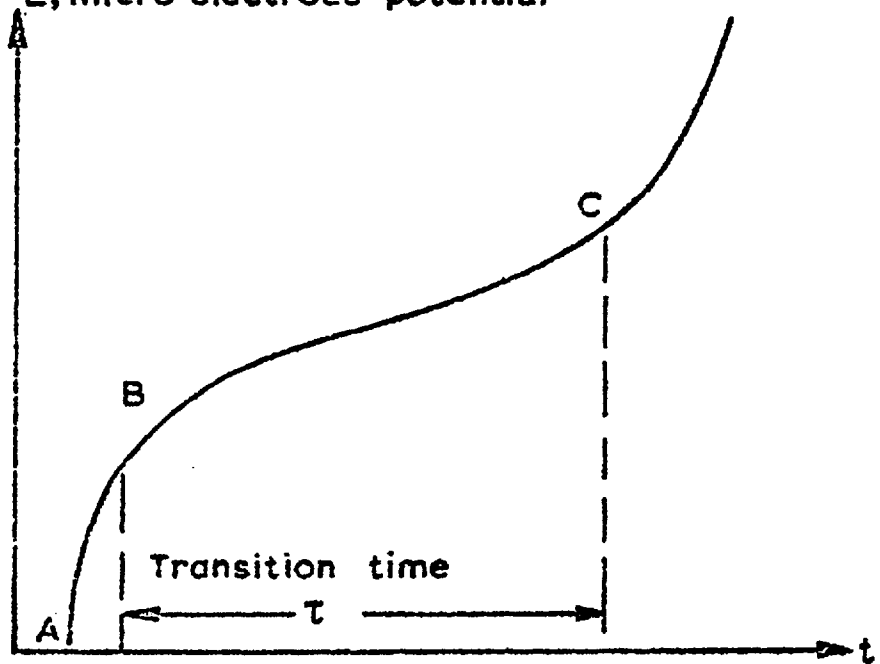
Chronopotentiogram

Fig.2.2

E

τ_1 τ_2
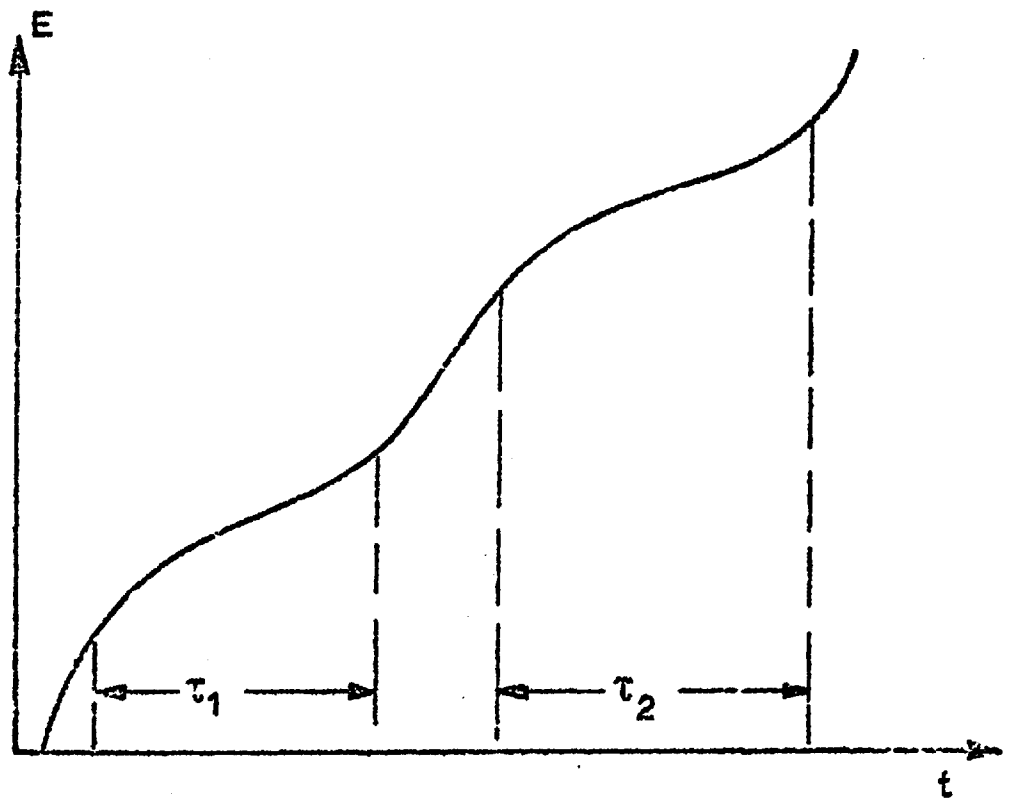
Stepwise reaction

concentration of the electroactive species at the electrode surface becomes essentially zero, and the current is distributed between continued electrolysis of the species and a further charging process.

The modern work began with Gierst and Juliard (36,37) in as much as the technique was applied to analysis and the study of an electrode process. Delahay and co-workers (38) expanded the theory to apply to more than just a simple, fast, charge transfer process.

2.1.2. Simple diffusion controlled electrode process.

Consider the simple electrode reaction, where substance O is reduced at a plane electrode and the product R is soluble either in the electrolyte or the electrode material.

$$O + n e \rightarrow R$$
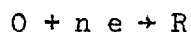
The rate of the reaction is controlled by the diffusion of O up to the electrode.

According to Fick's first law (39), the rate of diffusion per unit area i.e. the flux ."q", at a perpendicular distance "x" from the electrode at time "t" is given by

$$q(x,t) = Do \left(\frac{\partial Co(x\ t)}{\partial x} \right) \tag{2.1}$$

Do = the diffusion coefficient of the oxidized species O, and D_O = the concentration of species O.

Since the applied current density, "i", is constant, the following equation can be written:

$$i = n \, F \, D_O \left(\frac{\partial Co \, (x,t)}{\partial x} \right)_{x = o} \qquad (2.2)$$

Let $\quad \left(\frac{\partial Co \, (x,t)}{\partial x} \right)_{x = o} = \lambda \qquad (2.3)$

then $\lambda = \dfrac{i}{n \, FD_O} \qquad (2.4)$

The sum of the fluxes of the species O and R at the electrode surface must be equal, and of opposite sign.

$$Do \left(\frac{\partial Co \, (x,t)}{\partial x} \right)_{x = o} + D_R \left(\frac{\partial C_R(x,t)}{\partial X} \right)_{x = o} = 0 \qquad (2.5)$$

Equations (2.4) and (2.5) represent the two boundary conditions. In the initial conditions, the concentration of R is equal to zero, and the concentration of O is constant and equal to the bulk concentration c^O.

$$C_R \, (x,0) = 0 \qquad C_O \, (x,0) = c^O$$

For large distances from the electrode the functions $C_R \, (x,t)$ and $Co \, (x,t)$ will tend to the same value at the initial conditions. $C_R(x,t) \to 0$ and $Co(x,t) \to c^O$ as $x \to \infty$

The above boundary value problem was treated for the concentration of species O by Weber (32), Sand (33) and Rosebrugh and Miller (40). Karaglanoff (41) reported the solutions for the concentrations of both species O and R.

$$C_O \, (x,t) = c^O - \frac{2\lambda D_O^{\frac{1}{2}} t^{\frac{1}{2}}}{\pi^{\frac{1}{2}}} \, \exp\left(- \frac{x^2}{4 D_O t} \right) + \lambda \, x \, \text{erfc} \left(\frac{x}{2 Do^{\frac{1}{2}} t^{\frac{1}{2}}} \right) \qquad (2.6)$$

$$C_R \, (x,t) = \frac{2\lambda D_O t^{\frac{1}{2}}}{D_R^{\frac{1}{2}} \, \pi^{\frac{1}{2}}} \, \exp\left(\frac{-x^2}{4 D_R t} \right) - \frac{\lambda \, D_O}{D_R} \, \text{erfc} \left(\frac{x}{2 D_R^{\frac{1}{2}} t^{\frac{1}{2}}} \right) \qquad (2.7)$$

where erfc $(x) = 1 - erf(x)_{\gamma}$

and $erf(\phi x) = \dfrac{2}{\Pi^{\frac{1}{2}}}$ $\displaystyle\int_{0}^{x} exp\,(-z^2)\,dZ$

"Z" is an arbritrary integration variable.

At the electrode surface, i.e. x = o, substituting

equation (2.4), equations (2.6) and (2.7), become respectively:

$$C_{\bullet}\,(0,t) = C^{o} - \dfrac{2i\;\;t^{\frac{1}{2}}}{\pi^{\frac{1}{2}}nFDo^{\frac{1}{2}}} \qquad\qquad (2.8)$$

$$C_{R}\,(0,t) = \dfrac{2i\;\;t^{\frac{1}{2}}}{\Pi^{\frac{1}{2}}nFD_{R}^{\frac{1}{2}}} \qquad\qquad (2.9)$$

Defining the transition time "τ" as the time at which Co (o,t)

reaches zero, equation (2.8) becomes:

$$\tau^{\frac{1}{2}} = \dfrac{n\;F\;C^{o}\,\Pi^{\frac{1}{2}}\;Do^{\frac{1}{2}}}{2i} \qquad\qquad (2.10)$$

Equation (2.10) is known as Sand's equation, and for diffusion

controlled electrolysis at constant current density, the

quantity $i\tau^{\frac{1}{2}}/C$ will be independent of the applied current

density, the transition time and the concentration of the

diffusing species O.

2.1.3. Stepwise diffusion-controlled electrode process.

A species O is reduced in two steps, involving n_1 and n_2

electrons to R_1 and R_2 respectively.

$$O \xrightarrow{n_1 e} R_1 \xrightarrow{n_2 e} R_2$$
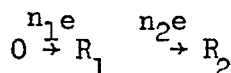
The chronopotentiogram will exhibit two steps (Fig. 2.2),

when the first wave, "τ_1" applies to the reduction of O to R_1,

and the second wave, "τ_2" applies to the reduction of O to R_2, and R_1 from the first transition to R_2.

The current during the second wave is divided between the reduction of O and R_1, and the sum of these two currents gives the boundary condition:

$$n_2 D_{R_1} \left(\frac{\partial C_{R_1}(x,t')}{\partial x}\right)_{x=o} + \frac{n_1}{(n_1 + n_2)} \, D_o \, \frac{\partial C_o(x,t\,1)}{\partial x}\Big)_{x=0} = \frac{i}{F} \quad (2.11)$$

Delahay (42). $\quad C_{R_1}(0,t') = \dfrac{2i}{n_2 F \Pi^{\frac{1}{2}} D_{R_1}^{\frac{1}{2}}} \dfrac{(n_1 + n_2)}{n_2} \tau^{\frac{1}{2}} - (\tau_1 + t)^{\frac{1}{2}} \quad (2.12)$

$$C_{R_2} = \frac{2i}{n_2 F \Pi^{\frac{1}{2}} D_{R_2}^{\frac{1}{2}}} (\tau_1 + t')^{\frac{1}{2}} - \tau_1^{\frac{1}{2}} \quad (2.13)$$

When $t' = \tau_2$, $C_{R_1}(0,\tau_2) = 0$,

therefore $\dfrac{n_1 + n_2}{n_1} \, \tau_1^{\frac{1}{2}} = (\tau_1 \tau_2)^{\frac{1}{2}}$ $\quad (2.14)$

also

$$\tau_2 = \tau_1 \left(\frac{2n_2}{n_1} + \frac{n_2^2}{n_1 2}\right) \quad (2.15)$$

Hence from the ratio of the two transition times it is possible to obtain the ratio of "n_2" to "n_1".

2.1.4. Consecutive diffusion-controlled electrode process involving two species.

When two species O_1 and O_2 are reduced at sufficiently different potentials, the chronopotentiogram will exhibit two waves. The first wave, corresponding to the reduction of O, will be described by the treatment in section 2.1.2. Species O_1 will however continue to diffuse up to the electrode after the first transition. The second wave will therefore include

some function which involves species O_1.

$$O_1 + n_1 \, \ell \rightarrow R_1$$

$$O_2 + n_2 \, \ell \rightarrow R_2$$
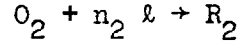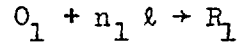
Let C^O_1 and C^O_2 be the bulk concentrations of species O_1 and O_2 respectively, and $t' = t - \tau_1$.

On this scale "τ_1" is equal to zero

The initial conditions, ($t' = 0$), are given by equation (2.6) when $C_{O_1} (x,t) = C_{O_1} (x,\tau_1)$ i.e. $C_{O_1} (x,0)$. also $C_{O_2} (x,0) = C^O_2$.

There are two boundary conditions to consider. Firstly, the flux at the electrode is the sum of the fluxes of the species O_1 and O_2.

$$n_1 \, D_{O_1} \left(\frac{\partial C_{O_1} (x,t')}{\partial x} \right)_{x = o} + n_2 \, D_{O_2} \left(\frac{\partial C_{O_2} (x,t')}{\partial x} \right)_{x = o} = i \, /F \qquad (2.16)$$

Secondly the concentration of species O_1 at the electrode surface is zero when t' is zero or greater than zero.

$$C_{O_1} (0,t') = 0 \qquad\qquad (2.17)$$

It can be said $C_{O_1} (x,t') \rightarrow C^O_1$ and $C_{O_2} (x,t') \rightarrow C_2^O$ as

$x \rightarrow \infty$.

The solution to this problem has been provided by Berzins and Delahay (42).

$$Co_2 (0,t') = C_2^{\ O} - \frac{2i}{\Pi^{\frac{1}{2}} n_2 F Do_2^{\frac{1}{2}}} (1 + t')^{\frac{1}{2}} - \tau_1^{\frac{1}{2}} \qquad (2.18)$$

by substituting the condition, $Co_2 (0,\tau_2) = 0$, into equation
(2.18), a simple relationship between "τ_1" and "τ_2" results.

$$(\tau_1 + \tau_2)^{\frac{1}{2}} - \tau_1^{\frac{1}{2}} = \frac{n_2 FC^{\ O}}{2i} n_2 \Pi^{\frac{1}{2}} Do_2^{\frac{1}{2}} \qquad (2.19)$$

Comparison of equation (2.19) with equation (2.10) provides
the relationship:

$$\tau_2'^{\frac{1}{2}} = (\tau_1 + \tau_2)^{\frac{1}{2}} - \tau_1^{\frac{1}{2}} \qquad (2.20)$$

"τ_2'" is the transition time expected for species O_2 if species
O_1 was absent.

2.1.5. Reactant adsorption

In the presence of adsorption of the reactant at the
electrode surface, the applied current will be divided between
the discharge of the adsorbed species and the discharge of the
diffusing species.

The product "$i \ \tau^{\frac{1}{2}}$" will not be constant (see section 2.1.2.)
but it will increase with increasing current density. The
number of models available to describe the division of the
current between the two processes is infinite, so that it is
feasible to consider only the limiting cases. In one case
it will be assumed that the adsorption equilibrium is established
before electrolysis, and that the rate of adsorption is a
slow process. Hence the time required to attain equilibrium
is very much longer than the transition time. The second
case considered is where the rate

of adsorption is fast, and hence there is a rapid equilibration
between the adsorbed and diffusing species during the transition
time.

2.1.5.1. Slow adsorption processes.

For a slow adsorption process, it is assumed that
the adsorbed reactants (A.R.) and the diffusing, or solution,
reactant (S.R.) undergo electron transfer as essentially
independent species. The kinetic scheme takes the following
form

$$O_{(Adsorbed)} \xleftarrow{Slow} O \text{ (solution)}$$

$$O_{(Adsorbed)} + ne \rightarrow R$$

$$O_{(Solution)} + ne \rightarrow R$$
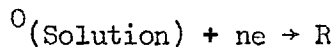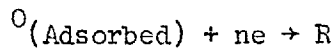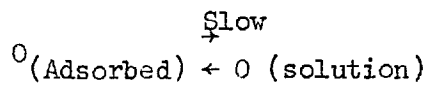
By Faradays' law

$$i_{ads} \, \tau_{ads} = nF\Gamma \tag{2.21}$$

where suffix "ads", applies to the adsorbed species, and "Γ"
is the molar surface excess concentration of the adsorbed species.

For the above kinetic scheme three limiting models can
be distinguished. The first model, the AR.SR model, assumes
that the adsorbed species is completely depleted before the
start of the electrolysis of the solution species (43-47).
The transition times for both processes will be additive,
and the applied current density will be the same for both
processes.

$$\tau = \tau_{ads} + \tau_{soln.} \tag{2.22}$$

$$i = i_{ads} = i_{soln.} \tag{2.23}$$

— 24 —

The suffix "soln" applies to the diffusion process, and symbols without the suffixes, "ads" or soln" apply to the overall process. A relationship for the AR.SR model can be obtained from equations (2.10) and (2.21-23).

$$i\tau = nF\Gamma + \frac{(nFC)^2 \Pi D}{4i} \qquad (2.24)$$

For the AR.SR model to be applicable, the plot of "iτ" versus "1/i" should linear. The surface excess may be calculated from the intercept, when 1/i is zero. The slope will be proportional to "$c^2 D$".

The second model, described as the SAR model, assumes A.R. and S.R. are depleted concurrently, and that there is a fixed division of the applied current between the two such that their concentrations at the electrode reach zero simultaneously.

$$\tau = \tau \text{ ads} = \tau soln \qquad (2.25)$$

$$i = i \text{ ads} + i \text{ soln} \qquad (2.26)$$

Equations (2.10, 2.19, 2.23 and 2.24) give rise to the relationship:

$$i = nF\Gamma + \frac{nFC \ (\Pi D)^{\frac{1}{2}}}{2} \tau^{\frac{1}{2}} \qquad (2.27)$$

The SAR model should apply if the plot of "iτ" versus "$\tau^{\frac{1}{2}}$" is linear. The value for the surface excess will be given by the intercept, when $\tau^{\frac{1}{2}}$ is zero, and slope will be proportional to "$CD^{\frac{1}{2}}$". The third model, the SR.AR model, requires that the absorbed layer be electrolyzed at the end of the transition time. A rigorous mathematical solution to this model has been given by Reinmuth (44) and Anson (48).

$$\frac{nF \ \tau ads}{i} - (\tau \text{ ads} + \tau \text{ soln}) \ \arccos \frac{(\tau soln - \tau ads)}{(\tau ads + \tau soln)} + 2 \ (\tau ads \ \tau soln)^{\frac{1}{2}}$$

$$(2.28)$$

A computer solution to equation (2.26) using the overall

transition time, "τ", has been published (49), but it is more

convenient to use the approximate solution put forward by

Lorenz (43,46).

$$(i\tau)^{\frac{1}{2}} = (nFT)^{\frac{1}{2}} + \frac{nFC}{2} \frac{(\pi D)^{\frac{1}{2}}}{i^{\frac{1}{2}}} \qquad (2.29)$$

The applicability of the SR.AR model can be shown by the

linearity of the plot $(i_\tau)^{\frac{1}{2}}$ versus $i^{-\frac{1}{2}}$. The surface excess

may be derived from the intercept, when "$i^{-\frac{1}{2}}$" is zero.

The slope of the plot will be proportional to "$CD^{\frac{1}{2}}$".

2.1.5.2. Fast adsorption processes.

In the case where the rate of adsorption is fast, the

assumption is made that there is rapid equilibration between

AR and SR according to a linear adsorption isotherm:

$$\Gamma = Ka.C \qquad (2.30)$$

The species actually undergoing electron transfer is unknown

in as much as the adsorption equilibrium shifts during the

electrolysis, the surface excess being determined by the

concentration of SR near the electrode surface. The expression

for the transition time was originally given by Lorenz (43).

$$\tau^{\frac{1}{2}} = \tau_\infty^{\frac{1}{2}} + \pi^{\frac{1}{2}}\frac{Ka}{2D^{\frac{1}{2}}} - \frac{\pi^{\frac{1}{2}} Ka \phi}{2D^{\frac{1}{2}}} \qquad (2.31)$$

$$\phi = \exp\left(\frac{D\tau}{Ka^2}\right) \text{erfc}\left(\frac{D^{\frac{1}{2}}}{K_a} \tau^{\frac{1}{2}}\right) \qquad (2.32)$$

"τ_∞" is the transition time which would be expected if Sand's

equation was obeyed, equation (2.10). At long transition times

"ϕ" will be small and hence a plot of "$\tau^{\frac{1}{2}}$" versus "$1/_i$" should

be linear. Extrapolation, from long transition times, to "$1/_i$"

is equal to zero, should give an estimate of "Ka", and the

slope will give an estimate of the diffusion coefficient. These

values may then be used to estimate the value of "ϕ" at

shorter transition times.

Equation (2.31) can be rewritten:

$$\tau^{\frac{1}{2}} + \frac{\Pi^{\frac{1}{2}}Ka}{2D^{\frac{1}{2}}} \quad \phi = \frac{nFCl^{\frac{1}{2}}D^{\frac{1}{2}}}{2i} + \frac{\Pi^{\frac{1}{2}}K_a}{2D^{\frac{1}{2}}} \qquad (2.33)$$

If the left hand side of equation is then plotted against "$1/i$",

better estimates for the diffusion coefficient and "Ka" can

be obtained. These values can then be used to gain a more

accurate view for "ϕ". The iteration should be continued

until it is ascertained whether a linear plot can be obtained.

2.1.5.3. Choice of adsorption model

It must be pointed out that, even though a single transition

time may be observed, the AR.SR or SR.AR models may still be

applicable. Two transition times would only be observed, if

the two processes occurred at widely separated potentials.

Another point, which should also be stressed is that the above

models represent limiting cases, and a fit to one of these

models will only indicate that the system approaches that

limiting case more closely than the next.

A range of transition times must be measured. Short

transition times will provide a maximisation of the adsorption

contribution whereas long transition times will lend to a

more accurate estimation of the diffusion coefficient.

Constancy of the value of the diffusion coefficient obtained

over a range of concentration provides an extra criterion to

the validity of the model.

Laitinen and Chambers (46) carried out trial calculations

assuming AR.SR model to be valid. They made plots for the

SAR and AR.SR model using the same synthetic data. The amount

of curvature however is very much dependent on the relative

surface and solution concentrations. For a surface excess of

8.3×10^{-10} mole, cm^{-2} (corresponding to a monolayer of 20

sq. $\overset{o}{A}$ molecular area) and a solution concentration of $10^{-2}M$

the curvature was barely detectable for the SAR and SR.AR models.

A more pronounced curvature would result if the solution

concentration was reduced. Lingane (50) used least

squares procedures to analyse extensive synthetic chronopotentiometric

data according to the four models described above. His work

illustrated the great difficulty in elucidating the adsorption

model, in that exceedingly large amounts of data were required

to satisfactorily detect which the model gave the best fit.

The surface excess values obtained from the intercept

of the best straight line decreases in the order AR.SR SAR SR.AR.

The magnitude of the variation increases with increasing

concentration (46). The safest procedure is to use the SAR

model, since this will give an intermediate value for the

surface excess concentration.

It is obvious that chronopotentiometry is of limited

value for the study of adsorption. It does however indicate

the presence of adsorption in an overall electrode process and
it does give an assessment of the probable magnitude of the
surface excess. From this point of view, it can be used to
monitor the effects, that changes in the system, have on
adsorption.

2.1.6. Chemical Kinetic Processes.

Consider the reduction of species O when the electrochemical
reaction is preceded by a chemical reaction according to the
following scheme:

$$mY \underset{k_b}{\overset{k_f}{\rightleftarrows}} pO$$

$$O + ne \rightarrow R$$
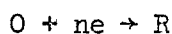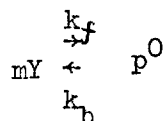
It is assumed that species Y is not electroactive near the
reduction potential for species O. Hence the rate of reduction
of species O may be no longer totally controlled by the rate
of mass transfer, c.f. section 2.1.2, but may also be
dependant on the rate of interconversion between species O and Y,
providing the rate is slow enough.

Three kinetic schemes have been considered for a preceding,
rate determining chemical reaction. The first scheme involves
the decomposition of a single species Y to a single electroactive
species, O, i.e. "m" and "p" in the chemical equation are
equal to unity. Examples of such a scheme are the breakdown of
a phosphate polymer (51) or the break down of the cadmium
cyanide complex species (37,53). The second scheme considers the
formation of an electroactive polymeric species, i.e. "m" is
greater than unity and "p" is equal to unity. The final scheme

describes the dissociation of a dimeric species to two

electroactive species, i.e. monomerization. In this case "m"

is equal to unity and "R" is equal to two.

2.1.6.1. Simple kinetic scheme

$$Y \underset{k_b}{\overset{k_f}{\rightleftarrows}} 0$$

$$0 + ne \rightarrow R$$
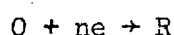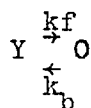
Delahay and Berzins (54) have treated this case and have

provided a rigorous solution to the boundary value problem.

The concentration of species 0 at the electrode surface is given

by equation (2.34)

$$C_0(0,t) = 1/(1 + 1/K) \left[C^0 + 2\lambda \left(\frac{Dt}{\Pi}\right)^{\frac{1}{2}} - \frac{\lambda D^{\frac{1}{2}}}{K(k_f + k_b)^{\frac{1}{2}}} \text{ erf } \left((k_f + k_b)^{\frac{1}{2}} t^{\frac{1}{2}} \right) \right]$$

$$C^0 = C_0(x,o) + C_Y(x,0)$$

$$K = \text{equilibrium constant} = k_f/k_b$$

The diffusion coefficient "D" is the common value for both

species Y and 0, i.e. it is assumed $D = D_Y = D_0$. "λ" is defined

by equation (2.4). The transition time "τ_k" is determined

by the condition $C_0(0,t) = 0$. Hence after substituting for

"λ" the following equation for "τ_k" can be obtained.

$$i\tau_k^{\frac{1}{2}} = \frac{nFC^0 \Pi^{\frac{1}{2}} D^{\frac{1}{2}}}{2} - \frac{\Pi^{\frac{1}{2}} i}{2K(k_f + k_b)^{\frac{1}{2}}} \text{ erf } ((k_f + k_b)^{\frac{1}{2}} \tau_k^{\frac{1}{2}}) \quad (2.35)$$

When the argument of the error function is greater than two,

the error function is virtually equal to unity (55). Therefore

in the case of transition times greater than $4/(k_f + k_b)$ the

relationship "$i\tau_k^{\frac{1}{2}}$" versus "i" is linear.

$$i\tau_k^{\frac{1}{2}} = \frac{nFC^0 \Pi^{\frac{1}{2}} D^{\frac{1}{2}}}{2} - \frac{\Pi^{\frac{1}{2}} i}{2K(k_f + k_b)^{\frac{1}{2}}} \quad (2.36)$$

The slope is inversely proportional to $K (k_f + k_b)^{\frac{1}{2}}$ and the

intercept, when "i" is zero, gives the product "$i\tau^{\frac{1}{2}}$, which

would be expected if Sands equation (2.10) was obeyed.

The error function may expand as a series.

$$erf(x) = \frac{2}{\Pi^{\frac{1}{2}}} \quad (x - \frac{x^3}{3x1} + \frac{x^5}{5 \times 2!} \frac{-x^7}{7 \times 3!} + \ldots) \quad (2.37)$$

In the case of transition times shorter than those applicable

to equation (2.36) it is necessary to take into account the

variations of the error function using the expansion (2.37).

For very small values of $(k_j + k_b)^{\frac{1}{2}}\tau^{\frac{1}{2}}$, only the first term of

the expansion need be used.

Thus

$$(i\tau_k^{\frac{1}{2}}) = \frac{nFC^O_{\Pi}{}^{\frac{1}{2}}D^{\frac{1}{2}}}{2(1 + 1/K)} \qquad (2.38)$$

At very short transition times, the amount of species "0"

produced by the chemical reaction is insignificant, and hence

only the equilibrium concentration of species "0", $(C^O/Cl + 1/K)$,

is involved. This results in a constant value for the product

"$i\tau_k^{\frac{1}{2}}$" c.f. equation (2.10).

2.1.6.2. Polymerization Scheme.

$$m\Upsilon \overset{kf}{\underset{kb}{\rightleftharpoons}} 0$$

$$0 + ne \rightarrow R$$
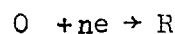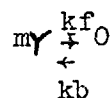
Reinmuth (44) has derived a theoretical treatment for

this scheme, with the restriction that the equilibrium must

strongly favour species Y, i.e. $C_y (x,o) \gg C_0(x,o)$

$$C_0 (o,t) = Km^m \left(C_T - \frac{2\lambda^{\frac{1}{2}} t^{\frac{1}{2}}}{\Pi^{\frac{1}{2}}} \right)^m - \frac{\lambda D^{\frac{1}{2}}}{k_f^{\frac{1}{2}}} \quad erf (k_b t^{\frac{1}{2}}) \qquad (2.37)$$

where $C_T = C_o(x,o) + C_y(x,o)/m$, and $D = Do = D_Y$

At the transition time "τ_k" the surface concentration of species O reaches zero.

Thus $i\tau_k^{\frac{1}{2}} = \dfrac{nFC_T \Pi^{\frac{1}{2}} D^{\frac{1}{2}}}{2} - \dfrac{nF\Pi^{\frac{1}{2}}D^{\frac{1}{2}}}{2m} i^{1/m} \left(\dfrac{\text{erf } (k_b\tau_k)^{\frac{1}{2}}}{nF D^{\frac{1}{2}} kf} \right)^{1/m}$ (2.40)

The concentration term has to be considered as species O.i.e. "C_T". If the concentration is in terms of species Y, i.e. "c^O" (for example if the species originally present was species Y) then it has to be converted to "C_T".

$c^O = mC_o(x,o) + C_Y(x,o) = m\ C_T.$

When the error function argument, $(kb\tau_K)^{\frac{1}{2}}$, is equal to or greater than two, the error function can be considered to be equal to unity (55).

Hence equation (2.40) becomes:

$i\tau_k^{\frac{1}{2}} = \dfrac{nFC_T \Pi^{\frac{1}{2}} D^{\frac{1}{2}}}{2} - (nFD^{\frac{1}{2}})^{(m-1)/m} \dfrac{\Pi^{\frac{1}{2}}}{2m} \left(\dfrac{i}{k_f} \right)^{1/m}$ (2.41)

It can be seen from equation (2.41) that if the transition time is greater than $4/k_b$, "$i\tau_k^{\frac{1}{2}}$" has a linear relationship with $i^{1/m}$, The intercept at zero current gives the product "$i\tau^{\frac{1}{2}}$" expected if Sands equation (2.10) was obeyed, i.e. totally mass transfer control. The slope will be inversely proportional to $kf^{1/m}$.

When the rate of attainment of equilibrium is very slow in comparison with the electrolysis time, i.e. when $(k_b\tau_k)^{\frac{1}{2}}$ is small, the first term in the error function expansion (2.37) need be used. The resulting expression corresponds to the Sand's equation (2.10) using the equilibrium concentration of species

"O", $K(mC_T)^m$

$$(i\tau^{\frac{1}{2}})_{k_\tau \to o} = \frac{nFK(mC_T)^m \pi^{\frac{1}{2}} D^{\frac{1}{2}}}{2} \qquad (2.42)$$

2.1.6.3. Monomerization scheme

$$\underline{Y} \underset{kb}{\overset{kf}{\rightleftarrows}} 2O$$

$$O + ne \to R$$
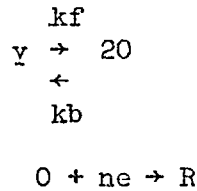
This scheme was originally treated by Koutecky et alia (56,57) and extended by Fischer et alia (58). The treatment involves the restriction that the equilibrium is displaced strongly in favour of species Y. They published the relationship for the intermediate case, i.e. $i\tau^{\frac{1}{2}}$ versus some function of current density, c.f. equations (2.36) and (2.40).

$$i\tau_k^{\frac{1}{2}} = \frac{nFC_T\pi^{\frac{1}{2}}D^{\frac{1}{2}}}{2} - \left(\frac{9\pi^6}{16nF_f^2 {}^4KD^2}\right)^{1/3} i^{4/3} \qquad (2.43)$$

$$C_T = C_o(x,o) + 2C_y(x,o)$$

and $D = D_y = Do$.

In the limiting case when the rate of attainment of equilibrium is slow in comparison with the electrolysis time, it is justifiable to substitute the equilibrium concentration of species O, $\dfrac{C_T K^{\frac{1}{2}}}{2}$

into Sand's equation (2.10).

$$(i\tau_k^{\frac{1}{2}})_{\tau \to o} = \frac{nFC_T^{\frac{1}{2}} K^{\frac{1}{2}} \pi^{\frac{1}{2}} D^{\frac{1}{2}}}{4} \qquad (2.42)$$

2.1.6.4. Choice of kinetic scheme

A decrease in the product, $i\tau^{\frac{1}{2}}$, with increasing applied current density is a diagnostic criterion for the occurrence of a preceding chemical reaction. The relationship of the

Fig. 2.3
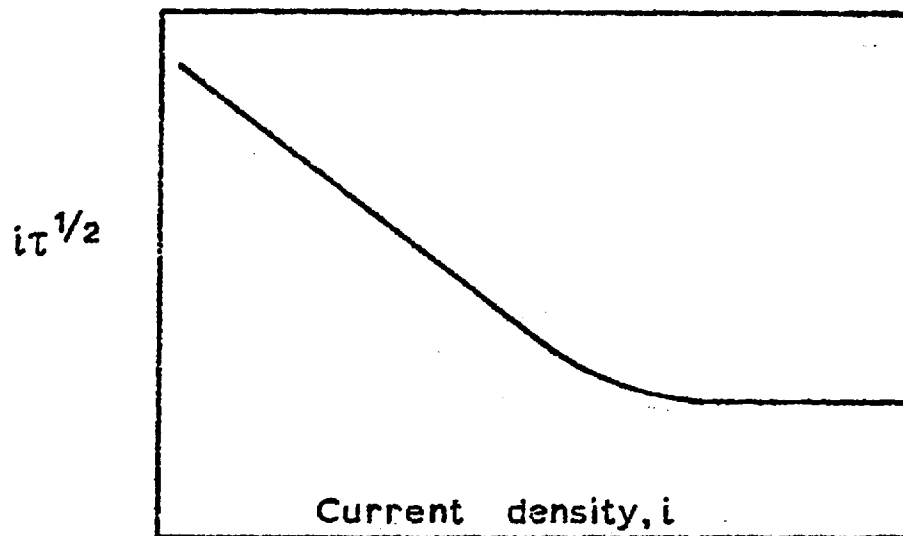
(a)   Simple kinectic scheme.
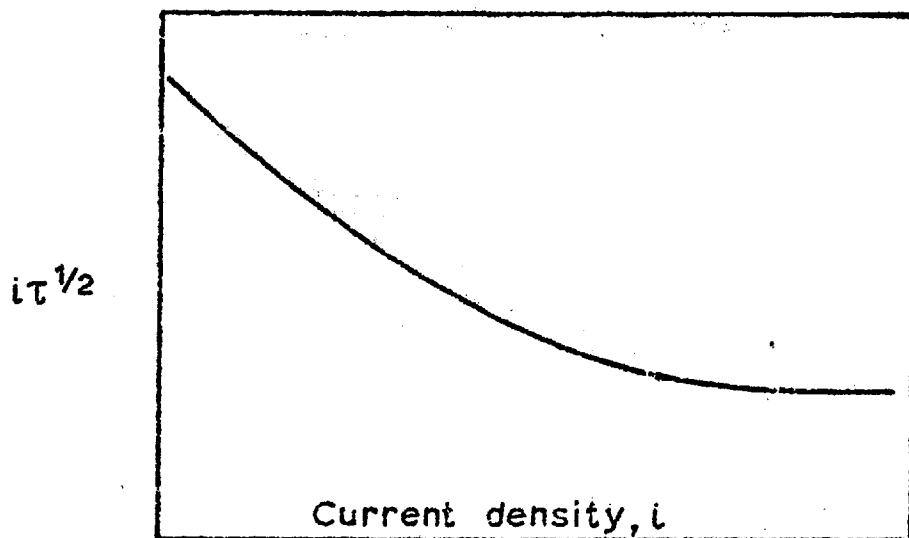
(b)   Polymerization scheme
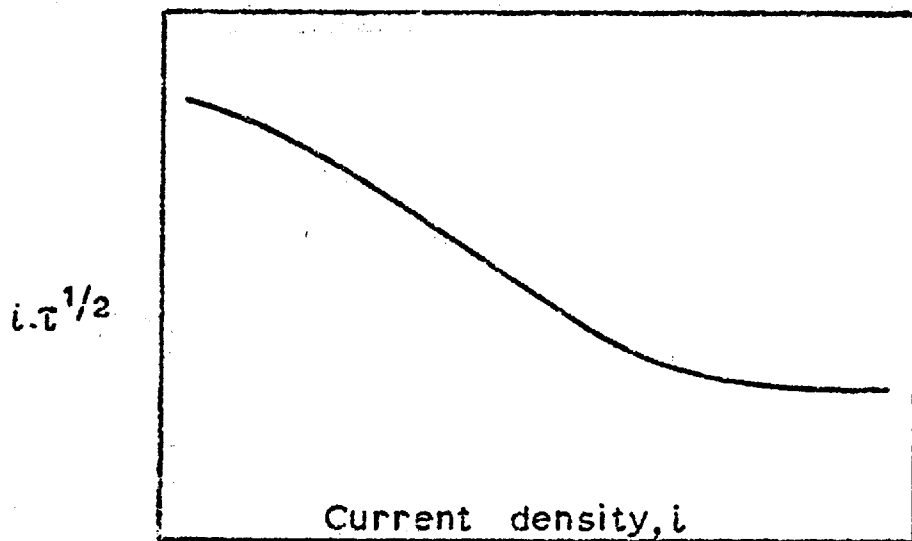
(c)   Monomerization scheme

product $i\tau^{\frac{1}{2}}$, to the applied current density, 'i', falls into two

parts; firstly there is the part where the product $i\tau^{\frac{1}{2}}$

decreases as a function of current density; and the second part,

at high current densities where $i\tau^{\frac{1}{2}}$ is constant, applies to the

situation when only the equilibrium concentration of species O

is electrolysed, (figure 2.3(a,b,c)).

The diagnostic criterion used in the choice of the model

is the form taken by the first part of the above relationship.

When the product, "$i\tau^{\frac{1}{2}}$" fits a linear function of current

density (figure 2.3(a)) c.f. equation (2.36), the simple kinetic

scheme will apply. The polymerization scheme will give a

concave plot for the product, "$i\tau^{\frac{1}{2}}$", versus "i" (figure 2.3(b))

according to the equation (2.41). Finally the monomerization

scheme is characterized by a convex plot for the product, "$i\tau^{\frac{1}{2}}$",

versus "i" (figure 2.3(C)) according to equation (2.43)

The polymerization and monomerizstion schemes are confirmed

by obtaining linear plots for $i\tau^{\frac{1}{2}}$ versus "$i^{1/m}$" and

"$i^{4/3}$" respectively.

2.1.7. Catalytic processes

Catalytic processes are those, in which there is regeneration

of the electrolysed species O. These processes, considering a

first order regeneration process, were first treated by

Brdicka and Wiesner (59) using the concept of a reaction layer

(60,61). The same scheme was later treated by Delahay et al

(62,63) as a boundary value problem.

$$O + ne \rightarrow R$$

$$O \overset{k_f}{\underset{}{\rightleftharpoons}} R + Z$$
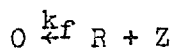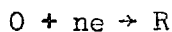
$$C_O(0,t) = C^O - \frac{i\,t^{\frac{1}{2}}}{\text{H}n\text{F}D^{\frac{1}{2}}\gamma}\ \text{erf}(\gamma) \qquad (2.45)$$

$$C_R(0,t) = C^O - C_O(0,t) \qquad (2.46)$$

and $\gamma = (k_f\,C^O\tau_c)^{\frac{1}{2}}$ $\qquad (2.47)$

Fig. 2.4.
Catalytic effect
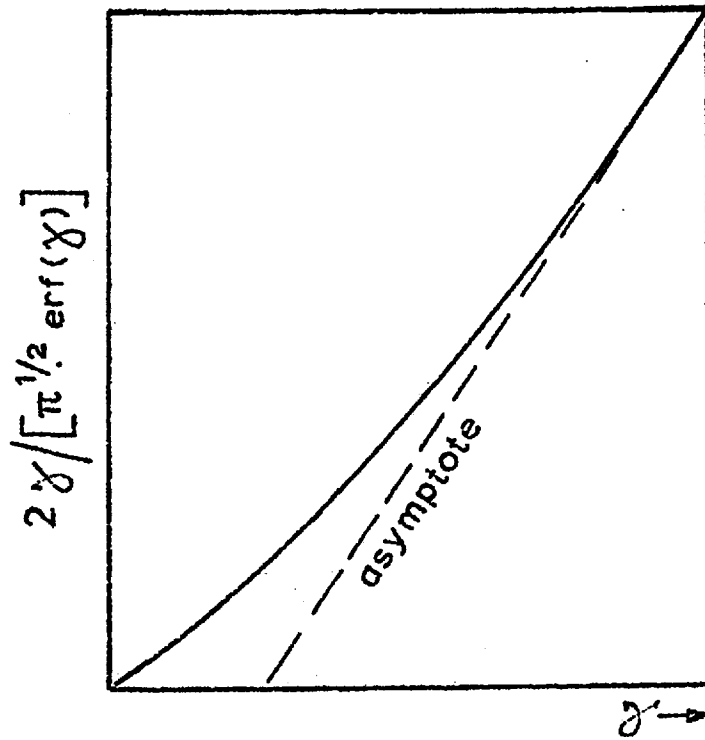
Fig. 2.5

Current reversal
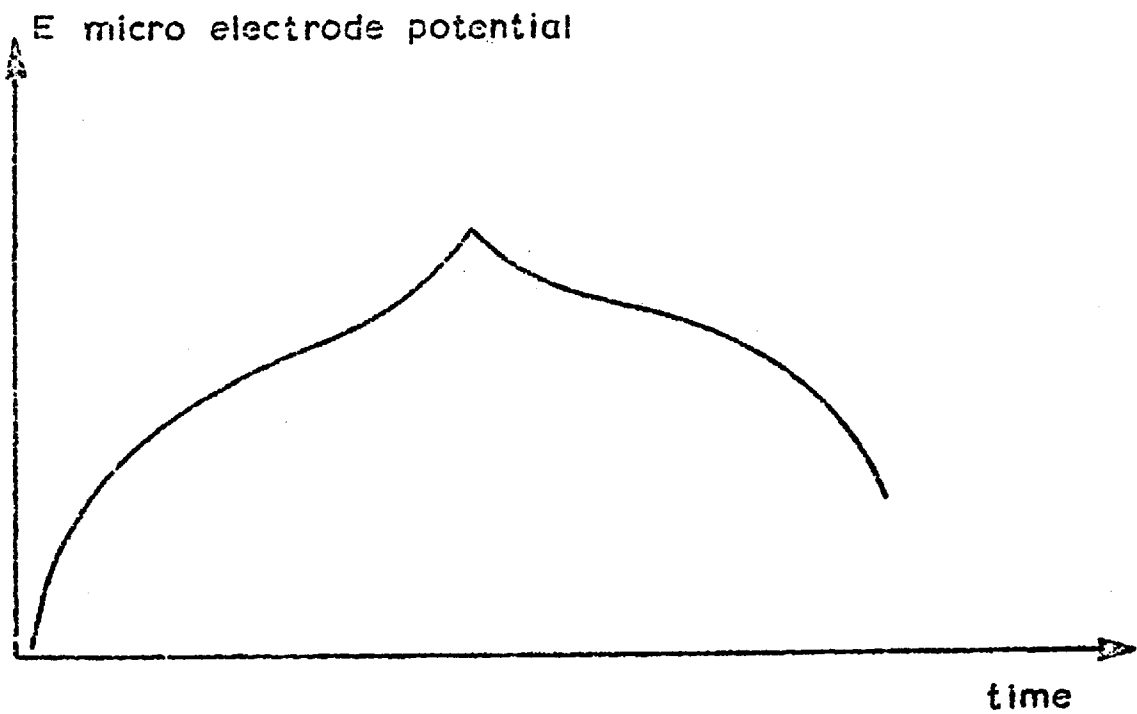
It is assumed that $D = D_O = D_R$. The catalytic transition time is "τ_c", and "k_f" is the formal rate constant for the regeneration of species O. From equations (2.10) and (2.45) it can be deduced that

$$\left(\frac{\tau}{\tau^c}\right)^{\frac{1}{2}} = \frac{2\gamma}{\Pi^{\frac{1}{2}}\text{erf}(\gamma)} \qquad (2.48)$$

The value for "τ" is given by Sand's equation (2.10). For very short transition times only the first term of the error function expansion, equation(2.37) is significant hence

$$\left(\frac{\tau_c}{\tau}\right)^{\frac{1}{2}} \to 1 \text{ as } \tau_c \to 0.$$

At long transition times, where the argument of the error junction is equal to or greater than two, the error function is virtually unity (55). Under these conditions the function $2\gamma(\Pi^{\frac{1}{2}}\text{erf}(\gamma))$ becomes asymptotic to $2\gamma/\Pi^{\frac{1}{2}}$, (figure 2.4). The first limiting condition will give the diffusion coefficient, using Sand's equation, and hence "τ" can be calculated for any current density. The value for "k_f" can be obtained from the second limiting condition, knowing "τ_c" and "τ".

2.1.8. Current Reversal

A species O is reduced to species R, and at the transition time, "τ" for this reduction, the current is reversed. Species R will then be oxidised back to species O, and a potential time curve will be observed for this process, (figure 2.5). Berzins and Delahay (42) have developed the following mathematical interpretation for the re-oxidation process.

The concentration of species R at the transition time "τ" is given by equation (2.7) in which time "t" is made equal to "τ". The resulting expression sets the initial

condition. The boundary condition is similar to that for section 2.1.2. c.f. equation (2.4)

$$\left(\frac{\partial C_R (x,t')}{\partial x}\right)_{x = 0} = \lambda' \qquad (2.49)$$

with

$$\lambda' = \frac{i'}{nFD_R} \qquad (2.50)$$

The time for the reverse electrolysis is "t'" and the current density is "$\bar{i}'$". For $x \to \infty$, $C_R(x,t') \to 0$.

Berzins and Delahay (42) solved the boundary value problem in terms of $C_R(x,t')$ and $C_O(x,t')$.

$$C_R(x,t') = 2\theta \left(\frac{D_R(\tau+t')}{\pi}\right)^{\frac{1}{2}} \exp\left(\frac{-x^2}{4D_R(\tau+t')}\right) - \theta x \operatorname{erfc}\left(\frac{x}{2D_R^{\frac{1}{2}}(\tau+t')^{\frac{1}{2}}}\right)$$

$$-2(\theta+\lambda')\left(\frac{D_R t'}{\pi}\right)^{\frac{1}{2}} \exp\left(\frac{-x^2}{4D_R t'}\right) + (\theta+\lambda')\, \operatorname{erfc}\left(\frac{x}{2D_R^{\frac{1}{2}} t'^{\frac{1}{2}}}\right) \qquad (2.51)$$

where

$$\theta = \frac{i}{nF\, D_R} \qquad (2.52)$$

With the assumption that D_O and D_R were equal

$$C_O (x,t') = c^O - C_R (x,t') \qquad (2.53)$$

The reverse transition time "τ'" is determined by the condition $C_R (0,\tau') = 0$. Hence from equations (2.51) and (2.53).

$$\tau' = \frac{\theta^2}{(\theta + \lambda')^2 - \theta^2}\, \tau \qquad (2.54)$$

When "i" and "i'" are equal, "θ" is equal to λ', and

$$\tau' = 1/3\tau \qquad (2.55)$$

The applicability of equation (2.55) can be used as a diagnostic criterion for the solubility of species R in the electrolyte. If species R is deposited on the electrode, as

would be the case if species R was a metal, then τ' would

be equal to τ.

2.1.9. Potential-time relationships

2.1.9.1. Reversible charge-transfer.

When charge-transfer is reversible, there is no

significant activation overpotential. Thus the electrode

potential "E" during electrolysis will be totally dependant on

the surface concentration of the oxidised and reduced species,

according to the Nernst equation.

$$E = E^O + \frac{RT}{nF} \ln \frac{C_O(0,t) \cdot f_O}{C_R(0,t) \cdot f_R} \qquad (2.56)$$

substitution of equations (2.8), (2.9) and (2.10) into

(2.54) gives the variable activity potential-time relationship.

$$E = E^O + \frac{RT}{nF} \ln \frac{f_O D_R^{\frac{1}{2}}}{f_R D_O^{\frac{1}{2}}} + \frac{RT}{nF} \ln \left(\frac{\tau^{\frac{1}{2}} - 1}{t^{\frac{1}{2}}} \right) \qquad (2.57)$$

In the case when the electrode substrate is the same material

as the reduced species or the reduced species is insoluble

the activity of the reduced species is unity, i.e.

$$C_R(0,t) \ f_R = 1$$

$$E = E^O + \frac{RT}{nF} \ln \left(\frac{2i}{nF\pi^{\frac{1}{2}}D_O^{\frac{1}{2}}} f_O \right) + \frac{RT}{nF} \ln (\tau^{\frac{1}{2}} - t^{\frac{1}{2}}) \qquad (2.58)$$

$$= E^O + \frac{RT}{nF} \ln f_O C^O + 1 \frac{RT}{nF} \ln \left(1 - \frac{t^{\frac{1}{2}}}{\tau^{\frac{1}{2}}} \right) \qquad (2.59)$$

If the activity coefficients "f" are assumed to be

unity and the diffusion coefficients for the two species to be

equal, equations (2.57) reduces to

$$E = E^O + \frac{RT}{nF} \ln \left(\frac{\tau^{\frac{1}{2}} - 1}{t^{\frac{1}{2}}} \right) \qquad (2.60)$$

and equation 2.59 reduces to

$$E = E^O + \frac{RT}{nF} \ln \quad C^O \quad + \frac{RT}{nF} \ln \left(1 - \frac{t^{\frac{1}{2}}}{\tau^{\frac{1}{2}}}\right) \qquad (2.61)$$

The quarter-time potential $"E_{\tau/4}"$ is the potential at time $t = \tau/4$, and the value of $E_{\tau/4}$ is obtained by substituting for "t" in the potential-time relationship. Thus for the variable activity relationship (2.60).

$$E_{\tau/4} = E^O \qquad\qquad (2.62)$$

and for the unit activity relationship (2.61)

$$E_{\tau/4} = E^O + \frac{RT}{nF} \ln \frac{C^O}{2} \qquad\qquad (2.63)$$

In both cases the quarter-time potential is independent of the applied current density. This criterion is diagnostic of a simple reversible electrode process.

A similar treatment can be applied to the second wave given by a stepwise electrode process, section 2.13. Equations (2.12) (2.13) and (2.14) are substituted into the Nernst equation (2.56). The variable activity relationship is given by.

$$E_2 = E_2^O + \frac{RT}{n_2 F} \ln \frac{(\tau_1 + \tau_2)^{\frac{1}{2}} - (\tau_1 + t')^{\frac{1}{2}}}{(\tau_1 + t')^{\frac{1}{2}} - \tau_1^{\frac{1}{2}}} \qquad (2.64)$$

and the unit activity relationship is given by

$$E_2 = E_2^O + \frac{RT}{n_2 F} \ln \frac{n_1}{n_2} C^O + \frac{RT}{n_2 F} \ln \frac{(\tau_1 + \tau_2)^{\frac{1}{2}} - (\tau_1 + t')^{\frac{1}{2}}}{\tau_1^{\frac{1}{2}}} \quad (2.65)$$

The equivalent to the quarter-time potential, $"E'_{\tau/4}"$, is the potential at $t' = \tau_2/4 + n_2 \tau_1 / 2 n_1$.

In the case of the variable activity relationship

$$E'_{\tau/4} = E^{o}_{2}$$ (2.66)

and in the case of the unit activity relationship

$$E'_{\tau/4} = E^{O}_{2} + \frac{RT}{n_{2}F} \ln\left(\frac{C^{O}}{2}\right)$$ (2.67)

If the second wave is a result of a reversible electrode process, then $E'_{\tau/4}$ will be independant of applied current density.

2.1.9.2. Totally irreversible charge transfer.

When the electrode process is totally irreversible with respect to charge-transfer, the electrode potential will be related to the surface concentration by the following equation, c.f. reference (64),

$$i = nFk^{o}_{fh}C_{o}(0,t) \exp\left(\frac{-\alpha nFE}{RT}\right)$$ (2.68)

where "k^{o}_{fh}" is the forward formal rate and "α" the charge transfer coefficient for the above charge-transfer process. Equations (2.8) and (2.10) can be introduced into equation (2.68) to give the potential-time relationship for a simple, totally irreversible charge transfer process.

$$E = \frac{RT}{\alpha nF} \ln\left(\frac{2k^{o}_{fh}}{\Pi^{\frac{1}{2}}D_{o}^{\frac{1}{2}}}\right) + \frac{RT}{\alpha nF} \ln(\tau^{\frac{1}{2}}-t^{\frac{1}{2}})$$ (2.69)

that is

$$E = \frac{RT}{\alpha nF} \ln\left(\frac{nFC^{o}k^{o}_{fh}}{i}\right) + \frac{RT}{\alpha nF} \ln\left(1-\frac{t^{\frac{1}{2}}}{\tau^{\frac{1}{2}}}\right)$$ (2.70)

Extrapolation of the plot "E" versus $\ln(1-t^{\frac{1}{2}}/\tau^{\frac{1}{2}})$ to t = o will give an estimate of the rate constant "k^{o}_{fh}". The slope of the plot will give a value for "αn". The slope of the

plot of "$E_{\tau/4}$" versus "$\ln i$" will be "$RT/\alpha nF$". The values

for "αn" obtained from both plots should not differ significantly

if the electrode process is controlled by the rate of charge

transfer.

2.1.10. Deviations from theoretical models.

The derivation of the above models was based on the assumption

that the following conditions were achieved. (a) The electrolyte

was not stirred, and the effects of convection could be

neglected. (b) A large excess of supporting electrolyte was

present such that migration of the electroactive species was not

significant. (C) The transport of the electroactive species

through the electrolyte was by means of semi-infinite linear

diffusion. If these conditions are applicable, the above

mathematical treatment will be valid. Thus it is necessary

to carry out measurements within the limits where these conditions

are applicable.

Other factors, which also need to be considered are the

influence of the double layer, surface roughness effects of

solid electrodes, oxide films on electrodes and the effect of

the adsorption of foreign substances.

2.1.10.1. Convection

At short transition times the effect of convection may

be neglected, but at long transition it will lead to the

enhancement of the product "$i\tau^{\frac{1}{2}}$". In aqueous studies at

room temperature ($25^\circ c$). Delahay and Mattax (65) found that

transition times of the order of one minute were not

influenced by convection. In high temperature studies, e.g.

fused salt studies, convection would have a much more marked

effect. The rate of natural convective heat transfer is

proportional the fourth root of the temperature difference, "$\Delta T^{1/4}$".(66)

To ensure that the effect of convection is not significant, the transition times should be less than two seconds.

2.1.10.2. Migration

The enhancement of the transition time by electrical migration, due to the absence of a supporting electrolyte was first observed by Sand's (33). He assumed that under these conditions the flux, "f", for the electroactive species at the electrode surface is given by:

$$f = \frac{i(1-t_+)}{nF} \tag{2.72}$$

where "t_+" is the transport number for the species. Sand's equation (2.10) has in this case to be modified.

$$i\tau^{\frac{1}{2}} = \frac{nFC^O\pi^{\frac{1}{2}}D_O^{\frac{1}{2}}}{2\ (1-t_+)} \tag{2.73}$$

This treatment is not rigorous since it is based on two erroneous assumptions. The solution is not homogeneous, but is less concentrated in the diffusion layer. The potential gradient in the diffusion layer is not linear, and hence Fick's second law must be modified to include the influence of the potential gradient. A more rigorous treatment has been applied by Morris and Lingane (67), assuming ideal ionic behaviour. The resulting equation has the same form as equation (2.73), but "Do" is replaced by "D_S", where

$$D_S = \frac{D_+D_-(n_+ + n_-)}{(n_+D_+ + n_-D_-)} \tag{2.74}$$

"D_+" and "D_-" are the diffusion coefficients for the reducible cation and its counter anion respectively, and "n_+" and "n_-" are their respective electronic charges. Morris and Ligane (67)

· have experimentally confirmed that their treatment satisfactorily predicts the enhancement of transition times by electrical migration.

2.1.10.3. Cylindrical and Spherical diffusion

It is not always feasible to use planar electrodes, and instead spherical electrodes e.g. liquid metal electrodes, or cylindrical e.g. wire electrodes, have to be used. Under these conditions semi-infinite linear diffusion need not be applicable. The cases of spherical and cylindrical diffusion have been treated by several authors (68-71). For cylindrical diffusion

$$i\tau^{\frac{1}{2}} = \frac{nFC^O\Pi^{\frac{1}{2}}Do^{\frac{1}{2}}}{2} \left(1 + \frac{\Pi^{\frac{1}{2}}D^{\frac{1}{2}}\tau^{\frac{1}{2}}}{4r} \right) \qquad (2.75)$$

and for spherical diffusion

$$i\tau^{\frac{1}{2}} = \frac{nFC^O\Pi^{\frac{1}{2}}D_O^{\frac{1}{2}}}{2} \left(1 + \frac{\Pi^{\frac{1}{2}}D^{\frac{1}{2}}\tau^{\frac{1}{2}}}{2r} \right)$$

The radius of the cylinder or sphere is denoted by "r". When the term "$D^{\frac{1}{2}}\tau^{\frac{1}{2}}/r$" is very small compared to unity equations (2.75) and (2.76) reduced to Sands' equation. The upper limit for the length of transition time will be dependent upon the radius and the diffusion coefficient.

2.1.10.4. Influence of the double layer

During electrolysis the potential of the working electrode varies, and hence the charge of the double layer varies, with the result a fraction of the applied current is used in the charging or discharging of the double layer. An approximate treatment of the influence of the double layer (differential) capacity "C_1" was discussed by Gierst (72).

The quantity of electricity "Q_i" required to charge the double

layer over the potential "ΔE" can be estimated using an average

value for the double layer †capacity $(C_1)_{Av}$.

$$Q_c = (C_1)_{Av} \Delta E \qquad (2.77)$$

If the approximation, that all the applied current "i" is involved

in the electrochemical reaction, is applied, then

$$Q_c = i\tau \qquad (2.78)$$

"Q_e" is the quantity of electricity used in the electrochemical

reaction.

$$\frac{Q_c}{Q_e} = (C_1)_{Av} \frac{\Delta E}{i\tau} \qquad (2.79)$$

Using Sand's equation;

$$\frac{Q_c}{Qe} = (C_1) \frac{Av \ \Delta E \cdot 4i}{n^2 F^2 (C^0)^2 \pi \ D_o} \qquad (2.80)$$

To minimise the influence of the double layer, e.g. Q_c/Q_e

is less than 0.01, the applied current density should be as low

as possible and the concentration as high as possible. It is

the concentration term, which will have the most significant

effect, since it is to the second power.

2.1.10.5. Surface roughness of electrodes.

The influence of the surface roughness of

electrodes has been discussed by several authors (73-77). Diffusion

up to or away from a rough electrode surface is not strictly

linear, and there is no exact theory for non-steady state

diffusion for such an electrode. A first approximation can be

made by representing the roughness of a sinusoidal function,

there would be a contribution from spherical diffusion.
Experimentally surface roughness gives rise to enhanced values
for transition times at low current densities, i.e. ·
when the diffusion layer thickness is small. The surface
roughness factor can be considered qualitatively in terms
of the diffusion layer thickness. When the diffusion layer
thickness is large in comparison with the amplitude of the
roughness, the diffusion area is identical to the projected
electrode area. With decreasing diffusion layer thickness,
the electrode roughness becomes more significant, since
the diffusion area will aproach the actual electrode surface area.

2.1.10.6. Surface oxide films

The formation or reduction of an oxide film may precede,
follow or occur simultaneously with the electrode reaction studied.
The effect of such a process is the same as for adsorption in
section 2.1. and the ARSR, the SRAR or the SAR model may be
applicable.

Bard (76) suggested a correction of the product $"i\tau^{\frac{1}{2}}"$
by allowing for the quantity of electricity involved $"Q"$. It
is virtually equivalent to the adsorption models mentioned
above.

$$i\tau^{\frac{1}{2}} - \frac{Q}{\tau^{\frac{1}{2}}} = \frac{nFC^O\Pi^{\frac{1}{2}}D_O^{\frac{1}{2}}}{2} \qquad (2.81)$$

2.1.10.7. Adsorption of foreign substances

Gierst and Juliard (37) observed that transition times
were markedly reduced by the addition of a strongly adsorbable
substance to the electrolyte. It was accounted for by assuming
that the effective electrode area was reduced by the adsorption.
The study of this process has been extended by several authors
(78-80).

2.1.11. Measurement of the transition time.

The methods for measuring the transition are all very empirical since there is no detailed theoretical description of the potential time curve in the presence of double layer charging. Noonan (81) has tested the different graphical constructions, used to measure the transition time, using his own experimental data. (See figure 2.63). He demonstrated that none of the techniques gave an adequate correction of the double layer charging. It is of interest to note that the double layer charging region at the start of his chronopotentiograms take the form of distinct rump, which could be due to a very large double layer capacity or adsorption of the electroactive species.

Electronic methods have been developed, involving the differentiation of the wave (86,87). These methods prove to be useful in cases where the wave is ill defined.

2.2. Steady-state voltammetry

2.2.1. Charge-transfer overvoltage.

Consider the simple electrode process

$$O + ne \underset{k_{bh}}{\overset{k_{fh}}{\rightleftarrows}} R$$
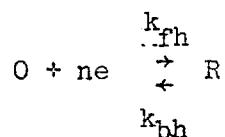
which involves two soluble species, and the forward and reverse formal rate constants at equilibrium are "k_{fh}" and "k_{bh}" respectively. Their forward and reverse current densities are "$\overrightarrow{i}$" and "$\overleftarrow{i}$" respectively. At equilibrium the two currents will be equal, and their value is defined as the ~~apparent~~ exchange current density "i^O". The current "i" following during an electrode reaction, will the net current density

$$i = \overrightarrow{i} - \overleftarrow{i} \qquad (2.82)$$
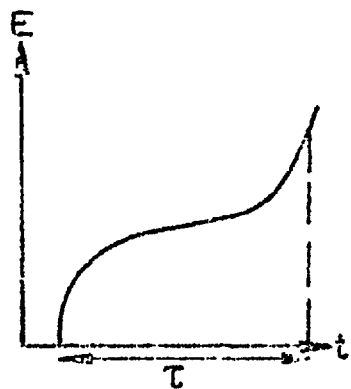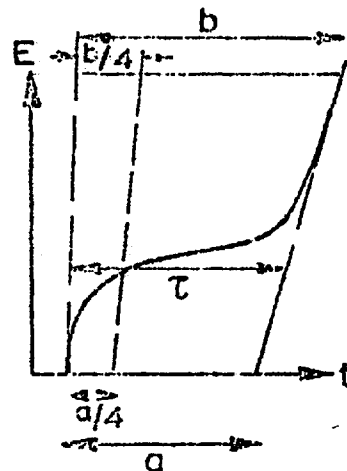
(a) Ref.(32)   (b) Ref.(83)   (c) Ref.(54)   (d) Ref. (77)
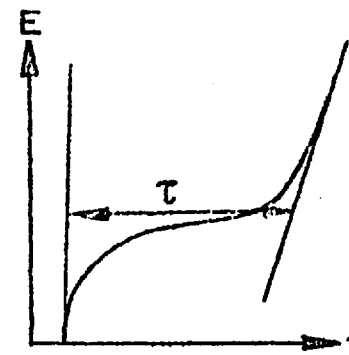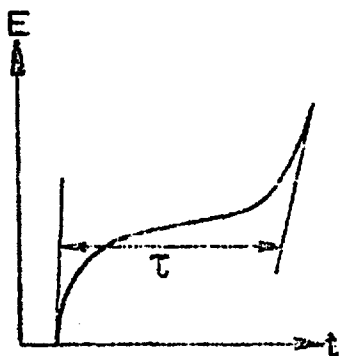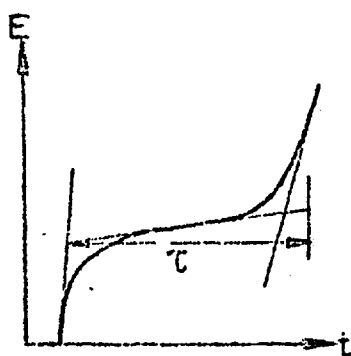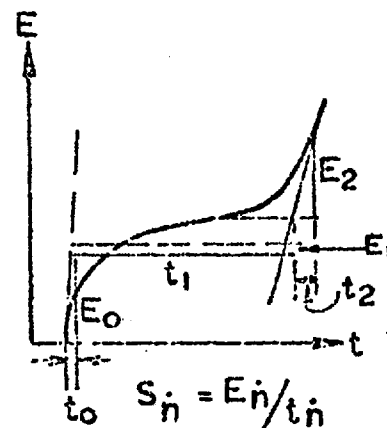
(e) Ref.(81)   (f) Ref.(84)   (g) Ref.(85)   (h) Ref.(81)
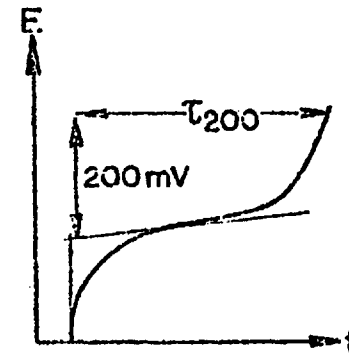
$S_{\dot{n}} = E_{\dot{n}}/t_{\dot{n}}$

$\tau = \tau_{200}$ -double layer correction for 200mV

$$\tau^{1/2} = \frac{1}{S_0} \sum_{j=1}^{n} [S_{j-1} - S_j] . \left[\sum_{k=j}^{n} t_k\right]^{1/2}$$

Fig.2.6 CONSTRUCTIONS FOR THE MEASUREMENT OF TRANSITION TIME "τ" (61)

Thus for a cathodic process the net current density will be

positive and for an anodic process the net current density will

be negative. (IUPAC Stockholm convention (88)). The current

potential relationship for pure charge-transfer was derived by

Erdey-Gruz and Volmer (89) and generally confirmed by Glasstone

and Laidler (64)

$$i = k_{fh}^{o} \cdot C_O \exp\left(\frac{-\alpha nF}{RT} E\right) - K_{bh}^{o} \cdot C_R \exp\left(\frac{(1-\alpha)nF}{RT} E\right) \quad (2.83)$$

At equilibruim the net current is zero hence

$$i^o = k_{fh}^{o} \cdot C_O \cdot \exp\left(\frac{-\alpha nF \ E_o}{RT}\right) \quad (2.84)$$

$$= k_{bh}^{o} \ C_R \ \exp\left(\frac{(1-\alpha)nF \cdot E_o}{RT}\right) \quad (2.846)$$

"E_o" is the equilibrium electrode potential, "α" is the

charge-transfer coefficient, the significance of which is well

reviewed by Bauer (90). The difference between the electrode

potential and its equilibrium potential is defined as the

overvoltage "η".

$$\eta = E - E_o \quad (2.85)$$

Equations (2.83), (2.84) and (2.85) give the following

relationship:

$$i = i_o \cdot \exp\left(\frac{-\alpha nF\eta}{RT}\right) - i_o \exp\left(\frac{(1-\alpha)nF\eta}{RT}\right) \quad (2.86)$$

$$\text{cathodic current} \qquad\qquad \text{Andodic current}$$

When the charge-transfer step is slow, such that it is

the rate controlling step, the overvoltage for the electrode

reaction will be given by equation (2.86). When the current

of the electrode process is large compared with the reverse current

equation (2.86) reduces to the Tafel equation (91).

$$\eta = a + b \ln|i|$$ (2.87)

where

$$a = \frac{RT}{\alpha nF} \ln i^o, \; b = - \frac{RT}{\alpha nF} \quad \text{(cathodic process)} \quad (2.889)$$

$$a = \frac{RT}{(1-\alpha)nF} \ln i^o, \; b = \frac{RT}{(1-\alpha)nF} \quad \text{(anodic process)} \quad (2.886)$$

The exponential terms may be expanded thus

$$\exp(x) = 1 + x + \frac{x^2}{2!} + \frac{x^3}{3!} + \ldots\ldots\ldots$$ (2.89)

When "x" is very small only terms, i.e. (1 + x), need be considered. Using this reasoning, at very low overvoltage equation (2.86) reduces to

$$i = - i^o \frac{nF\eta}{RT}$$ (2.90)

Allen and Hickling (92) another relationship, which is valid regardless of the magnitude of the over voltage. Equation (2.86) is rewritten

$$\frac{i}{1 - \exp(nF\eta/RT)} = i^o \exp\left(\frac{-\alpha nF\eta}{RT}\right)$$ (2.91)

Hence $\ln \dfrac{i}{1 - \exp(nF\eta/RT)} = \ln i^o - \dfrac{\alpha nF\eta}{RT}$ (2.92)

The slope of the plot (2.87) will yield the value for "an" and the intercept at η = 0 will yield the exchange current density "i^o". The slope of the plot of (2.90) will yield the value for "n". In the case of equation (2.92), "α" can be obtained from the slope and the exchange current density from the intercept at η = 0.

2.2.2. Reaction overvoltage.

Reaction overvoltage is a phenomena resulting from the

existence of a slow(rate - determining) chemical step in the

overall electrode reaction. The term was originally introduced

to electrochemistry by Vetter (93-95). By definition, this

chemical step is a reaction, whose rate constant is independent

of the electrode potential. For the reaction overvoltage to

appear separately, the other component steps of the overall

electrode reaction, such as charge transfer and diffusion,

can not be rate determining. The charge-transfer equilibrium is

assumed to be negligibly disturbed, that is the exchange

current density should be very much greater than the current

density flowing.

Consider the reaction

$$n_1 'S_1 ' + n_2 'S_2 ' + \ldots \rightarrow n_1 S_1 + n_2 S_2 + \ldots\ldots \nu S$$
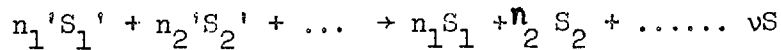
where "S" is the electroactive species, and "ν" is the

stoichiometric number of species "S" in the partial electrode

reaction. When "S" is the oxidised (S_o) or reduced (S_R) component

of the charge transfer reaction, $S_R \underset{\leftarrow}{\rightarrow} S_o + ze$ (redox) or

$S_M + S_R \underset{\leftarrow}{\rightarrow} So + Ze$ (metal/metal ion), "ν" + 1 or -1,

if "n" of the fast partial electrode reaction is equal to the

valence transfer "Z". The electrode potential "E" is given by

$$E = E' + \nu . \frac{RT}{nF} \ln C_{(o)} \qquad (2.93)$$

"E'" is not the standard electrode potential, but also includes

the contributions from the other components. "$C_{(o)}$" is the

concentration of S at the electrode surface. The equilibrium

potential "E_o" is given by

$$E_o = E' + \nu \frac{RT}{nF} \ln \bar{C} \qquad (2.94)$$

" $\bar{C}$ " is the equilibruim concentration of "S" given by the equilibruim

$$Y \overset{\rightarrow}{\leftarrow} Z + pS$$
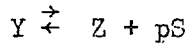
"Y" is equivalent to components "S_i'" "Z" to components S_i and "p" is equal to the order of reaction, in terms of "S", for the reverse reaction. From the definition of overpotential (2.85)., equations (2.93) and (2.94) reduce to

$$\eta = \nu \frac{RT}{nF} \ln \frac{C_{(o)}}{\bar{C}} = \nu \frac{RT}{nF} \ln u_{(o)} \qquad (2.95)$$

where $u = C_{(x)}/\bar{C}$.

At equilibrium the rate of formation "v_o" of "S" is equal to the rate in the reverse direction, i.e.

$$v_o = k\bar{c}^P \qquad (2.96)$$

The constant "k" includes the rate constant for the reverse reaction components "S" and the rates for the other components. Under non equilibruim conditions, the rate of reaction, "v"; will be the difference between the rate of formation of "S" and the rate of reaction in the reverse direction.

$$v = v_o - k \left(C(x)\right)^p \qquad (2.97)$$

Hence

$$v = v_o \left[1 - \left(\frac{C(x)}{\bar{C}}\right)^p \right] = v_o \left[1 - \left(u(x)\right)^p \right] \qquad (2.98)$$

2.2.2.1. Homogeneous, rate-determining reaction

The rate-determining chemical step essentially occurs within a reaction layer, thickness of which is smaller than the thickness of of the adhering diffusion layer. Vetter (94,95) used the extended Fick's second law, to obtain a solution.

$$\frac{\partial C(x,t)}{\partial t} = D.\frac{\partial^2 C(x,t)}{\partial x} + v \qquad (2.99)$$

and

$$\frac{\partial C(x,t)}{\partial t} = 0 \qquad (2.100)$$

under steady state conditions. The other assumption made was that the concentration of all the other components did not vary appreciably. The resulting solution was

$$i = \pm \frac{\bar{n}F}{\nu}\left(\frac{2p}{p+1}.\ v_0\ \overline{CD}\right)^{\frac{1}{2}}\left(1 + \frac{u_{(o)}}{p}\right)^{(p+1)} - \frac{p+1}{p}\ u_{(o)}\right)^{\frac{1}{2}} \qquad (2.101)$$

Introducing the overpotential from equation (2.95)

equation (2.101) becomes.

$$i = \pm i_r \left[1 + \frac{1}{p}\exp\left(\frac{n\ (p+1)\ F.}{\nu RT}\ \eta\right) - \frac{p+1}{p}\exp\left(\frac{nF.\eta}{\nu RT}\right)\right]^{-\frac{1}{2}} \qquad (2.102)$$

where the limiting reaction current density "i"

is defined thus

$$i_r = -\frac{n}{\nu}\ F\left(\frac{2p}{p+1}\ v_0.\ \overline{C.D}\right)^{\frac{1}{2}} \qquad (2.103)$$

The upper (+) sign of equation (2.101) applies to "$u_{(o)}$"
is greater than unity, the lower)-) sign to "$u_{(o)}$" is less than
unity. The sign ($\pm$) of equation (2.102) is chosen, such that

the currentdensity "i" has the same sign as the overvoltage.
At low overpotentials, the exponential terms can be written as
a series up to the squared term, c.f. equation (2.89), hence
equation (2.102) reduces to

$$\eta = |\nu|.\ \frac{RT.}{nF}\left(\frac{2}{p+1}\right)^{\frac{1}{2}}.\frac{i}{|i_r|} \qquad (2.104)$$

At higher overpotentials, when the sign which is opposite to
that of the limiting current, only the first exponential term
in equation (2.102) is significant, thus

$$\eta = -\frac{2\nu}{p+1} \cdot \frac{RT}{nF} \cdot \ln\left|\frac{i_r}{p^{\frac{1}{2}}}\right| + \frac{2\nu}{p+1} \cdot \frac{RT}{nF} \cdot \ln|i| \qquad (2.105)$$

c.f. the Tafel equation (2.87).

2.2.22 Heterogeneous, rate-determining, reaction.

The rate determining chemical step proceeds in an adsorption layer at the electrode surface. The heterogeneous chemical step has been treated by Vetter (95). On the basis of Faraday's law and the definition of the stoichiometric " ν ":

$$i = -\frac{n}{\nu} \cdot F \cdot v \qquad (2.106)$$

At the maximum rate of formation " v_0 " of species "S", " u " will be equal to zero. The limiting reaction current density " i_r " will be given by

$$i_r = -\frac{n}{\nu} \cdot F \cdot v_0 \qquad (2.107)$$

Substituting for " v " and " v_0 " into equation (2.98)

$$u \ (x = (1 - i/i_r)^{1/p} \qquad (2.108)$$

hence by equation (2.95) the relationship for overpotential becomes

$$\eta = \frac{\nu}{p} \cdot \frac{RT}{nF} \cdot \ln(1 - i/i_i) \qquad (2.109A)$$

or

$$1 - i/i_r = \exp\left(\frac{p}{\nu} \cdot \frac{nF}{RT} \cdot \eta\right) \qquad (2.109B)$$

At low overpotentials, where $\exp(x) \approx (1 + x)$, equation (2.109b) can be rewritten:

$$\eta = \left|\frac{\nu}{p}\right| \cdot \frac{RT}{nF} \cdot \frac{i}{|i_r|} \qquad (2.110)$$

When $(-i/i_r)$ is very much greater than unity, equation (2.109a) can be rewritten

$$\eta = -\frac{\nu}{p} \cdot \frac{RT}{nF} \cdot \ln|i_r| + \frac{\nu}{p} \cdot \frac{RT}{nF} \cdot \ln|i| \qquad (2.111)$$

c.f. the Tafel relationship (2.87).

2.2.2.3. Application of a homogeneous chemical step to the $E_\tau/4$ values

If the diffusion equations (2.8) and (2.9) are applicable, the point, at quarter of the transition time, is equivalent on all chronopotentiometric waves for the same species at the same concentration. This means that the concentrations of the oxidised and reduced species at the electrode surface will be the same for each wave at the quarter – time point. If a slow intervening chemcial step is present, this will no longer be the case, and the potential at quarter–time will include a reaction overpotential "η" component.

$$E_{\tau/4} = E' + \eta. \qquad\qquad (2.112)$$

The potential "E'" includes the potential contributions of all components at the electrode surface, apart from the species undergoing electron transfer. If "E'" remains essentially constant at different current densities, then changes in "$E_{\tau/4}$" can be considered as changes in overpotential. "E'" will only remain constant if the concentration of the other species at the electrode surface remain constant, i.e. the current density is sufficiently low. The invariance of the product $i\tau^{\frac{1}{2}}$ with current density will mean that the diffusion equations are obeyed when the components of the reaction are considered as one component, that is when no distinction is made between the species diffusing up to the electrode. Under these conditions "$E_{\tau/4}$" (equation (2.112)) may be substituted into equation (2.105), thus

$$E_{\tau/4} = \text{constant} + \frac{2\nu}{p+1} \cdot \frac{RT}{nF} \ln |i| \qquad\qquad (2.113)$$

C H A P T E R   3

S T R U C T U R A L   A S P E C T S

3.1. INTRODUCTION

Fused ionic salts are probably the most concentrated electrolytes obtainable by ordinary techniques, and for this reason are outside the range of applicability of the Debye-Huckel approach (96). The high electrostatic binding, which would be expected in fused ionic salts, gives rise to their high melting points and boiling points and also their fairly large surface tensions at elevated temperatures (17).

X-ray and neutron diffraction studies (97) show that on melting, the short range order of the salt is retained. The most frequent nearest neighbour interionic distance i.e. cation to anion, is shorter than that found in the solid state at the melting point. On the other hand the most frequent next-nearest neighbour approach, i.e. cation to cation and anion to anion, is nearly always larger than that found in the solid. The average co-ordination number for nearest neighbours is significantly lower than that for the typical solid structure. It can be considered therefore, that on fusion of ionic salts, a large number of vacancies, e.g. Schottky defects, are introduced into the crystal lattice. This would result in the reduction of the co-ordination number and a loss in long range order.

3.2. Quasi-lattice model

Ionic fused salts have an essentially disordered nature, in common with gases, when macroscopic distances are considered. However, it is clear that there is strong local ordering which

can be considered in terms of a lattice. Frenkel (98) and

Bresler (99) described the structure of an ionic fused salt in

terms of the quasi-lattice model. The model considers an

assembly of ions, in a vacuum, occupying positions in two

interlocking sub-lattices. One sub-lattice is available to

cations, and the other is available to anions.

In a thermodynamically ideal fused salt mixture, i.e.

where the activity "a" of ascomponent is equal to the ionic or

mole fraction "N" of that component, the different cations and

anions will be randomly distributed on their respective sub-lattices.

An ideal fused salt mixture containing ions all of the same

charge type will fit the Temkin model (100). The activity of a

component in such a mixture will be given by the product of the

ionic fractions of the cation and anion of that component.

Forland (101,102) extended the model in order to account for

mixtures of salts of different charge types, where there will

be a large number of vacancies in one of the sub-lattices. The

ionic fraction terms were replaced by equivalent ionic fraction

"N'" terms e.g. consider the mixture A_2X-BX. The cation equivalent

ionic fractions are

$$N_A' = \frac{n_A}{n_A + 2n_B} \qquad N_B' = \frac{2n_B}{n_A + 2A_B} \qquad (3.1)$$

where "n" denotes the number of particles. The Temkin model

assumes that the enthalpy of mixing is zero, but the enthalpy

of mixing for reciprocal salt mixtures was found not to be zero.

Flood et alia (103,104) further extended the model, still

assuming the random distribution of cations and anions on

their respective sub-lattices, but including a non-zero value for the enthalpy of mixing. For a system of AD and BC

$$\alpha_{AD} = N_A N_D \quad \exp \left(\frac{N_B N_C Z \Delta H}{RT} \right) \qquad (3.2)$$

where "Z" is the average co-ordination number of the quasi-lattice, and "ZΔH" is the approximate enthalpy change for the reaction

AD + BC → AC + BD.

3.3. Non-random mixing

Large deviations from ideality are found in many fused salt mixtures indicating that mixing is not random. These deviations from ideality may be explained in terms of ion association. A controvery exists as to the real significance of the ion association, whether it is purely coulombic, and hence a ~~kinetic~~ structural entity of the quasi lattice or whether it involves some form of orbital overlap, i.e. complex ion formation.

Non-random mixing can be considered in terms of complex ion formation if the life-time of the associated species is long compared to the life-time of the quasilattice "t". The life-time "t" of the quasi-lattice can be estimated from the relationship between Brownian movement and diffusion (105)

$$t = \bar{\Delta}^2 / 2D, \qquad (3.3)$$

where "$\bar{\Delta}$" is the average value for the displacement of an ion, an "D" is the diffusion coefficient. For ionic liquids "$\bar{\Delta}$" is about 10^{-8} cm and "D" is about 10^{-5} cm^2, sec^{-1}. These values suggest that the life-time of a quasi-lattice is of the

order of 10^{-11} second.

3.3.1. Evidence for complex-ion formation

The evidence for complex-ion formation is based on spectroscopic, ionophoretic, surface tension, cryoscopic, electrical conductivity and potenticometric data. None of this evidence proves to be conclusive.

The observation time for infra-red, Raman and atomic adsorption spectroscopy is the order of 10^{-12} second (105). That for electron spin resonance is of the same order as the relaxation time of the liquid. Hence these spectroscopic techniques, though giving a insight to the stereochemistry of the species, will not differentiate between complex-ions and quasi-lattice entities.

Fordyce and Baum (106-10 8), from infra-red spectroscopic measurements on tantalum (V) and niobuim (V) in fluoride melts, have shown the existence of $(Ta F_7)^{2-}$, $(TaF_6)^-$, $(NbF_7)^{2-}$, $(TaOF_6)^{3-}$ and $(NbOF_6)^{3-}$ entities. Infra red spectroscopy has shown the existence of ~~kinetic~~ structural entities (not necessarily complex-ions) in the $CuCl_2$-KCl system (105), and the ZrF_4 - alkali fluoride systems (109). Harrington and Sundheim (110) have reported on electronic absorption spectra for the first row transition metal ions infused salts. Gruen (111) reviews the electronic absorption spectra obtained for transition metal ions in fused salts. In both references they give positive identification for ~~kinetic~~ structural entities (not complex ions).

Nuclear magnetic resonance spectroscopy has an observation time of about 10^{-8} second (105). This time should be long

enough to allow the averaging out of quasi-lattice effects,
but still allow the observation of complex-ion formation.
The results from N.M.R. studies can be taken as direct evidence
for complex-ion formation in fused salts. Rowland and Bromberg
(112) and Hafner and Nachtrieb (113,114) have carried out N.M.R.
studies on thallium ions in fused salts. Their data provided
evidence for complex-ion formation between thallium ions and
halfide ions.

Ionophoretic measurements on binary and reciprocal salt
melts containing, transition metal ions, lanthanide ions or
actinide ions have produced evidence of cations migrating
to the anode (115-120). Since the extent of the solvent
movement in the electric field was unknown, no correction was
made for possible solvent flow. For this reason the data
cannot be considered as conclusive evidence for the formation of
anionic complexes. However, the fact that many other metal ions
in the same solvent moved towards the cathode (115-120) does
suggest that solvent flow is not significant.

Mellors and Senderoff (121, 122) observed that the
relationship of surface tension with concentration of zirconium
(IV) in alkali metal fluorides exhibited discontinuities.
In the lithium-potassium fluoride melt, they corresponded to
the stoichiometries for $(Zr\ F_7)^{3-}$ and $(ZrF_5)^-$. In the
lithium-sodium fluoride, the discontinuity corresponded to
$(ZrF_7)^{3-}$. Even though these results are not strictly diagnostic,
quasi-lattice effects would not be expected to give such
discontinuities, but rather some smooth relationship.

Van Artsdalen (123) and Van Artsdalen and Yaffe (124) have explained their cyoscopic and electrical conductivity measurements in terms of complex ion formation, but none of it proves to be diagnostic.

3.3.2. Ion association models in reciprocal salt melts.

The existence of complex entities can be most clearly visualized in a dilute reciprocal salt solution. Take for example a dilute solution of A^+ and C^- ions in a solvent of B^+ and D^- ions. The association

$$A^+ + C^- \rightleftharpoons AC,$$
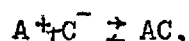
is represented two dimensionally in figure 3.1. The circled D^- anion is adjacent to one A^+ cation and (Z-1) B^+ cations. "Z" is the co-ordination number. The circled C anion is adjacent to "Z" B^+ cations. The interchange of these two anions results in an energy change of

$$\Delta e = \Delta E/N \qquad (3.3)$$

where "N" is Avogadros number. Letting the pair interaction energy of A^+-D^- be "e_1", B^+-C^- be "e_2", $A^{\pm} C^-$ be "e_3" and B^+-D^- be "e_4";

$$\Delta e = e_4 + e_3 - e_2 - e_1 = \Delta E/N \qquad (3.4)$$

A statistical treatment, based on the quasi-lattice model, has been used by Blander and Braunstein (125), and Blander (126,127) to describe the formation of associated entities. In the three approximate treatments applied, only nearest neighbour interactions were considered.

Fig. 3.1

TWO DIMENSIONAL REPRESENTATION OF
THE REACTION.

$$A^+ + C^- \rightleftharpoons AC$$
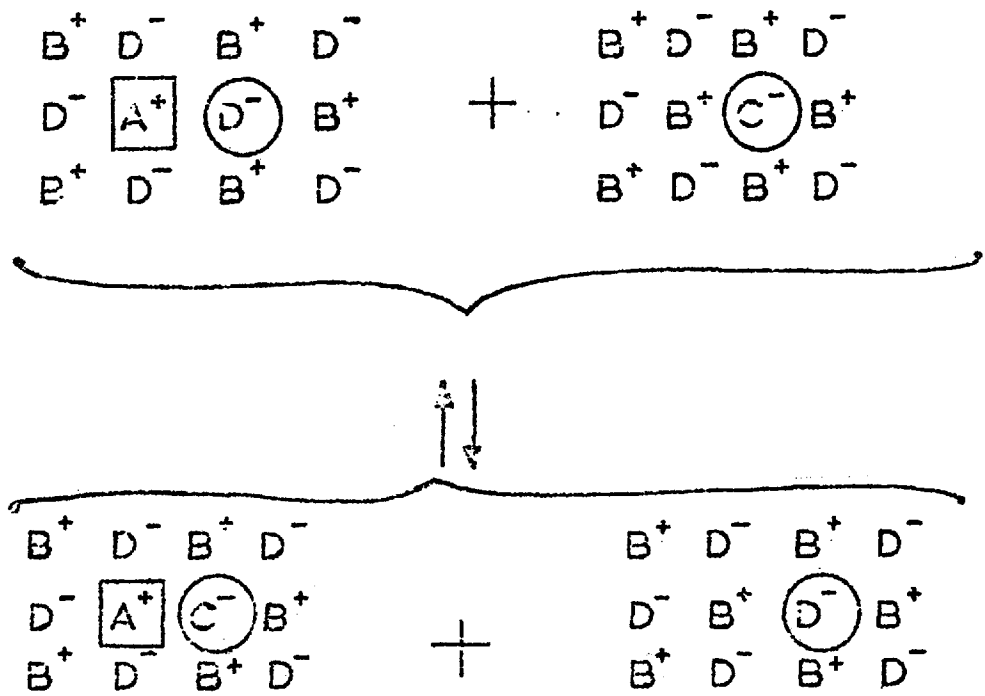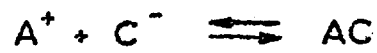
The symmetric approximation (125) takes into account the processes:

$$A_m C_n^{(m-n)+} + A^+ \rightleftarrows A_{(m+1)} C_n^{(m+1-n)+}$$

and $A_m C_n^{(m-n)+} + C^- \rightleftarrows A_m C_{(n+1)}^{(m-n-1)+}$ . .
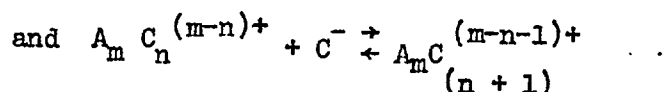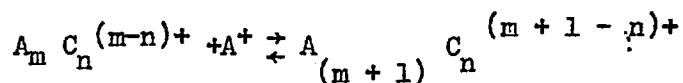
where $(m+1)$ or $(n+1)$ are less than or equal to "n".
The energy change for both processes is assumed to be the same, and independent of the value for "m" or "n" i.e. the bond energies are additive and there is non-interference of pair bonds.

The asymmetric approximation (126) only considers the interactions of one A^+ cation with up to as many as "Z" C^- anions.

$$AC_{(n-1)}^{(2-n)+} + C^- \rightleftarrows AC_n^{(1-n)+} \qquad \Delta e_n$$
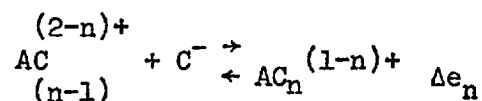
where "n" is limited between unity and "Z", and Δe_n is independent of the value for "n". The anion portion of the lattice is divided into two regions, (a) and (b). Region (a) includes all anion positions adjacent to an A^+ cation and $(Z-1)$ B^- anions. Region (b) includes all other anion positions.

Blander and Braunstein (125) found close agreement between theoretical calculations based on the two above approximations and experimental data. They attributed the difference found to a saturation effect on the pair bonds, that is

$$\Delta e, \neq \Delta e_2 \neq \Delta e_n \neq \ldots \neq \Delta e_E \qquad (3.4)$$

A generalised treatment, based on the asymmetric approximation, was derived by Blander (127) to take into account this interference between pair interactions.

3.3.3. Ion association models in binary salt melts

It is not so easy to visualize complex entities in a binary salt system, i.e. only one anion present, as it is in a reciprocal system.

In a binary salt system the solute cations are surrounded by anions in groupings, which are distinctly separated from each other. These groupings can be divided into two types, firstly those involving one solute cation, i.e. mononuclear, and secondly those involving more than one solute cation i.e. multinuclear.

The mononuclear groupings will be distinguished by a co-ordination number and stereochemistry, which can be different to that of the quasi-lattice of the surrounding solvent. Such groupings should be apparent from spectroscopic data (105-111,128) and other thermodynamic measurements, for example, surface tension measurements indicated the presence of $(ZrF_7)^{3-}$ and $(ZrF_5)^-$ in fluoride melts (121,123).

Up to now there have been no reports of definitive or diagnostic evidence for multinuclear species, involving cations, in fused salts. However, in light of the fact that transition metals have a great tendency to form such species in the solid state (to be discussed in section 3.4) it is probable that such species could exist in fused salts. Such multinuclear groupings may be visualized in terms of solute cations occupying adjacent positions in the cation sublattice,

with the anions e.g. chloride ions, acting as ligand bridges.
Such a model could be fitted to the analysis of Martin and Winter
(129). In this analysis the bridging ligands modify an
intramolecular metal-metal interaction in one (or both) of two
ways. Firstly, by multicentre bonding involving direct overlap
of the orbitals of the bridging ligands and the two metal ions.
Secondly, by localised super-exchange, which involves no direct
overlap of the orbitals of the two cations; however, the
magnetic properties from such an exchange would be the same
as for the direct overlap of the metal ion orbitals.

3.3.4. Solvent cation effects

It has been shown that the stability of "complex" species
is strongly affected by varying solvent cations (130-138).
The solvent cation effect can be considered in terms of its
charge density. The charge density of an ion is equal to its
charge "Z" divided by the cube of its radius "r" that is
"Z/r^3". The greater the charge density the greater the solvent
cation-anion interaction, that is the shorter the interionic
distance. Take for example the alkali metal chlorides where
the cationic radii are:

Li^+, 0.78Å; Na, $^+0.98\text{Å}$; K^+, 1.33Å; Rb^+, 1.48Å, and Cs $^+1.69\text{Å}$ (139)

The interionic distances have been collated by Bauer and Porter
(140) $LiCl$, 2.02Å; $NaCl$, 2.36Å; KCl, 2.67Å; $RbCl$, 2.79Å, and
$CsCl$, 2.91Å.

An increase in the interionic distance, between solvent cations
and solvent, should lead to an increase in the solute cation -
anion interaction, since there is a decrease in the competition
for the anion. Hence it can be said that for solvent cations
of the same charge, the stability of ionic associations of the

stability of ionic associations of the solute will increase with increasing solvent cation size.

3.4. Refractory metal ion-halide ion interactions

It has already been mentioned that refractory metals show a great tendency to form multinuclear groupings in the solid state. In view of the similarities in structure between the solid and liquid states for ionic systems (see section 3.1) it is probable that such multinuclear groupings can be found in ionic melts containing refractory metal ions. For this reason it is necessary to consider the interactions existing in the solid state as well as the liquid state.

3.4.1. Interactions with fluoride ions.

Wilmshurst (109) observed that infra red spectra of the molten systems $LiF-KF-ZrF_4$ and $NaF-KF-ZrF_4$ were consistent with the assumption of a "complex" zirconium species. This is in support of the observations of Mellors and Senderoff (121, 122) who from surface tension measurements, postulated the existence of $(ZrF_7)^{3-}$ and $(ZrF_6)^-$ in the $LiF-KF-ZrF_4$ system, and $(ZrF_7)^{3-}$ species in the $LiF-NaF-ZrF_4$ system.

Fordyce and Baum (106-108) carried out infra red spectroscopic measurements on tantalum (V) and niobuim (V) in molten fluorides. They have shown, that in the case of tantalum (V), the $(TaF_7)^{2-}$ is the predominant species in KF, LiF-KF and LiF-NaF melts. In the LiF-NaF melt, the $(TaF_6)^-$ species were also shown to be present. Similarly for niobium (V) they have demonstrated that $(NbF_7)^{2-}$ is the predominant species in molten LiF-KF. They observed that $(TaOF_6)^{3-}$ and $(NbOF_6)^{3-}$ were the predominant species in melts containing hydrolysed

entities of tantalum (V) and niobium (V).

The pentafluorides of niobium and tantalum have been shown by X-ray single-crystal techniques, to have a trimeric structure in the solid (141). The metal atoms are at the corners of a square and linked by linear bridging fluoride atoms. These two compounds are iso-structural with molybdenum pentafluoride (142). These fluorides also appear to have a polymeric form when molten (143). Lower valent fluorides have been reported for niobium (144). Out of these lower fluorides, $NbF_{2.5}$ appears to be built up of $Nb_6 F_{12}$ groups involving fluoride bridges.

3.4.2. Interactions with chloride ions.

It is apparent that the chemistry of the refractory metal chlorides, in particular the lower chlorides, is dominated by the tendency to form apparent metal-metal bonds (c.f. Martin and Winter (129)) and polymeric structures.

Dahl et alia (145), on the basis of X-ray powder diffraction patterns, propose a structure for Zr Cl_3 and Hf Cl_3, which consists of infinite chains of MCl_6 tetrahedra joined at opposite faces by chloride bridges. A number of chlorides approximating to trichlorides, i.e. Nb $Cl_{2.33}$, Nb $Cl_{2.67-3.13}$ Ta $Cl_{2.5}$ and $TaCl_{2.9 - 3.1}$ have been reported (144). They all appear to be built up from metal clusters involving bridging chloride ions. McCarley and Torp (146) found that the halides or niobium (IV) and tantalum (IV) are diamagnetic even though both have a d' electronic configuration. These results evidence the existence of some form of metal-metal bond. McCarley and Brown (147) obtained similar results for tungsten (IV) halides, but since tungsten (IV) is a d^2 ion, their results do not necessarily require

the postulation of metal-metal bonds. The dichlorides of molybdenum (148) and tungsten (149) are not simple compounds, but contain metal atom clusters which involve bridging chloride ions.

3.4.3. Concluding comments.

The question of whether ionic association in fused salts exists in the form of quasi-lattice entities or of discrete complex ions, in many studies is purely a semantic one. However, such a question when considered in terms of structural influences on an electrode reaction, is important, since the break down of a complex species could in fact constitute a slow step in an electrode process.

C H A P T E R 4
E L E C T R O C H E M I C A L A S P E C T S

4.1. Introduction

It has already been mentioned briefly in the general introduction that one of the requirements in the design of an electrodeposition process is the understanding of the kinetics and the mechanisms involved in the overall electrode process. Up to this date the study of the electro-reduction of refractory metals has been concerned with the determination of the stoichiometry of the electrode process, the diffusion coefficients of the ions and whether the process is slow or fast. There appears to have been very little work carried out to ascertain the nature of any slow steps in the electrode process.

4.2. The electrochemistry of refractory metal ions

4.2.1. Titanium

Baboian et alia (150) used potentiometric and polarographic techniques to study titanium (II) and titanium (III) ions in lithium chloride-potassium chloride eutectic at $450^{\circ}C$ and $550^{\circ}C$.

They demonstrated that the reduction

$$Ti^{3+} + e \rightarrow Ti^{2+}$$
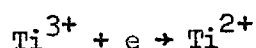
was reversible, but the reduction of titanium (II) to the metal gave ill defined and not reproducible polorographic waves. They also determined the equilibrium constant, "K", for the equilibrium

$$Ti^{\circ}_{(solid)} + 2Ti^{3+} \rightleftarrows 3Ti^{2+}$$
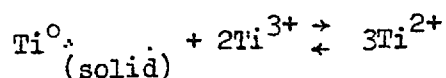
The value for "K" was in the range of 10^3 to 10^4, which means the equilibrium is far to the right. This supports the findings of Rossokhin et alia (151) from their potentiometric investigation into the equilibrium in fused potassium chloride, where

$$\log_{10} K = -6.956 + 8165/T^\circ K$$

The same authors have extended their study to the fused chloride solvents of magnesium, calcium and barium (152). They found that the equilibrium constant decreased with increasing ionic radius of the solvent cation. In other words the increase in the titanium-chloride pair bond energy stabilises titanium (III) ions to a greater degree than titanium (II). The addition of fluoride ions was also found to stabilize the titanium (III) ion (153,154).

Menzies et alia (155) examined the electro-deposition of titanium from lithium chloride-potassium chloride and sodium chloride - potassium chloride eutectics. They observed, that the change over from large dendritic deposits to fine powder deposits, occurred over a small change in conditions e.g. concentration of titanium or current density. In polarographic experiments they observed that a limiting current for titanium was only present under conditions which gave dendritic deposits. They suggested that the powder deposits were produced from the reduction of titanium ions by electrodeposited alkali metal, i.e. secondary deposition.

Anodic dissolution of titanium from pure titanium anodes in chloride electrolytes gives divalent titanium (150, 154) If titanium carbide anodes (156) or titanium dioxide - carbon anodes (157) are used, trivalent titanium goes into solution according to the following equations

$$TiC_{(s)} \rightarrow Ti^{3+} + C_{(s)} + 3e$$

$$TiO_{2(s)} + C_{(s)} \rightarrow Ti^{3+} + O_{2(g)} + 3e$$
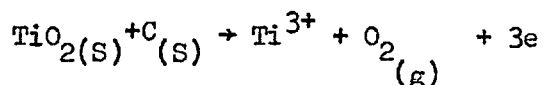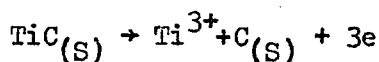
Mellors and Senderoff (135) were not able to obtain primary electrodeposit; i.e. dendritic or coherent, for titanium from pure fluoride melts. Delimarskii and Chernov (158) carried out an oscillopolarographic study of potassium hexafluorotitanate and potassium hexa fluorotitanate - sodium chloride melts. The former system exhibited three polarographic waves. The first waves were reproducible where as the final wave was not. Similar results were obtained for the latter system. The second wave however tended to disappear with increasing titanium concentration. The data was very inconclusive, but it did provide some evidence for a slow chemical step.

4.2.2. Zirconium and Hafnium

Baboian et alia (159) have carried out a potentiometric and polarographic investigation of solutions of zirconium and hafnium ions in molten lithium chloride-potassium chloride eutectic at 450°C to 550°C. Anodic dissolution of zirconium at 450°C yielded zirconium (IV) but at 550°C it chiefly yielded zirconium (II). At 500°C anodic dissolution yielded an average valency between 2 and 4. This led to the postulation of the equilibrium:-

$$Zr^{4+} + Zr^{o}_{(s)} \rightleftharpoons 2Zr^{2+}$$
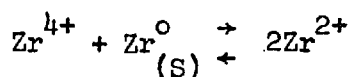
Anodic dissolution of hafnium yielded only hafnium (IV) over the
whole range of temperature. At $450^{\circ}C$ one polarographic reduction
wave was observed for the zirconium solution. The potential -
current relationship fitted a reversible four electron step. At
higher temperatures zirconium solutions gave two polarographic
reduction waves which were not very reproducible. The second
wave was much longer than the first wave. The first wave was
ascribed to the reduction of zirconium (IV), and the second wave
to the reduction of zirconium (II) the metal. Hafnium
gave only a single polarographic reduction wave, which fitted a
reversible four electron step. The equilibrium between zirconium
(IV) and zirconium (II) put forward by Baboian et alia (159) has
been confirmed in molten equimolar sodium chloride-potassium
chloride (150), molten potassium chloride (161) and in molten
caesium chloride (164).

Sakura (163) used chronopotentiometry to determine the diffusion
coefficients of zirconium (II) and zirconium (IV) in equimolar
sodium chloride-potassium chloride at temperatures from $700^{\circ}c$
to $900^{\circ}c$. Zirconium was added to the melt by anodic dissolution
and then was converted to the divalent state by reduction with
hydrogen gas or converted to the quadrivalent state by
oxidation with chlorine gas. The reduction of zirconium (II)
exhibited a single chronopotentiometric wave, and the product
"$i\tau^{\frac{1}{2}}$" was independent of applied current density. The diffusion
coefficient for zirconium (II) ion was equal to (5.4 ± 0.8)
$10^{-3} \exp (-11,000 \pm 300)/RT \ cm^2 \ sec^{-1}$. Plots of E versus
$\log (1-t^{\frac{1}{2}}/ \tau^{\frac{1}{2}})$ i.e. equation (2.69) gave slopes for an
irreversible process with equivalent $\alpha n = 1$, i.e. $\alpha = 0.5$.
Intercepts gave values for the rate constant, "k°_{fh}" ,
varying between 10^{-14} and $10^{-13} \ cm^2 \ sec^{-1}$. The reduction of
zirconium (IV) proceeded in two steps, which were exhibited

by two chronopotentiometric waves presumably

$$Zr^{4+} \underset{2e}{\rightleftharpoons} Zr^{2+} \underset{2e}{\rightleftharpoons} Zr^{0}$$
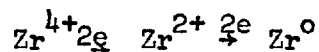
The first wave did not obey Sand's equation. The plot
of "$I\tau^{\frac{1}{2}}$" versus "$1/i$" gave a negative intercept "a" on the
"$\tau^{\frac{1}{2}}$" axis i.e. diagnostic of a preceding chemical reaction.
The value of "$\tau^{\frac{1}{2}}$" was empirically corrected by adding the
value of the intercept "a" to "$\tau^{\frac{1}{2}}_{i}$". Using the corrected value
for "$\tau^{\frac{1}{2}}$" the diffusion coefficient for the zirconium (IV) ion
became $(6.2 \pm 1.0) \, 10^{-3} \exp (-9800 \pm 500) \, /RT) \, cm^2 \, sec^{-1}$. The
first wave was not examined in terms of the preceding chemical
reaction, which is suggested by the negative intercept
mentioned above.

Mellors and Senderoff (164) have investigated the
electro-reduction of zirconium (IV) added as K_2ZrF_6 dissolved
in lithium fluoride-sodium fluoride-potassium fluoride eutectic
(Flinak). They obtained chronopotentiograms over the temperature
range of $500^{\circ}C$ to $750^{\circ}C$. The reduction went in one step, i.e.
only a single wave on the chronopotentiogram. At low current
densities, 50-100mA, cm^{-2}, very poorly defined waves were
obtained, but at higher current densities greater than 300 m A, cm^{-2}m

the waves were very much better defined. The $E_{\tau/4}$
values were in the order of 200 mV more cathodic at the higher
current densities. The process was not a simple diffusion
controlled process, since plots of $i\tau^{\frac{1}{2}}$ versus concentration of
zirconium (IV) were non-linear. They do not give any
information concerning the form taken by the non-linearity.
The potential time relationship for the waves at $500^{\circ}C$ and $650^{\circ}C$

fit that for a reversible system with a variable activity
product c.f. equation (2.60). The values for "n" were 3.0 at
500°c and between 2.6 and 10 at 650°C. At 750°C it was
impossible to fit the wave to any relationship. From the variable
$E_{\tau/4}$ values and the potential-time relationships one can infer
that the electrode process is irreversible. Since only one
wave is present, the process probably goes by a single four-electron
transfer. It has been reported by Manning and Mamantov (165)
that polarographic measurements on the same system at 500°C
indicated that zirconium (IV) was reduced in a single reversible
four-electron step.

4.2.3. Niobium

An investigation has been made into the electrochemistry
of niobium ions in molten lithium chloride potassium-chloride
eutectic and molten equimolar sodium chloride-potassium chloride
(166). Anodic dissolution at low current densities yielded
sparingly soluble niobium (III) in both melts. Higher current densities
yielded blue solutions of niobium (IV). Electrolysis of
niobium (III) in lithium chloride-potassium chloride gave
cathode deposits of niobium which were attached to the electrode,
indicating single primary reduction;

$$Nb^{3+} + 3e \rightarrow Nb^{o}$$
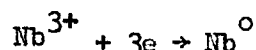
On the other hand when equimolar sodium chloride-potassium
chloride was used as the solvent, electrolysis produced
powdery deposits of niobium at an appreciable distance from
the cathode. Such deposits suggest a secondary reduction
process:

$4Na^+ + 4e \rightarrow 4Na$

$Nb(IV) + 4Na \rightarrow Nb^\circ$
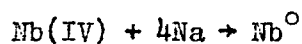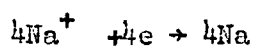
Pimenov and Baimakov (167) had used the chronopotentiometric technique to determine the diffusion coefficient of niobium (III) in molten lithium chloride-potassium chloride eutectic at $400^\circ c$ to $610^\circ C$ and the diffusion coefficients of niobium (II) and niobium (III) in equimolar sodium chloride potassium chloride melts at $700^\circ C$ to $840^\circ C$.

$$D_{Nb(III)} = 2.18.10^{-3} \exp (-7,000/RT) \ cm^{-2} \ sec^{-1}, \ (LiCl\text{-}KCl)$$

$$D_{Nb}(III) = 4.36.10^{-3} \exp (-10,500/RT) cm^2 \ sec^{-1} \ (NaCl\text{-}KCl)$$

$$D_{Nb}(II) = 9.2.10^{-3} \exp (-9,150/RT) \ cm^2, \ sec^{-1} \ (LiCl\text{-}KCl)$$

Their published chronopotentiograms show a single reduction wave for all the systems, but without further information it is difficult to draw any conclusions about the electrode process. It appears, however, that their work is in conflict with that of Dartnell et alia (166) who suggested that the reduction of niobium ions in the sodium chloride-potassium chloride melt occurred via a secondary reduction process, which could not give a reduction wave. Saeki et alia (158) studied the electrolytic reduction of anodically dissolved niobium (in solution as $Nb \ Cl_{2.67}$ (159))in alkali metal chloride melts, including the lithium chloride-potassium chloride eutectic melt. Their chronopotentiometric data suggested that the reduction occurred via a diffusion controlled, reversible two electron step followed by an irreversible step. These results are again inconsistent with those of other workers.

Senderoff and Mellors (170) carried out a chronopotentiometric investigation into the electro-reduction of niobium (V), added as K_2NbF_7 dissolved in molten Flinak. The investigation was carried out over the temperature range of $650^\circ C$ to $800^\circ C$. At $650^\circ C$ the chronopotentiograms consisted of two waves. The ratio of the two transition times "τ_2/τ_1" was 0.55 ± 0.11, and since the valence of the niobium was five, i.e. $n_1 + n_2 = 5$, the number of electrons involved in the first step should be four, and the number of electrons in the second stage should be unity (when $n_1 = 4$ and $n_2 = 1$, $\tau_2/\tau_1 = 0.56$, c.f. section 2.1.3). At $750^\circ C$ and low current densities the first wave was resolved into two waves, a new wave appearing at less cathodic potentials. This wave disappeared when the mean valence of the niobium in solution was reduced to 4.2. The first wave in the reduced solution fitted a reversible process with a variable activity product (equation (2.60))where the estimated number of electrons involved was 3.04 ± 0.49. The overall electrode process may be summarised as follows:-

$$Nb^{5+} \xrightarrow{e} Nb^{4+} \xrightarrow{3e} Nb^{+} \xrightarrow{e} Nb^{\circ}$$
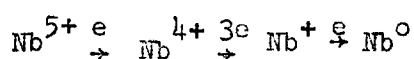
Both the first waves i.e. for reduction of niobium (V) and niobium (IV) obeyed Sand's equation. The diffusion coefficients for niobium (V) and niobium (IV) calculated from Sand's equation, at $750^\circ C$ were 2.03×10^{-5} cm^2 sec^{-1} and 5×10^{-5} cm^2 sec^{-1} respectively. Reversal of the applied current density during the first wave gave a reverse transition time, which was greater than one third of the forward electrolysis time c.f. section 2.1.8. This can be interpreted in terms of adsorption or partial solubility of the niobium (I) species. The final step i.e. the reduction of niobium (I) gave a value for $i\tau^{\frac{1}{2}}/C$

which decreased with increasing concentration, and hence it cannot

be totally diffusion controlled. Contrary to the ideas of

Senderoff and Mellors (170) this inconstancy cannot be considered

a criterion of irreversibility i.e. a slow stage charge transfer

or otherwise, for the final step.

4.2.4. Tantalum

Suzuki (171) has shown, from potentiometric measurements at

$500^{\circ}C$ and $600^{\circ}C$ that tantalum anodically dissolves in molten

lithium-chloride-potassium chloride eutectic as quadrivalent ions.

In a further study, Suzuki (172) examined the electro-reduction

and electro-oxidation of tantalum (IV) in the molten lithium

chloride-potassium chloride eutectic at $500^{\circ}C, 600^{\circ}C$ and $675^{\circ}C$

using chronopotentiometry. The chronopotentiograms showed that

the reduction of tantalum (IV) occurred in two steps. The

potential-time relationship for the first step supported a

reversible two electron transfer process, the product from which

was soluble in the melt. The value of $i_\tau^{\frac{1}{2}}/c$ for the first step

was constant showing the first step to be diffusion controlled.

The diffusion coefficients, calculated from Sand's equation

for tantalum (IV) at $500^{\circ}C, 600^{\circ}C$ and $675^{\circ}C$ were 9.0×10^{-5}.

2.5×10^{-4} and 4.6×10^{-4} cm^2 sec^{-1} respectively. Values for

$i\tau^{\frac{1}{2}}/C$ for the second step were not constant, but decreased with

increasing concentration. The inconstancy is given to be an

indication of irreversibility, slow charge transfer, but this

is not correct, since the length of the transition time is

not dependant on charge transfer rates. Anodic chronopotentiograms

showed one oxidation step for the tantalum (IV) ion. The

potential-time relationship supported a reversible one-electron

transfer process in which the product was soluble in the melt.

The value of $i\tau^{\frac{1}{2}}/C$ was constant, supporting a diffusion controlled process. The diffusion coefficients for tantalum (IV) at $500°C$, $600°C$ and $675°C$ were estimated to be 4.4×10^{-5} 1.4×10^{-4} and 2.3×10^{-4} cm^2, sec^{-1} respectively. The diffusion coefficients from both the reduction and oxidation measurements are larger than would be expected for such a highly charged cation, c.f. $D_{Nb(III)} = 2.84.10^{-5}$ cm^2 sec^{-1} at $600°C$ in the same melt (167).

Senderoff et alia (173) used chronopotentiometry to investigate the electro-reduction of tantalum (V) dissolved in molten Flinak. The tantalum (V) was added as $K_2 Ta F_7$ and the experiments were carried out in the temperature range of $640°C$ to $860°C$. The chronopotentiograms exhibited two reduction steps at all temperatures. The value of $i\tau^{\frac{1}{2}}/C$ for the first wave was constant indicating that it is purely diffusion controlled. The potential-time relationship for the first step fitted a reversible process with a soluble product. The average value for · number of electrons involved was three. The ratio of the two transition times τ_2/τ_1 was 1.8 ± 0.7. Total number of electrons involved in the reduction, $(n_1 + n_2)$ must equal five, and the only "n" values, which satisfy this and give

$\tau_2/\tau_1 = 1.8$ are $n_1 = 2$ and $n_2 = 5$ (c.f. section 2.3).

The reduction may therefore be written:

$$Ta^{5+} \xrightarrow{3e} Ta^{2+} \xrightarrow{2e} Ta^{0}$$
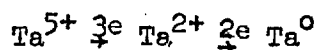
The diffusion coefficient for tantalum (V) at $750°C$ calculated from Sand's equation, is 1.5×10^{-5} cm^2 sec^{-1}.

Reversal of the applied current density during the first wave gave a

reverse transition time which was 80-90% of the forward electrolysis time, c.f. section 2.1.8. This can be interpreted in terms of strong adsorption or insolubility of the tantalum (II) species. The second step, i.e. the reduction of tantalum (II) did not give a constant value for $i\tau^{\frac{1}{2}}/C$, but it decreased with increasing concentration.

4.2.5. Molybdenum

It has been demonstrated potentiometrically that anodic dissolution of molybdenum in fused lithium chloride-potassium chloride eutectic (137,171,174) fused lithium chloride (175) and fused equimolar sodium chloride-potassium chloride (174) results in solutions of molybdenum (III)

The kinetics of the electrode, Mo-Mo^{3+}, have been examined by Selis (174) in various molten alkali metal chloride and bromide melts using a galvanostatic technique. The values obtained for exchange current densities were those for reversible charge transfer process, for example with a molybdenum (III) concentration of 10^{-2}M in the solvents lithium chloride - potassium chloride eutectic at 667°C and equimolar sodium chloride-potassium chloride at 769°C the exchange current densities were 0.50 and 0.34 A, cm^{-2} respectively.

The electro-reduction of molybdenum (III) ions in molten lithium chloride-potassium chloride eutectic at 600°C, 700°C and 800°C has been investigated by Senderoff and Mellors (176) using chronopotentiometry. They observed that the solutions of molybdenum (III) were unstable and concluded that a disproportionation reaction, which yielded a volatile higher chloride of molybdenum, was occurring, e.g.

$$5 \text{ Mo Cl}_{3(1)} \rightleftharpoons 2\text{Mo}_{(s)} + 3\text{Mo Cl}_{5(g)}$$
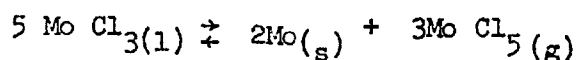
The instability of these solutions increased with decreasing

molybdenum (III) concentration and increasing temperature. As

a result of such behaviour they postulated the possible existence

of polynuclear molybdenum (III) ions which have a slow rate of

decomposition e.g.

$$\text{Mo}_n^{3n+} \underset{\leftarrow}{\overset{\text{slow}}{\rightarrow}} n \text{ Mo}_o^{3+}$$
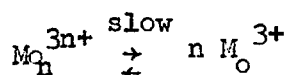
A single chronopotentiometric wave was observed for the reduction

of molybdenum (III). The value of $i\tau^{\frac{1}{2}}/C$ for the reduction wave

was not invariant, and at temperatures $500^{\circ}C$ and $700^{\circ}C$ increased

with increasing concentration. The values for $i\tau^{\frac{1}{2}}/C$ though

were considered constant enough to justify the application of

Sand's equation in order to calculate diffusion coefficients.

The diffusion coefficients for molybdenum (III) at $600^{\circ}C$ $700^{\circ}C$

and $800^{\circ}C$ were 1.43×10^{-5}, 2.89×10^{-5} and 3.87×10^{-5} $\text{cm}^2 \text{ sec}^{-1}$

respectively. The potential-time relationships for waves at

$600^{\circ}C$ did not fit any of the models described in section 2.1.9.

At $700^{\circ}C$ the potential-time relationship fitted an irreversible

charge-transfer process or a reversible process with an insoluble

product i.e. equations (2.61) or (2.69) with a value for "αn"

or "n" of 2.66 ± 0.28. The potential difference between the

reduction and oxidation processes was obtained by current

reversal during the reduction wave. The potential difference

at $500^{\circ}C$ was three times and at $700^{\circ}C$ two times that expected

from the ohmic resistance of the melt. At $800^{\circ}C$ the potential

difference was very close to that expected from ohmic resistance.

It was suggested therefore that the reduction process approach

closely to reversibility at $800^{\circ}C$.

Senderoff and Mellors (177) have investigated the reduction
of molybdenum (III) in molten Flinak at 600°C, 700°C and 800°C
using chronopotentiometry. Their chronopotentiograms consisted
of single reduction wave, which was too irreproducible for any
conclusions to be drawn from them. Only at 800°C did the
potential-time relationship approach a fit to any model described
in section 2.1.9. At 800°C the relationship approached the
irreversible charge transfer model with a value for
"an" of 2.0 $\pm$ 0.2 i.e. α = 0.67.

The potential difference between the reduction and
oxidation process obtained by current reversal were always
very much greater than that expected from the ohmic
resistance of the melt.

4.2.6. Tungsten and Platinum

Senderoff and Mellors (177) have examined the electro-
reduction of tungsten ions in molten Flinak at 600°C, using
chronopotentiometry. The mean valence of the tungsten ions was
4.48 but during the experiment the valence would rapidly
increase to 5 or above. At mean value of 4.48 one irreproducible
chronopotentiometric wave was observed. The potential difference
between cathodic and anodic processes, from current reversal,
was 0.65 volt, which is very large compared with the potential
difference 0.05 volt, expected from the ohmic resistance of
the melt. This indicates a very high degree of irreversibility.
At mean valencies of 5 or greater, a second chronopotentiometric
wave appeared, which probably corresponded to the reduction
of a higher valence state.

Schmidt et alia (178) have investigated the reduction of platinum (II) molten lithium chloride potassium chloride eutectic at $450^{\circ}C$ using polarography. The polarographic waves were described by the Kolthoff Lingane equation, i.e. assuming unit metal activity, for a reversible two electron transfer. The diffusion coefficient for platinum (II) was calculated to be 1.49×10^{-5} cm^2, sec^{-1}. Inman et alia (186) have examined the complex-ion formation of platinum (II) with a bromide ions in lithium chloride potassium chloride eutectic. The potentiometric data indicated that the platinum (II) - bromocomplexes were stronger than the platinum (II) - chloro complexes.

4.2.7. Discussion

The polorographic studies of the electro-reduction of titanium ions (150, 155) zirconium ions and hafnium ions (159) in chloride electrolytes, and zirconium ions in fluoride electrolytes (165) all support fast processes. However, it was observed by Menzies et alia (155) that at lower concentrations of titanium there was no limiting current for the titanium reduction. This suggests the presence of slow step, resulting in secondary deposition (see section 4.3.2.) which is supported by the fact that these same conditions gave rise to powder electro-deposits of titanium metal.

Chronopotentiometric studies of the reduction of zirconium ions in chloride electrolytes (163) and fluoride electrolyte (164) support a slow step in the reduction process. These apparent anomalies can in some degree be accounted for by the different current density ranges employed by the two techniques. The current densities in polarography are low, that is below the limiting current for the process, where as the current densities used in chronopotentiometry are high, that is above the limiting current for the process. Thus the chronopotentiometric

technique will tend to place greater emphasis on any slow step than a polarographic technique.

The anomalies between the studies of electro-reduction of niobium ions in chloride electrolytes, carried out by Darnwell et alia (166), Pimenov and Baimakov (167) and Saeki et alia (168) cannot be easily accounted for. This is mainly as a result of the lack of information in their works. It could possibly be attributed to impurities present in the electrolytes e.g. oxides.

It has been shown that the molybdenum-molybdenum (III) couple is electro-chemically reversible in chloride melts (174). The electro-reduction of molybdenum (III) to the metal has been shown by chronopotentiometry (176) to be slow, but the potential time relationships at lower temperatures do not fit an irreversible charge-transfer model. These facts tend to support a rate controlling step, which involves a chemical reaction i.e. dissociation of a complex species. The absence of adsorption suggests such a reaction would be homogeneous.

~~The electro-reduction of niobium (V) (170) and tantalum (V) (173) in fluoride electrolytes have to be shown to occur via three steps and two steps respectively. In the former the first two steps suggest such a reaction would be homogeneous.~~

The electro-reduction of niobium (V) (170) and tantalum (V) (173) in fluoride electrolytes have been shown to occur via three steps and two steps respectively. In the former the first two steps were fast, and in the latter the first step was fast. It was proposed that the final steps in both processes

were slow on the criterion that $i\tau^{\frac{1}{2}}/C$ decreased with increasing

concentration. This is not a criterion of irreversibility,

but indicates that the process is not totally diffusion controlled.

The only evidence for the above final steps being slow is that,

even though the preceding steps are fast, coherent and not

dendritic electro-densities of the metals are obtained from this

electrolyte (see section 1.3).

Zirconium (IV) (165) molybdenum (III) and tungsten (IV)

(177) ions in pure fluoride electrolyte, have been shown to be

reduced to the metal in a single slow step. The chronopotentiometric

potential-time relationships did not support an irreversible

charge-transfer process. The inconstancy of $i\tau^{\frac{1}{2}}/C$ indicated

the process was not totally diffusion controlled.

There is a considerable amount of evidence that the presence

of a slow step, in the electro-reduction of refractory metal

ions in chloride and fluoride electrolytes is the rule rather

than the exception. However, there is very little evidence

to support an irreversible charge-transfer process as the slow

step, in fact there is considerable evidence to the contrary.

On this evidence it is suggested that the break down of

multi-nuclear complex species could play an important role in

the mechanism of the slow step. Evidence for the existence

of such complex species in the solid state has been discussed

in chapter 3.

The evidence for adsorption of niobium (I) (170) and tantalum

(II) (173) and the decrease in $i\tau^{\frac{1}{2}}/C$ with increasing concentration

in the final step for all the processes in the fluoride electrolyte

suggest such a slow chemical step in fluorides could be heterogeneous

in nature.

4.3. Electrodeposition

4.3.1. Simple electrodeposition model

4.3.1. Simple electrodeposition model.

The dependence of the nature of electro-deposits on the kinetics of the overall electro-reduction process has already been discussed briefly in section 1.3. It was shown that the diffusion overvoltage at a substrate electrode sphere would be less than at a planar electrode substrate, for the same current density, if the radius of the sphere was less than the diffusion layer thickness. It will also mean that for a given diffusion over voltage, the current density will be greater at such a sphere than at a planar electrode. Consider a fast overall electrode reaction, i.e. diffusion controlled. At the start of metal deposition, the metal will build up at certain growth sites and as the deposition continues metal atoms will build up on these sites. These aggregates of metal atoms will be equivalent to very small substrate electrode spheres with radii less than the diffusion layer thickness. The current density, i.e. the rate of deposition, will be greater at these metal aggregates than at surrounding electrode substrate, and hence there will be a tendency for dendrites to grow out into the electrolyte.

If the electro reduction process is not fast, i.e. the overpotential for the process is not a result of diffusion, equation (1.1) will not be applicable. Under these conditions, where the overpotential for diffusion is small compared to the total over potential, one would expect a multilayer coherent deposit, since the rate is not strictly determined by the geometry.

There are situations where the overpotentials are so large
that the potentials required to deposit the metal are more
cathodic than those required to reduce the solvent cation. Such
a situation would arise, if the electro-reduction process was
very irreversible or if the applied current density was very large
and hence giving a very large diffusion overpotential. The
reduced solvent cations, which will be thermodynamically unstable,
will then reduce the solute cations around the electrode. The
resulting metal deposits will be powdery in form and not
necessarily attached to the electrode. This type of deposition
is generally described as secondary deposition. Take for example
the reduction of a solute cation M^{n+} in an alkali metal halide
electrolyte AX, where secondary deposition occurs, then

$$nA^{+} + ne \rightarrow nA^{o}$$
$$nA^{o} + M^{n+} \rightarrow nA^{+} + M^{o}$$
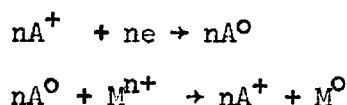
The picture drawn of metal deposition has been very much
simplified in order to illustrate the effect of the electrode
kinetics on metal deposition. A very thorough treatment of the
mechanism of electrodeposition of metals has been provided by
Bockris and Damjanovic (174).

4.3.2. Electrodeposition of refractory metals from molten fluorides

Mellors and Senderoff (135) have attempted to relate the
polarising power of the solvent cations, c.f. section 3.3.4.Z/r^3
ratios, to the nature of the electrode deposits. The polarising
power of the solvent cations should reflect in the stability
of the solute complexes, and hence should be related to the
reversibility of the overall electroreduction process.

In order to quantify the concept of the polarising power of the solvent cations they define the molar dissociation coefficient, "M", for the solvent

$$M = \sum_i n_i \, Zi/r_i^3$$

where n_i is ionic fraction of solvent cation "i", "r" is the ionic radius and "Z" is the valency. According to the concepts discussed in section 3.3.4. an increase in the value of "M" will result in a decrease in the stability of any solute cation complex species. The parameter used to judge the solute complex stability was $M.Z/r^3$, where "Z" and "r" apply to the solute cation.

It was found that it was possible to obtain coherent deposits for tantalum, niobium and zirconium solutes in molten flinak. It was found though that the deposition of zirconium was difficult and deposition of titanium was impossible. The values of the parameter MZ/r^3 for titanium (II) and zirconium (IV) in molten Flinak were 16.4 and 19.3 respectively. These results indicate that, if the parameter is greater than 19.3 coherent deposits should be obtainable. Hence the minimum value of "M" required to give coherent deposits from titanium (II) would be 2.90. The use of the solvent (0.36 NaF: 0.54 LiF 0.10KF), which has an "M" value of 2.96 produced titanium plates of limited thickness.

The applicability of the concept of the molar dissociation coefficient is useful in the way it emphasises the important part played the solvent cations in electrode processes. It cannot though be considered as diagnostic evidence of chemical kinetic effects in the overall electrode

process, since the solvent cation effect on the electrode

potential could be equally important.

C H A P T E R 5

E X P E R I M E N T A L

5.1. Apparatus

5.1.1. Furnace and Controls

A conventional wire wound furnace was used. The furnace
tube was made of a vitreous silica (Thermal Syndicate Ltd.)
with an internal diameter 100 m.m.,wall thickness 6.00 m.m.
and length 18 ins. Since the tube was made of silica the upper
operating temperature was limited to $1000^{\circ}C$. The tube was
stagger wound logarithmically with 16 s.w.g. Kanthal Al wire,
and the wire was held in place with alumina cement. The
resistance of the furnace was 19 ohms, which limited the maximum
power to about 3 K.watts. The furnace tube was insulated with
a layer of "Triton" ceramic fibre and finally M.I.28 bricks
(Morgan Crucible Ltd.), such that the insulation was 18 in
cube around the tube. The tube and insulation was contained
in a "Syndanyo" box with a welded mild steel frame. The furnace
and box were counterbalanced with lead weights so that it
could move easily up and down within an outer welded mild
steel frame. (Similar to the principle of sash cord windows).
The cell was clamped at the top of the outer frame by a
water-cooled brass collar. The whole arrangement facilitated
the slow heating and cooling of the cell, by raising or
lowering the furnace from around the cell. An earth shield
of Nimonic 75 alloy lined the inside of the furnace tube
to minimize electrical noise.

The furnace temperature was controlled by a Eurotherm
P.I.D.15 controller, which is solid state, proportional,

integral, differential controller. The proportional band range
was variable, but the integral and differential terms were
fixed. The controlling thermocouple, which was platinum-platinum,
13% rhodium, was sheathed in alumina, and situated six inches
from the bottom inside the furnace tube. The constant temperature
zone (hot zone) started four inches from the top of the furnace
tube and was eight inches in length. The temperature of the
constant temperature zone could be controlled with in $\pm 1^{\circ}C$.

5.1.2. <u>Dry box assembly</u>.

The basic glass fibre glove box, with perspex windows,
but without posting ports, was made by Marine and Industrial
Plastics Ltd. A horizontal side posting port 7.5 inches in
diameter and 24 inches in length, and a vertical bottom posting
port 5.5. inches in diameter and 22.5 inches in length were
added to the basic box. The ports were made of brass and the
ends were sealed by aluminium covers fitted with O-rings. The
ports were capable of holding a vacuum of 10^{-2} torr. The
bottom port facilitated passing the cell in and out of the glass
box without having to lay it horizontally. The side port was
used for passing other articles in and out of the box. The
atmosphere in the ports was evacuated via one inch diameter
copper tubing. Articles to be passed into the box were placed
in the posting port, which was then sealed. The atmosphere
in port was then evacuated down to a reasonable vacuum,
10^{-1}-10^{-2} torr, and then filled with argon dried over molecular
sieve. This procedure was repeated three times, and then the
inner cover was removed and the articles taken into the
box. The atmosphere inside the box was dry argon at slightly
greater than atmospheric pressure. The atmosphere inside the
box was continually circulated through a molecular sieve
drying train by a Dymax Mk II diaphragm pump. The pressure

inside the glove box was controlled by two electromagnetically operated valves. (Magnetic Valve Co. Ltd.) via a modified diaphragm pressure switch (Londex Ltd.) The pressure switch was modified by incorporating two micro-switches, which were operated by the diaphragm. One switch controlled the argon inlet magnetic valve, opening the valve if the pressure in the box dropped below 0.1 ins water, gauge, and switching off when the pressure reached 0.8 ins water, gauge. The other switch controlled the outlet magnetic valve, opening the valve if the pressure went above 1.3 ins water, gauge and closing it when the pressure reached 0.8 ins water gauge. The argon gas was dried over molecular sieve before passing into the box.

The box containing a Kern single pan top loading balance which could weigh up to 150 g plus a tare up to 40 g. The balance was capable of weighing to $\pm$ 0.2 m.g. As a precautionary measure all the chemicals were stored in closed bottles or desiccators.

A schematic diagram of the glove box assembly is shown in figure 5.1.

5.1.3. Vacuum and gas system

An integrated vacuum system, which supplied the dry box, the vacuum pre-electrolysis cell and the electrolytic cell, was used. The main vacuum lines were one inch diameter glass tubing to allow high pumping speeds. The vacuum pump was a two stage rotary pump with a pumping speed of 82 litres, min^{-1} and an ultimate vacuum of 5×10^{-4} torr (Edwards ED75 pump). Volatile compounds were removed from the vacuum system by a liquid nitrogen cooled trap. The vacuum was

measured by Edwards GSC1 Pirani head and Edwards 8-1 Pirani
gauge. An Edwards type CF3 vacuum dial gauge, 0-760 torr, was
used to measure higher pressures, e.g. when bringing the cell
or glove box ports back to atmospheric pressure.

The argon gas system to the vacuum pre-electrolysis
cell and the electrolytic cell were integrated. High purity
argon (British Oxygen Co.) was dried over magnesium perchlorate
and thenpassed over calcium granules at $650^{\circ}C$ to remove residual
nitrogen and oxygen.

5.1.4. Electronic Equipment

The circuit for the constant current pulse generator used
through out the chronopotentiometric study is shown in figure
5.2. The current step output was supplied by single side
stable, mercury wetted relay (RL1), Elliots EBSC 65015,
triggered from a 30 volt D.C. supply. The constant current
pulse could be reversed or switched off a fixed time after
the start off the pulse by the adjustment of the resistance R_2
and the capacitance C. The current reversal was effected by
the mercury wetted relay, RL2, (Elliots EBSC65015). The
forward and reverse current pulses were supplied by two 50 volt
D.C. stabilized power supplies, through a variable resistor
(R_1) to the micro electrode (W) and the counter electrode (C).
Resistance, R_1, was selected from 44 resistors ranging from 1.0
K.ohms to 2.2. Meg. ohms. The height of the constant current
pulse was determined by measuring the potential difference
across a 100 ohm standard resistor, built in series with the
pulse circuit. The oscilloscope time base was triggered by
the same voltage that triggered relay, RL1. The working
and counter electrodes could be shorted closing by switch (X).
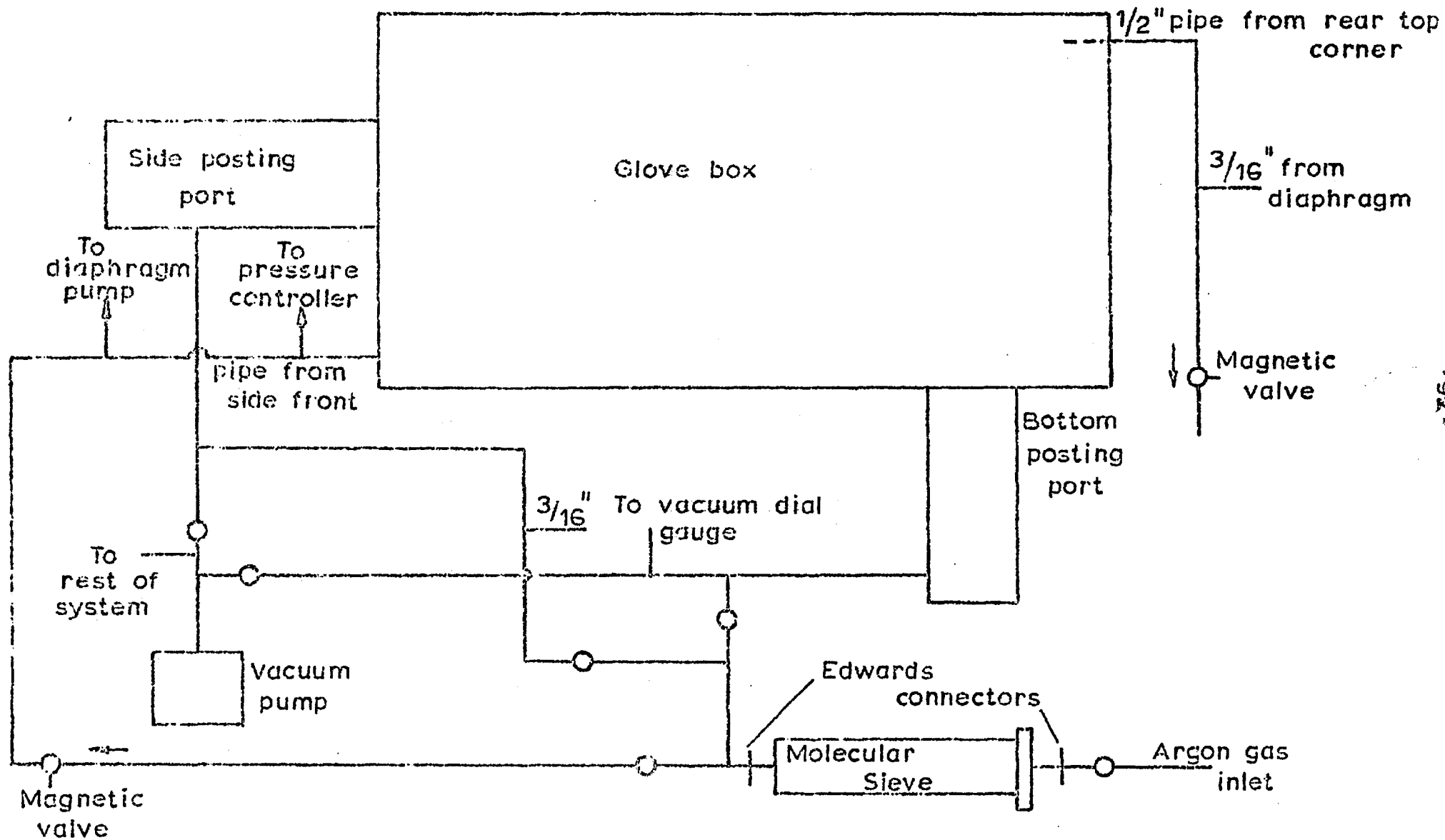
Fig.5.1 SCHEMATIC DIAGRAM OF GLOVE BOX ASSEMBLY

Fig. 5.2   CHRONOPOTENTIOMETRIC   CURRENT   PULSE   UNIT

Fig.5.3

CONSTANT CURRENT POWER SUPPLY

Transistor NPNS
2S012   40W   1Amp >> 20v max.gain >10

ZL10   10v 5% 1·5w Zener diode.

ZL6·8   6·8v 5% 1·5w   "   "   .

Fig. 5.4

CONSTANT VOLTAGE POWER SUPPLY

Transistor 2S012   NPNS 4w, 1 amp, >>20v, gain > 10.

Transistor 2N2929S   200mW 100mA 18V gain > 30

ZL 8·2   8·2v 5% 1·5w Zener diode

The circuit diagram for the constant current power supply used for anodic dissolution is given in figure 5.3. The power supply was able to give a constant current of up 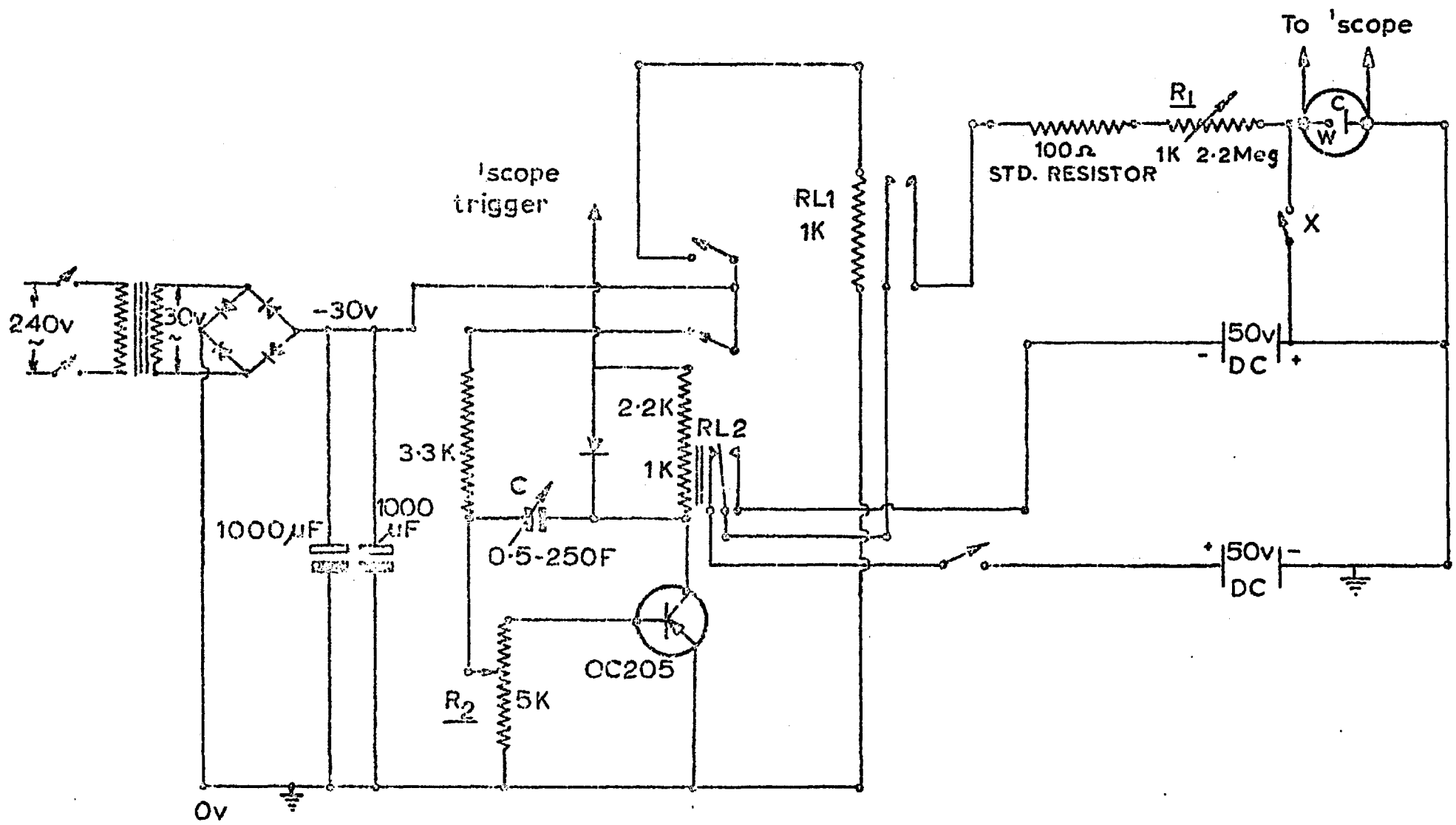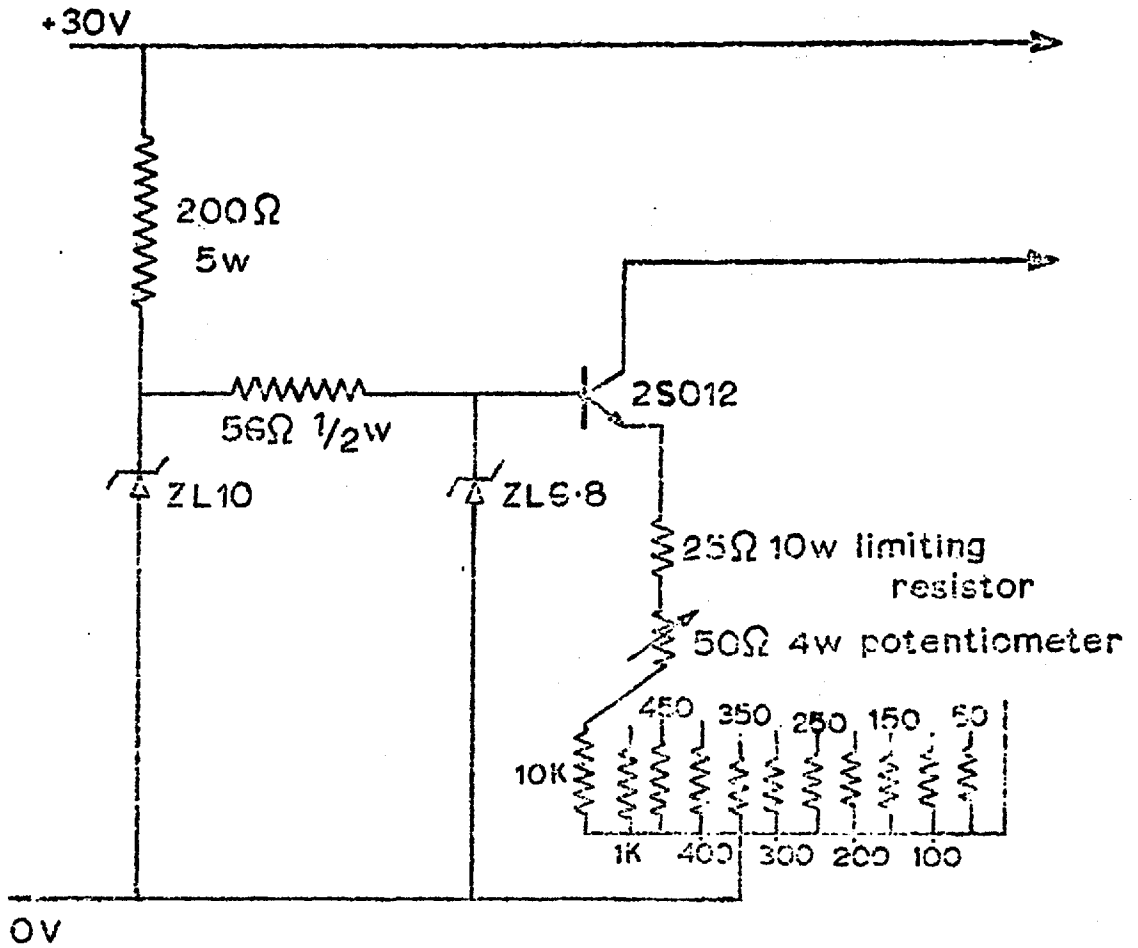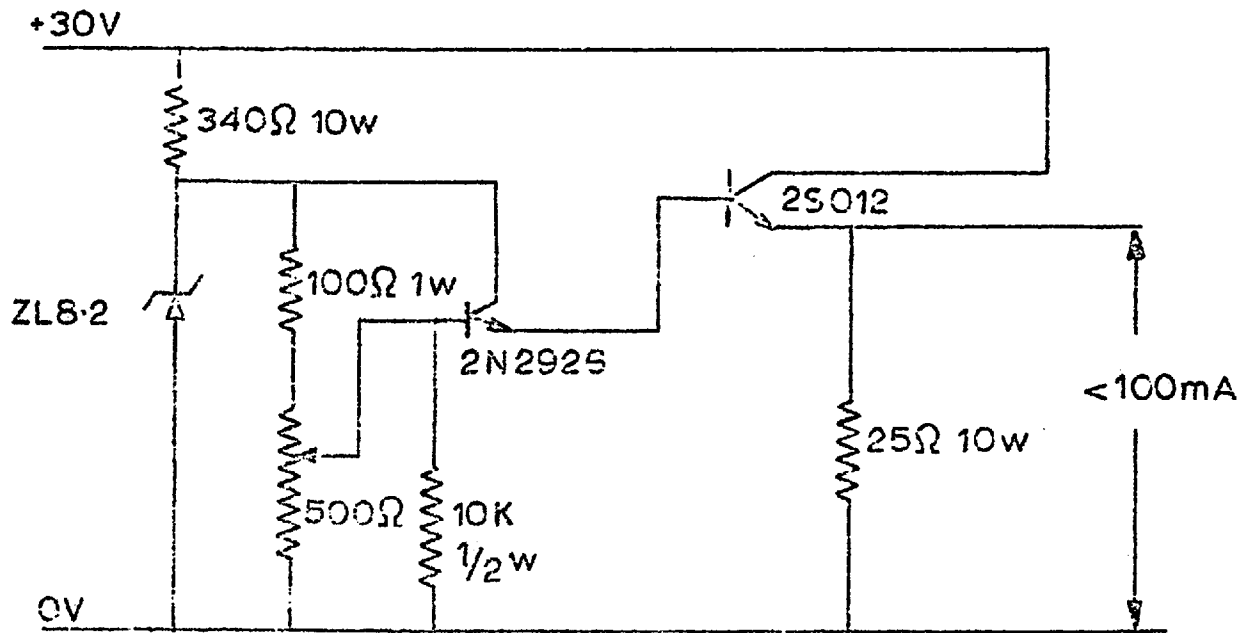to 250 m A. Its maximum operating voltage was 27 volts. The current flowing was determined by measuring the potential difference across a 10 ohm standard resistor.

The constant voltage power supply used in the vacuum pre-electrolysis of melts, would supply up to 3 volts. The maximum current capable of being drawn from the unit was 100 mA. A circuit diagram for the unit is shown in figure 5.4.

A Tektronic 564 oscilloscope, with a 2B67 time base unit and a 3A8 operational amplifier unit. This oscilloscope is capable of storing traces on the screen for at least an hour. The 3A8 unit consists of two operational amplifiers. One of the amplifiers was used as a unity gain amplifier, with a very high impedence input and a low impedance output. Signals from the electrodes were fed into the unity gain amplifier, and the output from the amplifier was fed into the oscilloscope. The high impedence input was used to ensure that the current drawn from the electrode system was insignificant. The other operational amplifier was used to differentiate signals from the electrode system.

A solatron digital voltmeter type LM 1420.2 was used to measure all potentials

5.1.5. Electrolytic Cell

The cell is shown diagrammatically in figure 5.5. It consisted af outer envelope (A), of external diameter 3 ins

and length 14 ins. capped by a water cooled brass head (B).
The pot (C) containing the electrolyte rested on a bed of small
ceramic beads (D) at the bottom of the envelope.

The materials used for the outer envelope varied according
to the experiment. For low temperature studies, that is below
$570^{\circ}C$, Pyrex glass was used. In high temperatures studies in
chloride electrolytes outer envelopes of transparent silica
were used. It was found that silica could not be used with molten
fluorides at high temperatures, because it was disastrously
attacked by the fluoride vapour. It was found necessary to use
outer envelopes fabricated from "Mullite" (Thermal Syndicate
Ltd). These envelopes were also attacked by the fluoride vapour,
but not to such a serious extent. They were also considerably
cheaper than silica, and could therefore be discarded after a
few experiments. The cell head fitted over the top of the
outer envelope, and a vacuum and gas tight seal was achieved
by means of a Wilson O-ring seal (E). Seven holes (F), 7 mm
in diameter, were drilled through the cell head. The tops
of the holes were chamfered at 45° in order to accommodate
O-ring seals (G). The electrodes etc. were located through
these holes. The O-rings were compressed around the electrode
and against the cell head by an upper plate (H), and thereby
achieving a gas and vacuum tight seal. By slightly slackening
off the screws holding the upper plate down on to the O-ring,
one was able to easily raise and lower the electrodes. The
centre hole in the cell head was used to accommodate the gas
outlet and solute addition tube (I) which was fitted with a B 10
socket. When all the seals are tight the cell was able to
maintain a vacuum of better than 5×10^{-3}torr.

A diagram of the cell head is given in figure 5.6.

5.1.6. Thermocouples, etc.

The thermocouples used to measure the melt temperature were platinum-platinum, 13% rhodium. For the low temperature ($570^{\circ}C$) work Pyrex sheaths were used. Silica sheaths were used in the high temperature studies in molten chlorides. It was necessary to use alumina sheaths for the fluoride studies. The same materials were used for the gas bubblerswhich were also used to apply the vacuum, figure 5.7(a).

Pyrex pots were used to contain the low temperature melts ($570^{\circ}C$). The high temperature chloride melts were contained in silica or vitreous carbon (Vitreous Carbon Ltd.) pots. Vitreous carbon pots were also used to contain the pure fluoride melts.

5.2. Materials

5.2.1. Lithium chloride-potassium chloride

The lithium chloride-potassium chloride (58.8 mole% LiCl + 41.2% KCl) eutectic mixture was used. The lithium chloride used was Hopkin and Williams G.P.R. grade and the potassium chloride was Hopkin and Williams A.R. grade. The purification of this melt is very necessary since there are three major sources of impurity. Lithium chloride is very hygroscopic and attempts to remove the water lead to the hydrolysis of the salt. Lithium chloride in particular contains heavy metal ions and carbon. The different purification processes have been discussed by Wrench (180). The method used in this study involved the vacuum pre-electrolysis of the molten eutectic using a carbon anode and a stainless steel cathode, followed
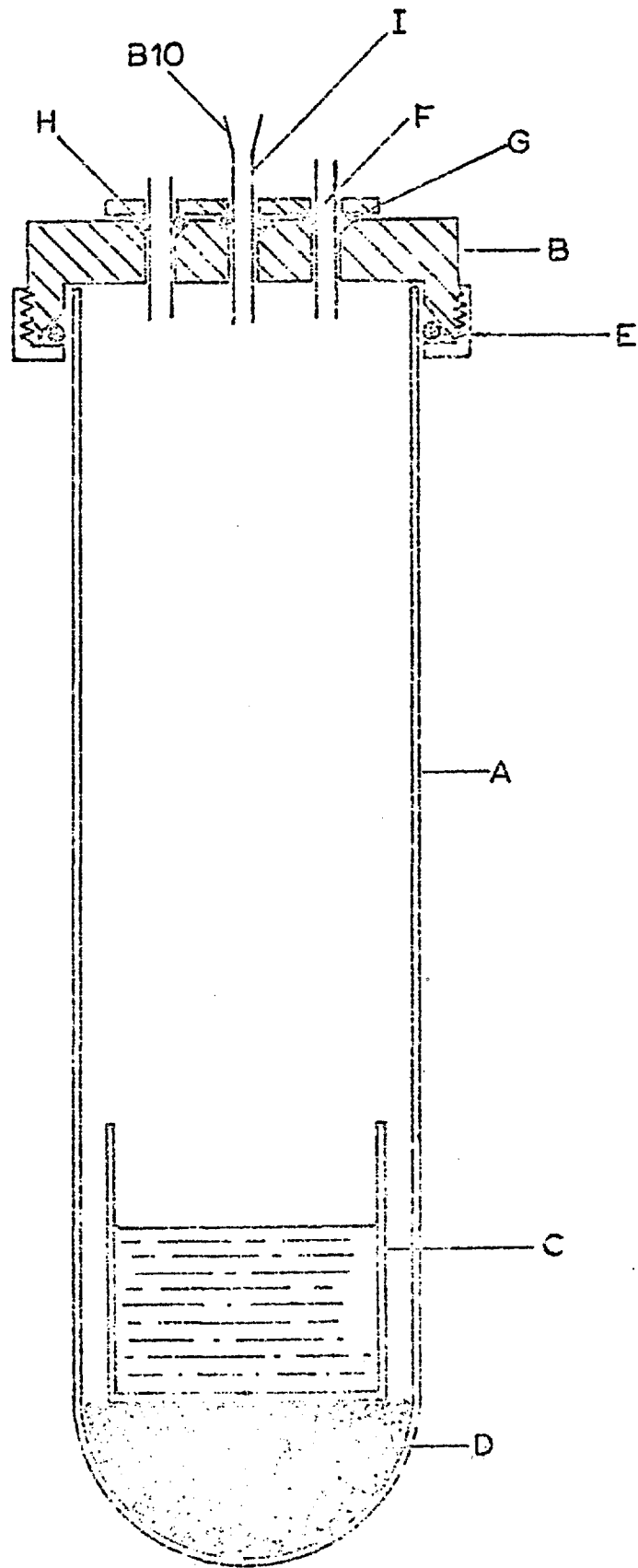
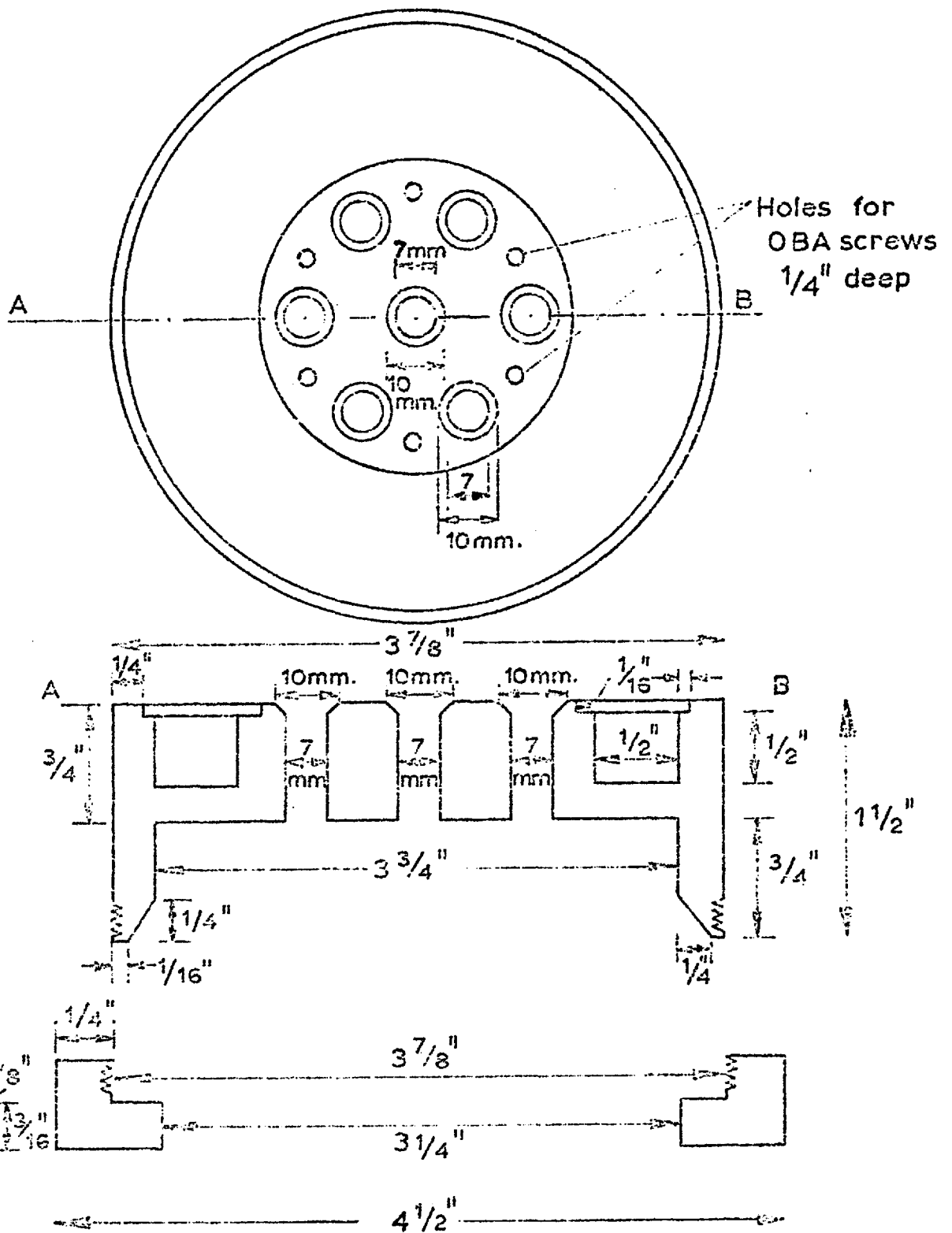Not drawn to scale.

Fig.5.5 ELECTROLYTIC CELL

Fig.5.6   BRASS CELL HEAD

by filtration. Details of the purification apparatus and technique have been given elsewhere (180). After cooling, the solid eutectic was transferred to the dry box in a polythene bag, which had been flushed with argon. The eutectic was transferred to the electrolytic cell in the dry box, and used immediately. The absence of transitions on the chronopotentiograms for the pure melt were considered a criterion for a pure melt.

The expression of the melt density "ρ" g cm^{-3} versus temperature can be obtained from data given by Van Artsdalen and Yaffe (181).

$$\rho = 1.885 - 5.274 \times 10^{-4} \; T^{o}C \qquad (5.1)$$

5.2.2. Sodium chloride -potassium chloride

It was found in the studies of niobium ions in sodium chloride - potassium chloride melts that A.R. grade salts melted under vacuum gave melts free of any impurities detectable by chronopotentiometry. In the studies of molybdenum ions in sodium chloride-potassium chloride melts the A.R. grade was not sufficiently pure. This is probably due variability in the quality of batches of the salts.

A technique was developed to purify the salts separately using sublimation under vacuum at $760^{o}C$. The sublimation was carried out in the electrolytic cell. A stainless steel condenser plate was suspended from the bottom of the cell head by four stainless steel rods, screwed into the underside of the cell head. The plate was 2.5 ins in diameter and 0.125 ins thick and the rods were 0.25 ins in diameter and 3.0 ins long.

About 120 g of A.R. grade salt was mixed intimately with about 5 g of ammonium chloride and placed in a silica pot

inside the silica envelope. The cell head was assembled, without the condenser, with a connection to the argon/vacuum supply and a gas outlet. The cell was assembled and the evacuated and flushed with argon three times. The temperature of the cell was very slowly raised to $760^{\circ}C$, with argon passing slowly through the cell. When the cell had reached $760^{\circ}C$, it was placed under vacuum for two hours to ensure that the more volatile impurities had sublimed off. When cool the cell was unloaded in the glove box, the pot containing the salt was left in the box and the cell was washed clean of sublimed salt. The condenser was then fitted to cell head and the cell was reloaded with the remaining salt. The cell was heated up to $760^{\circ}C$ under vacuum and held there for about 18 hours. This was sufficient time for most of the salt to sublime, but some unsublimed salt, which should contain the involatile impurities, remained. The cell was dismantled in the glove box, and the crystals were removed from the condenser plate. The layer of crystals up to 1/8 inch away from the condenser plate was discarded. The remaining crystals were ground to powder inside the glove box.

The initial treatment with ammonium chloride, was carried out to ensure removal of any oxides present. The sublimation treatment was found to give melts free of detectable impurities.

The melt densities can be calculated from their individual densities, since sodium chloride and potassium chloride form virtually ideal mixtures with each other (182) i.e.

$$\rho_{melt} = W_{NaCl}\,\rho_{NaCl} + W_{KCl}\,\rho_{KCl} \qquad (5.2)$$

where W = weight % and ρ = density in g, cm^{-3}.

5.2.3. Potassium chloride - caesium chloride

It was found that A.R. caesium chloride could be purified by recrystallization from distilled water. The A.R. potassium chloride did not require such purification. Fusion of mixtures of the two salts under vacuum provided melts of sufficient purity.

5.2.3. Sodium fluoride - potassium fluoride

Mixtures of A.R. grade sodium fluoride and GPR grade potassium were fused under vacuum, and then held at $850^{\circ}C$ under vacuum for two hours. This treatment tended to give a melt of reasonable purity, but it was not really satisfactory, as impurity waves were frequently present on chronopotentiograms.

5.2.4. Complex fluoride salts of refractory metals

The salts potassium heptafluoroniobate (K_2NbF_7) and potassium heptafluorotantalate (K_2TaF_7) were obtained from Alpha Inorganics, U.S.A.

The analysis of these salts is given in table 5.1.

5.2.5. Metals

The metals used for the electrodes were supplied by Alpha Inorganics, U.S.A. except for the platinum which was supplied by Johnson Matthey. The purities of the metals are listed below.

Molybdenum	99.95%
Tantalum	99.9%
Niobium	99.8%

5.3. Electrodes

5.3.1. Microelectrodes and counter electrodes

Four types of microelectrodes were used in this study. They

Table 5.1.

Maximum limits of impurities in complex fluoride salts.

	K_2NbF_7	K_2TaF_7
Nb	–	40 p.p.m.
Ti	10 p.p.m.	10 p.p.m.
Fe	800 p.p.m.	35 p.p.m.
Sn	10 p.p.m.	10 p.p.m.
Si	350 p.p.m.	100 p.p.m.
Cr	–	10 p.p.m.
Mo	–	10 p.p.m.
Ni	–	10 p.p.m.
N	–	75 p.p.m.
Ta	3,700	–

were a tungsten planar electrode, a platinum spherical electrode, a platinum flag electrode and a tantalum flag electrode. The electrode areas of the flag electrodes were not so well defined, since it was not always possible to accurately assess their depth of immersion in the electrolyte. It was for this reason flag electrodes were only used for the study in pure fluoride electrolytes, where any insulating material e.g. silica would be severely corroded. These electrodes are illustrated in figure 5.7(b).

The tungsten planar electrodes were prepared by sealing the tungsten rod 2 mm in diameter into silica using the G.E.C. graded seal G.S.10. The tungsten was then ground down on grade 90 carborundum paper until the tungsten was flush with the seal. The end of the electrode was then polished on grade 800 carborundum paper. Finally the electrode was polished on a lapping wheel using firstly 3μ diamond paste and in alloy 1μ diamond paste. The electrode was then examined under a magnifier to ensure it was free from scratches. Tungsten may be sealed directly into Pyrex glass for the low temperature studies, but these electrodes were found to be less reliable perhaps because of lower thermal shock resistance. Thus the silica variety of tungsten planar electrode was used even for the low temperature studies. It was found that a new tungsten electrode should be used for each series of experiments, if it was to be relied upon.

The platinum spherical electrodes were used in the platinum study at $480^{\circ}C$, and hence the platinum could be sealed into pyrex glass. The platinum wire, 22 S.W.G. was sealed into pyrex glass with about 2 mm of the wire

protruding. The protruding platinum was then fused, using a fine oxy-gas flame, to produce a sphere. Immediately prior to using the platinum electrode, it was soaked in concentrated hydrochloric acid and heated in coal gas flame.

The flag electrodes used were approximately 2 mm square and were spot welded to 10 mil wire. The area of the platinum flag electrode and the spherical electrode were calibrated in an aqueous solution of 10^{-3} M potassium iodide plus 1M sulphuric acid. Using the chronopotentiometric constant 0.700 Amp, $\sec^{\frac{1}{2}}$, mole, cm^{-1} (183). The tantalum flag electrode was calibrated against the platinum flag electrode during a fluoride experiment. The area of the tungsten electrodes were estimated geometrically. The area of the electrodes at the experimental temperature were calculated from the coefficients of expansion "α" supplied by Smithells (184).

$$\alpha . 10^6 \text{ for } (20 \text{ to } t^{\circ}c)$$

Platinum   9.6

Tungsten   6.6

The counter electrodes, which were also used as the anode in anodic dissolution, were fabricated from the same metal as the ions being studied. The dimensions of the metal foil used was 3.5 cm by 3 cm and 10 mil thick.

5.3.2. Reference electrodes

Reference electrodes were only used in the chloride electrolyte studies. The couple used for all the reference electrodes all the reference electrodes was the silver-silver (I) couple.

The reference electrode used in the low temperature studies (<570°C) consisted of a dilute solution of silver chloride in the lithium chloride-potassium chloride eutectic, which was contained in a Pyrex glass bulb. This type of electrode was originally developed by Inman (185). The Pyrex glass acted as a membrane, in which the alkali metal ions are in equilibrium with the alkali metal ions in the electrolyte. The solution of silver (I) ions was prepared by anodic dissolution at 470°C under an argon atmosphere, and its concentration was determined by atomic adsorption spectroscopy. A single 100 g batch of the solution was prepared, and lasted the whole study. The concentration of silver was 7.22×10^{-3} moles per 1000 g.

The reference electrode used in the high temperature studies consisted of a dilute solution of silver chloride in equimolar sodium chloride potassium chloride. The membrane used in this case was "Mullite" in the form of a closed end tube. The silver chloride was prepared from sodium chloride and silver nitrate in the usual way. The concentration of the silver chloride solution was 0.1 moles per 1000 g.

Diagramatic representation of the reference electrodes are shown in figure 5.8.

5.3.3. Anodic dissolution cathodes

Two types of anodic dissolution cathodes have been used, those employing liquid bismuth. The requirement of the cathode is to prevent the electrochemically produced alkali metals entering the bulk of the electrolytes. Illustrations of the types of cathodes employed are in figure 5.9.

The graphite cathode, consisted of graphite electrode 5 cm long and 6 mm in diameter enclosed in a cathode compartment 5 cm long and internal diameter 1.0 c.m. The bottom of the compartment was closed by a No. 2 porosity sintered disc. The graphite electrode was electrically connected to the outside of the cell via a steel wire. A complete new assembly was used for each series of experiments, and since this proved to be expensive, a liquid bismuth cathode assemble was employed in all the later experiments.

The liquid bismuth cathode was contained in a cathode compartment, which consisted of a closed end tube 4.5 cm long and 1.0 cm in diameter, contact was made with the electrolyte via a small side arm which was situated 2.0 cm from the bottom, and packed with silica wool. Electrical contact was made with the molten bismuth through a tungsten rod (1 mm diameter). The tungsten rod could be raised and lowered without breaking the vacuum and gas-tight seal by employing a precision sliding glass joint greased with Apieson T. grease. Only the cathode compartment needed replacing after each series of experiments.

The cathode assemblies were fabricated from Pyrex glass for use in the low temperature studies, and silica for use in the high temperature studies.

5.4. Experimental procedure

5.4.1. Chronopotentiometric measurements

Constant current pulses of varying heights were applied between the micro electrode (cathode) and the counter electrode (anode). The change in potential difference between the two
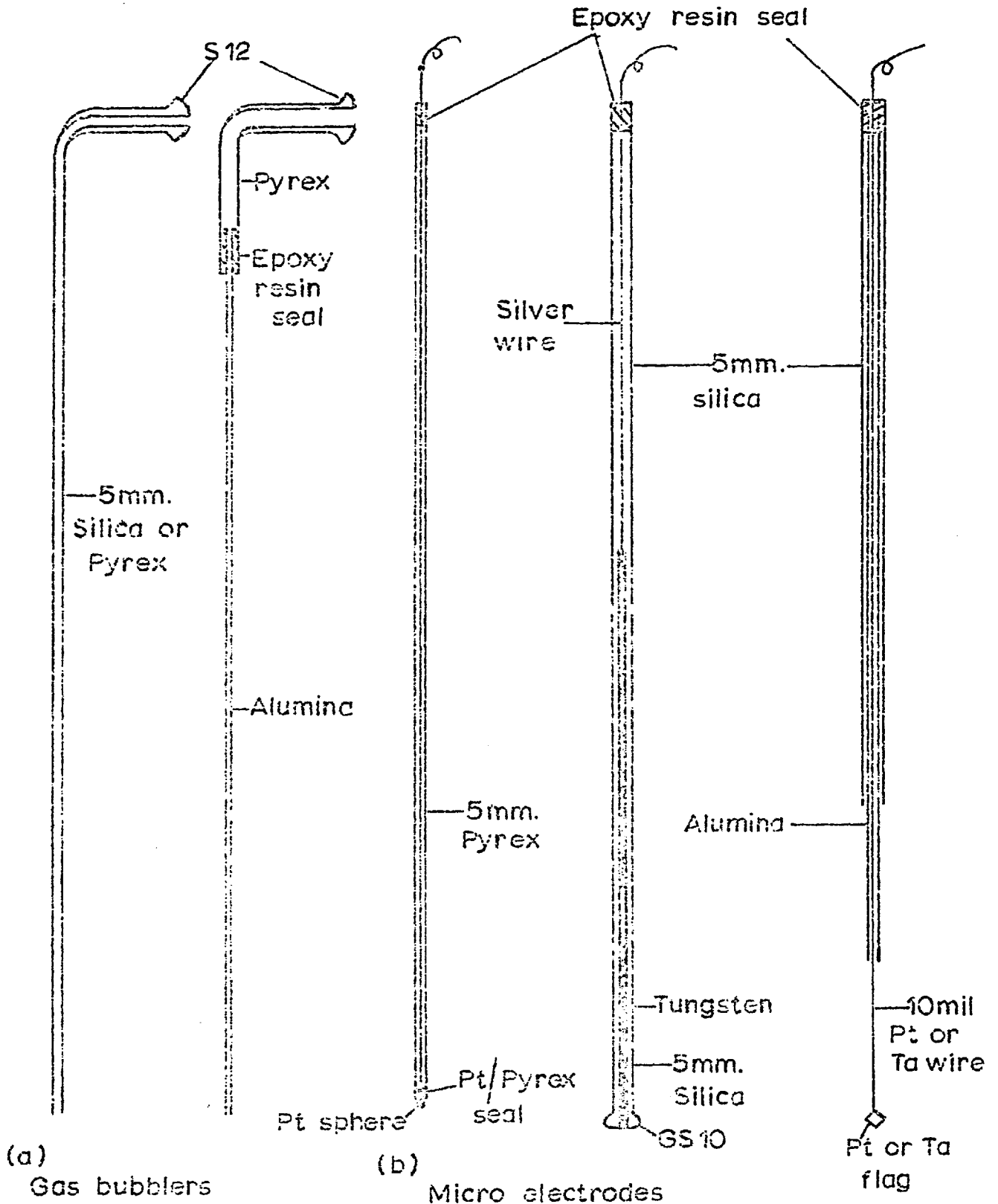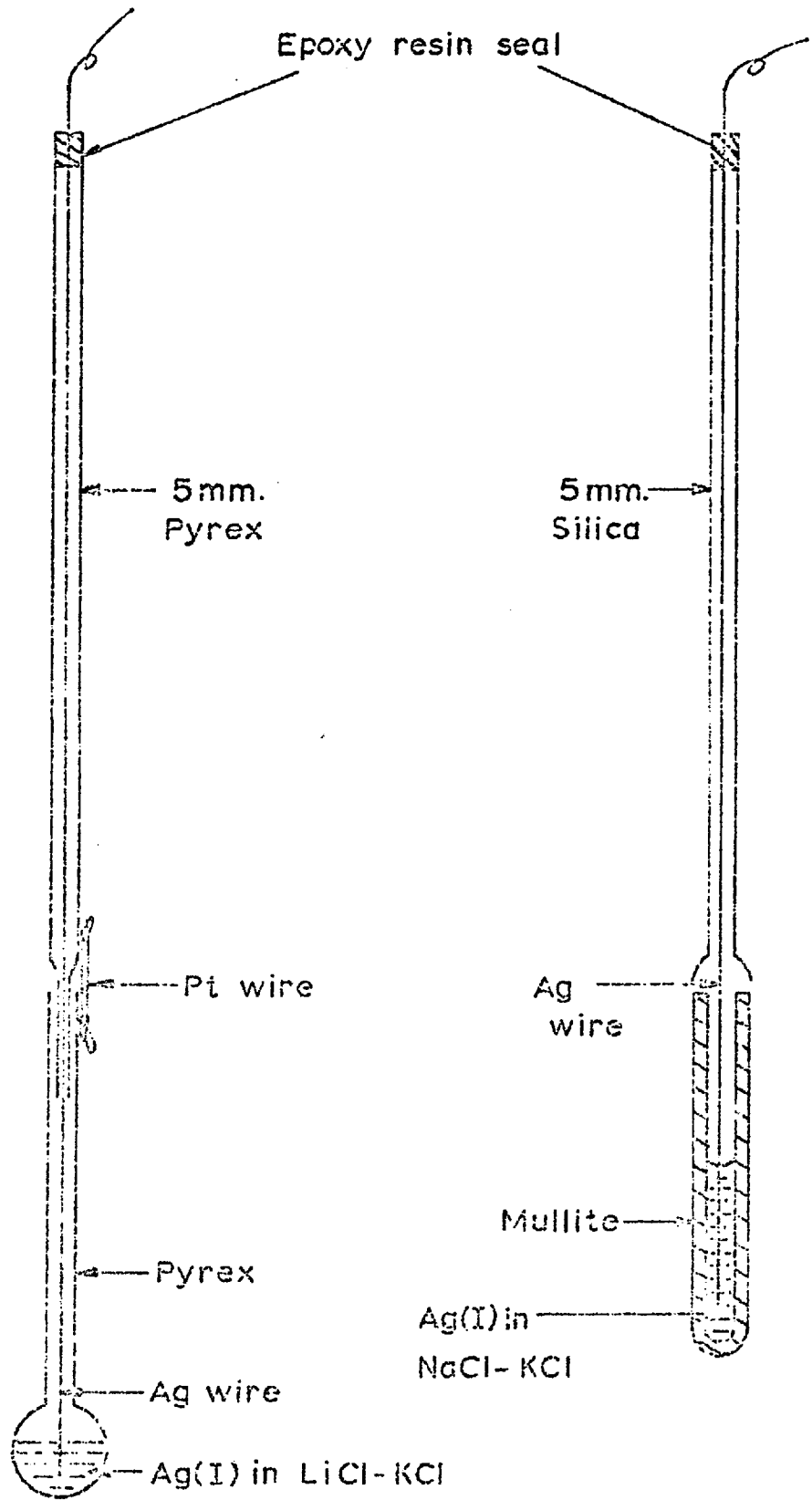
(a) Gas bubblers

(b) Micro electrodes

Fig. 5.7

Epoxy resin seal

5mm.
Pyrex

5mm.
Silica

Pt wire

Ag
wire

Pyrex

Mullite

Ag wire

Ag(I) in
NaCl-KCl

Ag(I) in LiCl-KCl

Fig. 5.8   REFERENCE   ELECTRODES

Connected to
atmosphere in
electrolytic cell

— Epoxy resin

— Silver wire

Precision
sliding joint

— Steel rod

Tungsten
rod

— Silica

— Graphite

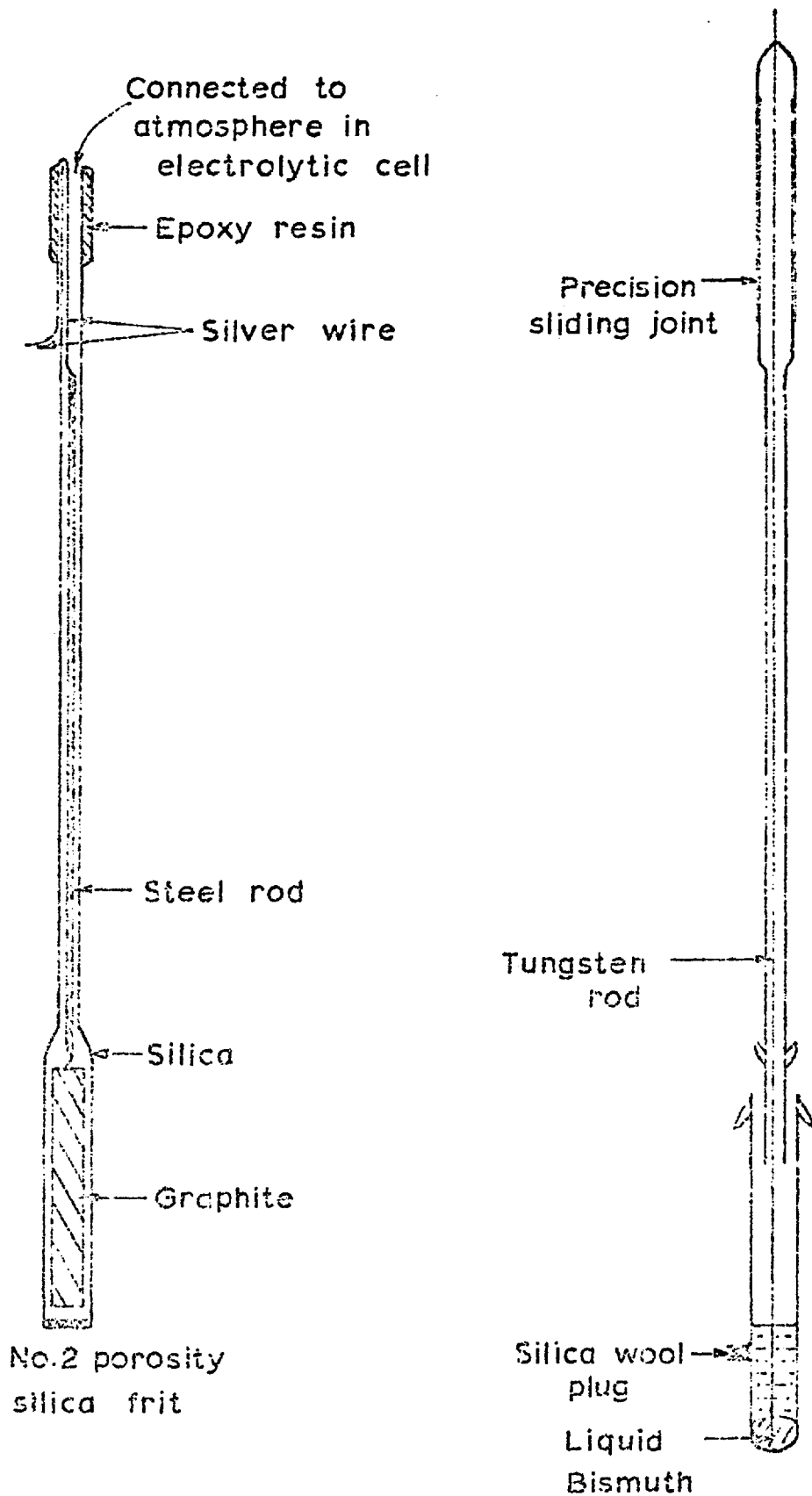No.2 porosity
silica frit

Silica wool
plug

Liquid
Bismuth

Fig.5.9 ANODIC DISSOLUTION CATHODES.

electrodes with respect to time (chronopotentiogram) was observed on the oscilloscope screen. Since the microelectrode was very much smaller in area than the counter electrode (about 500 times in terms of geometry) the current density at the counter electrode was insignificant compared to the current density at the micro electrode. The potential of the counter electrode could be assumed to stay constant during the electrolysis, and any changes in potential difference between the two electrodes could then be assumed to be due to changes in the potential of the micro electrode. The current was reversed at the end of each pulse, to remove the reduced species from the electrode surface. The micro electrode was then allowed to return to a steady potential before the next pulse was applied. Several constant current pulses of the same value were applied to the cell to ensure the chronopotentiograms were reproducible.

Two methods were used to measure the length of transition times. The earlier measurements were taken directly off the screen of the storage oscilloscope. To facillitate the direct measurement of the transition times the chronopotentiograms were electronically differentiated. The potential-time measurements were taken directly from the undifferentiated wave. In the majority of experiments undifferentiated chronopotentiograms were recorded photographically, using a Tetronic C.12 camera. The camera was fitted with a Graflex back which accommodated a 12 exposure, 120 roll film holder. The 120 roll film used was Kodak Panatomic-X, which had a film speed of 32 A.S.A. To overcome parallax effects between the oscilloscope graticule and screen, an external

graticule was used. The virtual image of the external graticule

was projected on the same plane as the oscilloscope screen.

The use of a projected graticule also allowed a more complex

graticule to be employed, and hence make measurements from

the chronopotentiogram simpler. Since the double layer charging

part at the start of the chronopotentiograms was very steep a

simple tanget construction was used to estimate the length

of the transition time (see figure 5.10). All the measurements

were made from prints about 1.16X the actual screen size.

5.4.2. Solute addition

The complex fluoride salts (K_2 NbF_7) and the simple

fluorides (NaF and KF) were added as pellets which were prepared

in the dry box. The solute addition assembly, shown in

figure 5.11, fitted into the gas outlet of the cell, using

B10 cone and socket joints. To add the solute, the plunger (A)

was retracted, the sample tube (B) was rotated a little over

$90°$ from the vertical and one of the weighed pellets was tapped

into the horizontal tube (C). The plunger was then used to push

the pellet into the vertical tube (D), from which it dropped

into the electrolyte underneath. The pellet was allowed to

dissolve, and the electrolyte was stirred by bubbling argon

gas through it.

The addition of refractory metal ions to chloride

electrolytes was achieved by anodic dissolution of the counter

electrode. The current was applied between the counter and

the anodic dissolution cathode by the constant current power

supply described in section 5.1. The electrolysis time for

the dissolution was accurately timed using a stop watch, and

hence the amount of the ion added was calculated from the
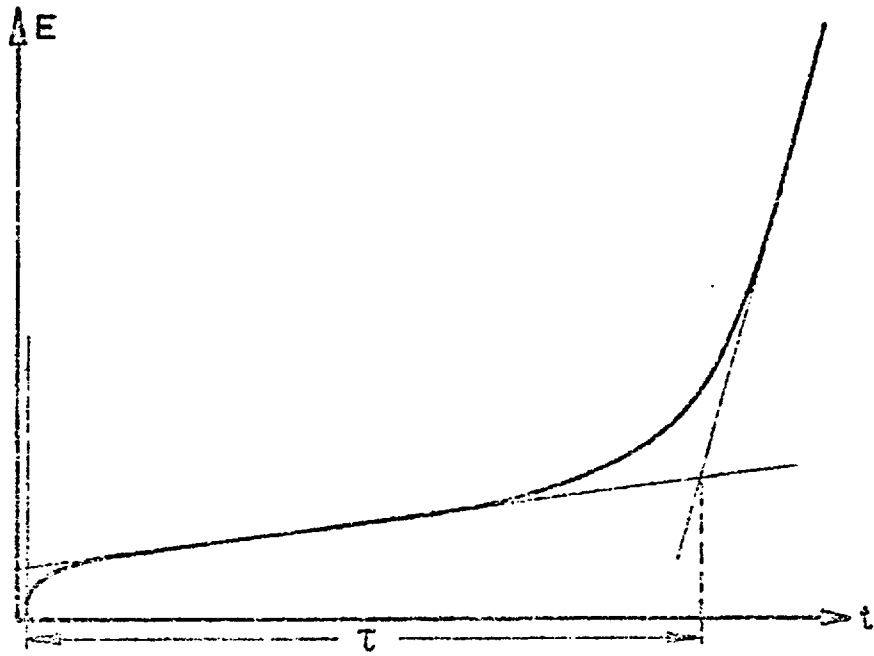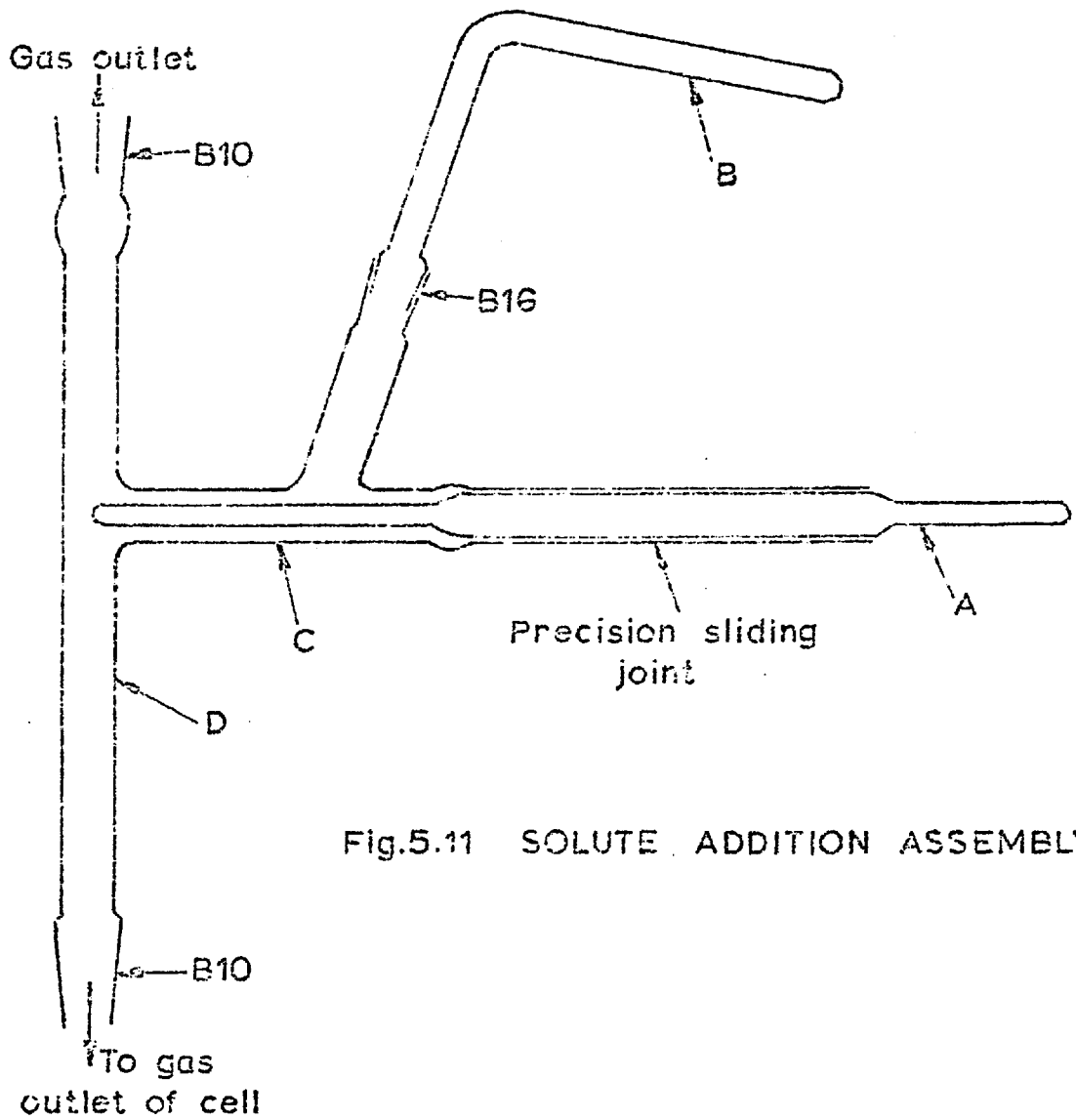
TANGENT CONSTRUCTION TO MEASURE 'τ'
Fig.5.10

Fig.5.11 SOLUTE ADDITION ASSEMBLY

quantity of coulombs passed. The melt was stirred after dissolution.

5.4.3. Preparation of apparatus.

Prior to an experiment all glassware and silica ware was cleaned by the following procedure. They were soaked in a 1:1 mixture of concentrated nitric and concentrated sulphuric acids for at least one hour, washed with distilled water, followed by A.R. acetone, and finally dried in an oven at $110^{\circ}C$. The counter electrodes were cleaned by dipping them briefly into a 1:1:1 mixture of concentrated nitric, concentrated sulphuric and 40% hydrofluoric acids. (Great care and full safety precautions must be taken in preparing this mixture). The electrodes were then washed with distilled water and finally with A.R. acetone, and allowed to dry. The other micro electrodes were washed with distilled water and A.R. acetone.

The cell was assembled, transferred into the dry box where it was loaded with the solid electrolyte. The reference electrode and the solute addition tube were also loaded in the glove box. The sealed cell was then taken from the glove box, and fitted into the water cooled collar on the furnace. The cell was then connected to the argon-vacuum system and the gas outlet system. The gas outlet system included a dibutyl phthalate bubbler to ensure no air diffused back into the cell. The cell head was earthed to minimise pick up of electrical interference. The cell was then evacuated and flushed with argon three times. With argon passing slowly through it, the cell was heated to the experimental temperature and evacuated. When the electrolyte was completely molten, the cell was brought back to atmospheric pressure by admitting argon, and the electrodes together with the thermocouple were lowered into the melt.

If pyrex or silica was used the lowering of the electrodes may be carried out visually by briefly lowering the furnace. When a "Mullite" outer envelope was used the lengths of the electrodes needed to be known accurately and the melt level accurately estimated. In the case of the fluoride electrolyte the thermocouple sheath was not lowered into the melt until the end of the series of experiments, so that its corrosion was minimised. A very small flow of argon was maintained over the melt throughout the series of experiments.

5.4.4. Study of niobium ions in chloride melts.

Experiments were carried out in the lithium chloride-potassium chloride eutectic at $724^{\circ}C$ using about 100 g of melt, equimolar sodium chloride-potassium chloride at $755^{\circ}C$ using about 120 g of melt and equimolar potassium chloride-caesium chloride at $750^{\circ}C$ using about 120 g of melt. The niobium was added to all the melts by anodic dissolution, except for one experiment where potassium potassium heptafluoroniobate was added to the caesium containing melt. The current density used for the anodic dissolution was about 5m A, cm^{-2}. Also a very high current density was achieved by just touching the anode on the melt surface. The chronopotentiometric measurements were carried out using tungsten micro electrodes also steady state current-voltage measurements were made for the anodic dissolution in the caesium containing melt. The potential of the anode was measured against the reference electrode.

5.4.5. Molybdenum ions in chloride melts

The melts investigated in this study were the lithium chloride-potassium chloride eutectic at $570^{\circ}C$ using about 100g of melt, equimolar sodium chloride - potassium chloride

at 765°C using about 120 g of melt, and sodium chloride -

20 mole % - potassium chloride 80 mole % at 765°C using

150g of melt. The molybdenum ions were added by anodic

dissolution. The fluoride ions were added as pellets of

sodium fluoride at low the temperature and pellets of sodium

fluoride 20 mole% - potassium fluoride 80 mole % at the high

temperature.

All the measurements made were chronopotentiometric using tungsten

micro electrodes.

5.4.6. Platinum ions in chloride melts

The melt investigated was the lithium chloride-potassium

chloride eutectic at 470°C using about 100 g melts. The platinum

ioms were added by anodic dissolution, and the fluoride ions were

added as pellets of sodium fluoride. Chronopotentiometric

and potentiometric measurements were made using platinum electrodes.

5.4.7. Tantalum ions in fluoride melts

The study was carried out in sodium fluoride 40 mole % -

potassium fluoride 60 mole % at 728°C using about 100 g of melt

The tantalum was added as pellets of potassium heptafluorotantalate.

The chronopotentiometric measurements were made on platinum and

tantalum flag electrodes.

CHAPTER 6

RESULTS AND DISCUSSION

6.1. Niobium ions in chloride melts

6.1.1. Results in lithium chloride-potassium chloride

No chronopotentiometric reduction wave was observable in
the eutectic melt at $724^{\circ}C$ using anodic dissolution current
densities of about $5mA$, cm^{-2}. When anodic dissolution was
carried out at a high currents, with the anode just touching
the melt surface, a chronopotentiometric reduction wave was
observed. A large amount of precipitation occurred during
anodic dissolution and hence the concentration was not known.
The precipitate was very dark in colour.

The wave produced by anodic dissolution at high current
densities diminished with time. See table 6.1 where the values
of the product $i\tau^{\frac{1}{2}}$ are listed in the order they were measured,
i.e. $i\tau^{\frac{1}{2}}$ decreased with time. The plot of the micro electrode
"E" versus $\log_{10} (\tau^{\frac{1}{2}}/t^{\frac{1}{2}}-1)$ was virtually linear for example
with a slope of 207 mV (figure 6.1). The slope corresponds
to n = 0.96, see equation (2.60). The plot of "E" versus $\log_{10}$
$(1-t^{\frac{1}{2}}/\tau^{\frac{1}{2}})$ was totally non linear (see figure 6.1).

6.1.2. Results in sodium chloride-potassium chloride

Anodic dissolution when carried out at current densities
of about $5m A$, cm^{-2} did not produce a chronopotentiometric
reduction wave in the equimolar sodium chloride-potassium
chloride at $760^{\circ}C$. Anodic dissolution, carried out at high
currents and with the anode just touching the melt surface,

Table 6.1.

Niobium ions in Li Cl-KCl eutectic at 724°C.

i,mA.	τ,sec	$i\tau^{\frac{1}{2}}10^5$,A.sec.$^{\frac{1}{2}}$
0.604	0.019	8.33
0.510	0.025	8.06
0.385	0.040	7.70
0.337	0.050	7.54
0.270	0.080	7.64
0.204	0.140	7.62
0.185	0.167	6.91
0.135	0.305	7.44
0.128	0.322	7.25
0.116	0.390	7.25
0.114	0.415	7.33
0.0962	0.590	7.39
0.0772	0.850	7.12

Fig.6.1 NIOBIUM IONS IN LiCl-KCl EUTECTIC AT 722°C.
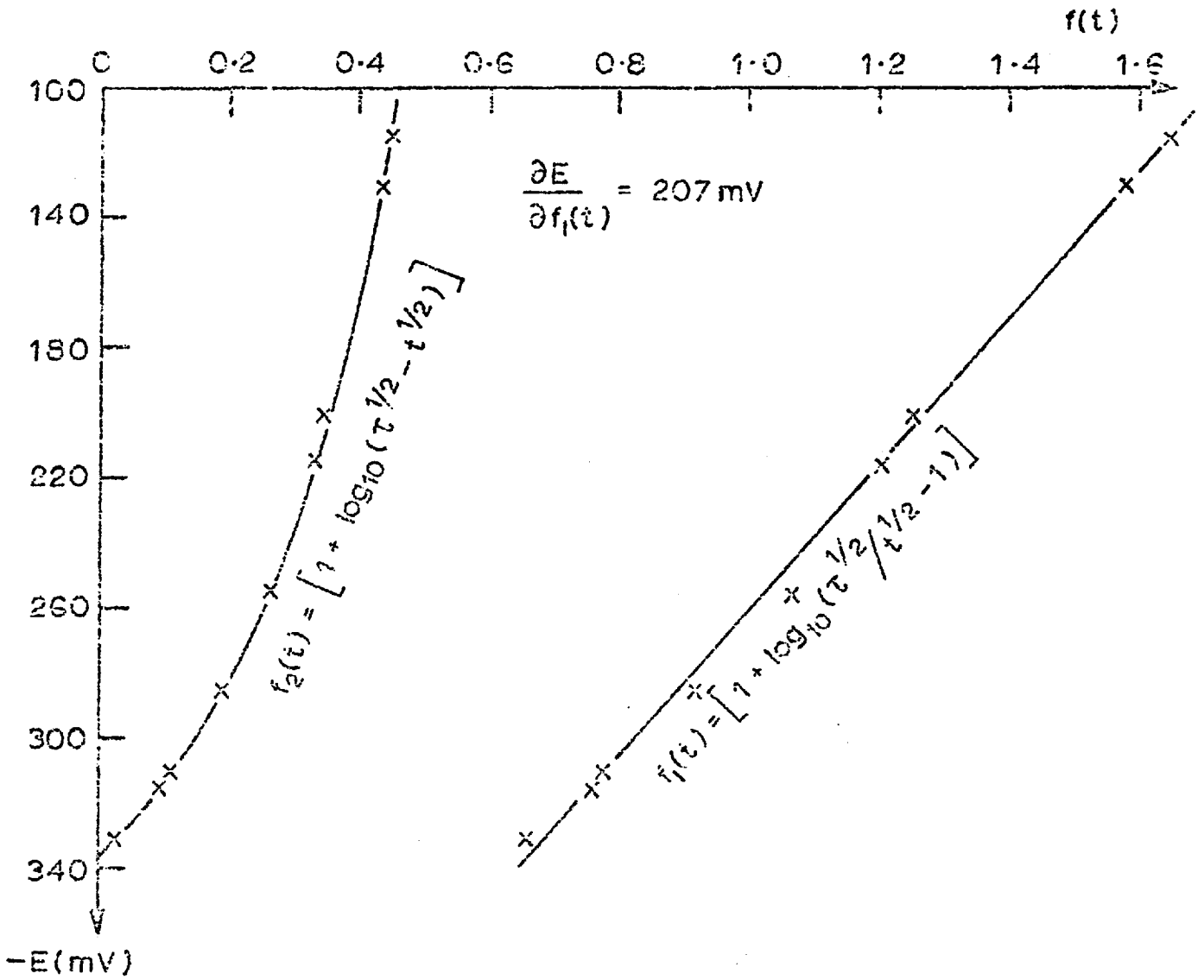
Table 6.2.

Niobium ions in equimolar NaCl-KCl at $760^{\circ}C$

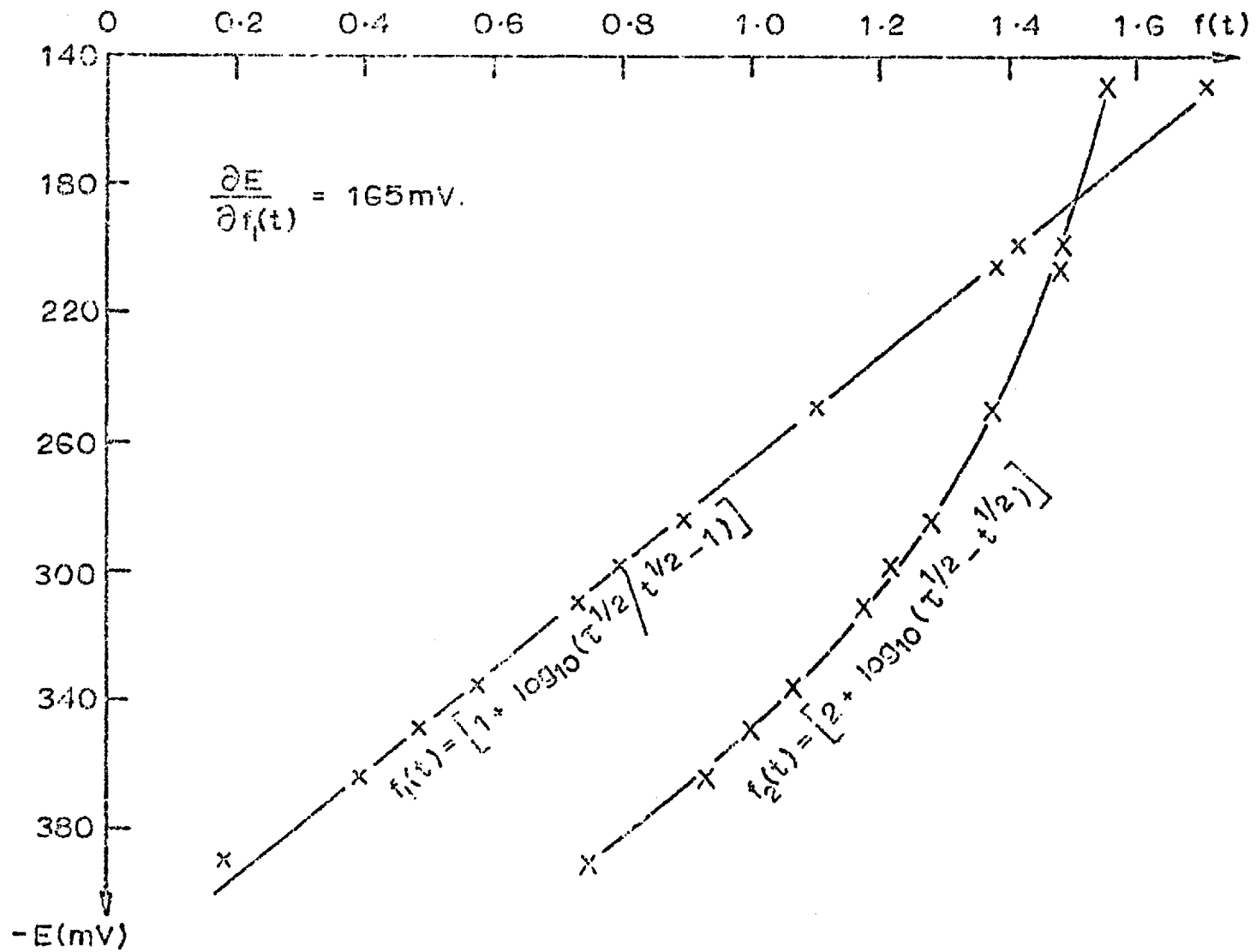| i,mA	τ,msec	$i\,\tau^{\frac{1}{2}}10^3$,A.msec.$^{\frac{1}{2}}$
1.421	13.5	5.22
1.198	14.3	4.53
1.046	18.4	4.49
0.817	31.6	4.59
0.757	36.5	4.58
0.604	48.9	4.22
0.509	55.2	3.78
0.384	72.2	3.26
0.336	82.6	3.05
0.269	107	2.78
0.2033	147	2.46
0.1844	154	2.29
0.1342	231	2.04
0.1274	244	1.99
0.1157	259	1.86
0.1132	278	1.89
0.0959	353	1.80

Fig.6.2 NIOBIUM IONS IN EQUIMOLAR NaCl-KCl AT 760°C.

produced a chronopotentiometric reduction wave. (See photograph 6.1.(a)) It was not possible to estimate the concentration of the niobium species, owing to the large amount of precipitation. On cooling the melt was blue in colour.

The reduction wave for the species produced by the anodic dissolution at high current densities were not very reproducible and diminished with time. Table 6.2. lists the values of the product $i\tau^{\frac{1}{2}}$ in the order they were measured. The plot of the micro electrode potential "E" versus $\log_{10}$ $(\tau^{\frac{1}{2}}/t^{\frac{1}{2}}-1)$ was linear. An example is shown in figure 6.2 which has a slope of 165 m V. The slope corresponds to n = 1.23, see equation (2.60). The plot for "E" versus $\log_{10}$ $(1-t^{\frac{1}{2}}/\tau^{\frac{1}{2}})$ was non-linear, see figure 6.2.

6.1.3. Results in potassium chloride-caesium chloride

No chronopotentiometric reduction wave was observed in the equimolar potassium chloride-caesium chloride melt at $760^{\circ}C$, when anodic dissolution was carried out at current densities about 5mA, cm^{-2}. A chronopotentiometric reduction wave was obtained at high anodic dissolution current densities and with the anode just touching the melt surface. A large amount of precipitation occurred during anodic dissolution, and hence it was impossible to estimate the concentration of the niobium species. The colour of the melt, when cooled, was blue.

The reduction wave for the species (see photograph 6.1(b)) produced by the anodic dissolution at high current densities was reproducible and invariant with time. The product $i\tau^{\frac{1}{2}}$ was independent of current density (see table 6.3) i.e. a plot of "$\tau^{\frac{1}{2}}$" versus 1/i passed through the origin, figure 6.3. The plot of the electrode potential "E" versus $\log_{10}$ $(\tau^{\frac{1}{2}}/t^{\frac{1}{2}}-1)$ was

almost linear. An example is shown in figure 6.4 where the slope is 214 mV. The slope corresponds to n = 0.96, see equation (2.60). The plot of "E" versus $\log_{10}(1-t^{\frac{1}{2}}/\tau^{\frac{1}{2}})$ was not linear, see figure 6.4.

The addition of niobium (V) as the complex fluoride, K_2NbF_7, produced a multiple wave which disappeared too rapidly to make any measurements.

Steady state anode current-anode potential measurements were carried out on a melt apparently saturated by the species produced by anodic dissolution as about 5m A cm^{-2}, i.e. precipitation had occurred. The measurements were carried out in the anode current density range - 4.84 x 10^{-5} to -2.16 x 10^{-3} Amp, cm^{-2}, and anode over potential "η" range 4.6 to 128 m V. The Tafel plot of "η" versus $\log_{10}|i|$ was linear at high overpotentials see figure 6.5. The slope was equal to 85.1 mV and the intercept, at $\eta = 0$, was -3.76. This gave a value for $(1-\alpha)n$ of 2.4 and an exchange current density "i_0" of 1.74 x 10^{-4} Amp, cm^{-2}, if the process is an irreversible charge transfer process, c.f. equation (2.88b). The plot of "η" versus "i" shown in figure (6.6), gave limiting slope, as "i" tended to zero, of -98.3 V cm^2, Amp^{-1}. Applying equation (2.90) the exchange current density "i_0" is 3.02 x 10^{-4} Amp.cm^{-2} if n = 3 and 2.27 x 10^{-4} Amp cm^{-2} if n = 4.

6.1.4. Discussion

The work of Dartnell et alia (166) and Saeki and Suzuki (169) indicate that the anodic dissolution of niobium at low current densities in chloride electrolytes produces

Photograph 6.1.
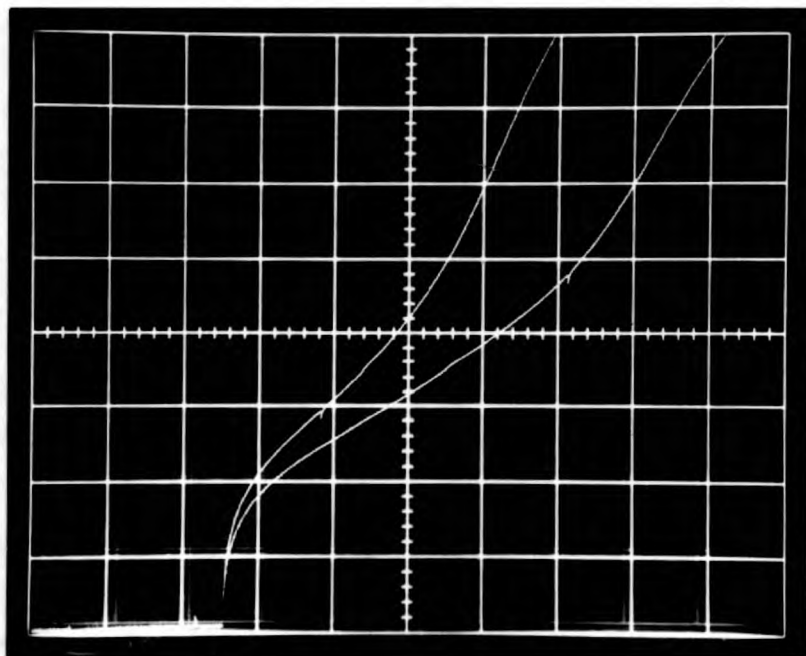
(a) Nb ions in Na Cl - KCl
y = 0.1 V,cm^{-1} x = 2 msec, cm^{-1}.
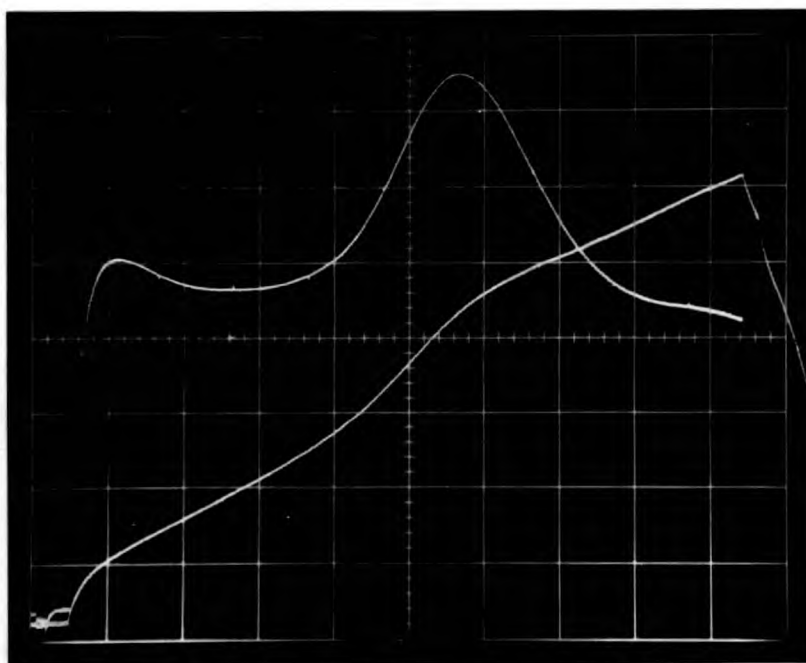
(b) Nb ions in KCl - CsCl
0.2 V,cm^{-1}. x = 10 msec. Cm^{-1}.

Table 6.3

Niobium ions in equimolar KCl - CsCl at 760°C.

i,mA	τ m sec	$i_\tau^{\frac{1}{2}}10,^3$ A.msec$^{\frac{1}{2}}$
1.198	16.5	4.87
1.046	22.4	4.95
0.817	34.6	4.81
0.757	40.4	4.81
0.604	67.6	4.97
0.509	92.0	4.88
0.384	159	4.84
0.336	204	4.80
0.269	306	4.71
0.2033	528	4.68
0.1844	644	4.68
0.1342	1330	4.89
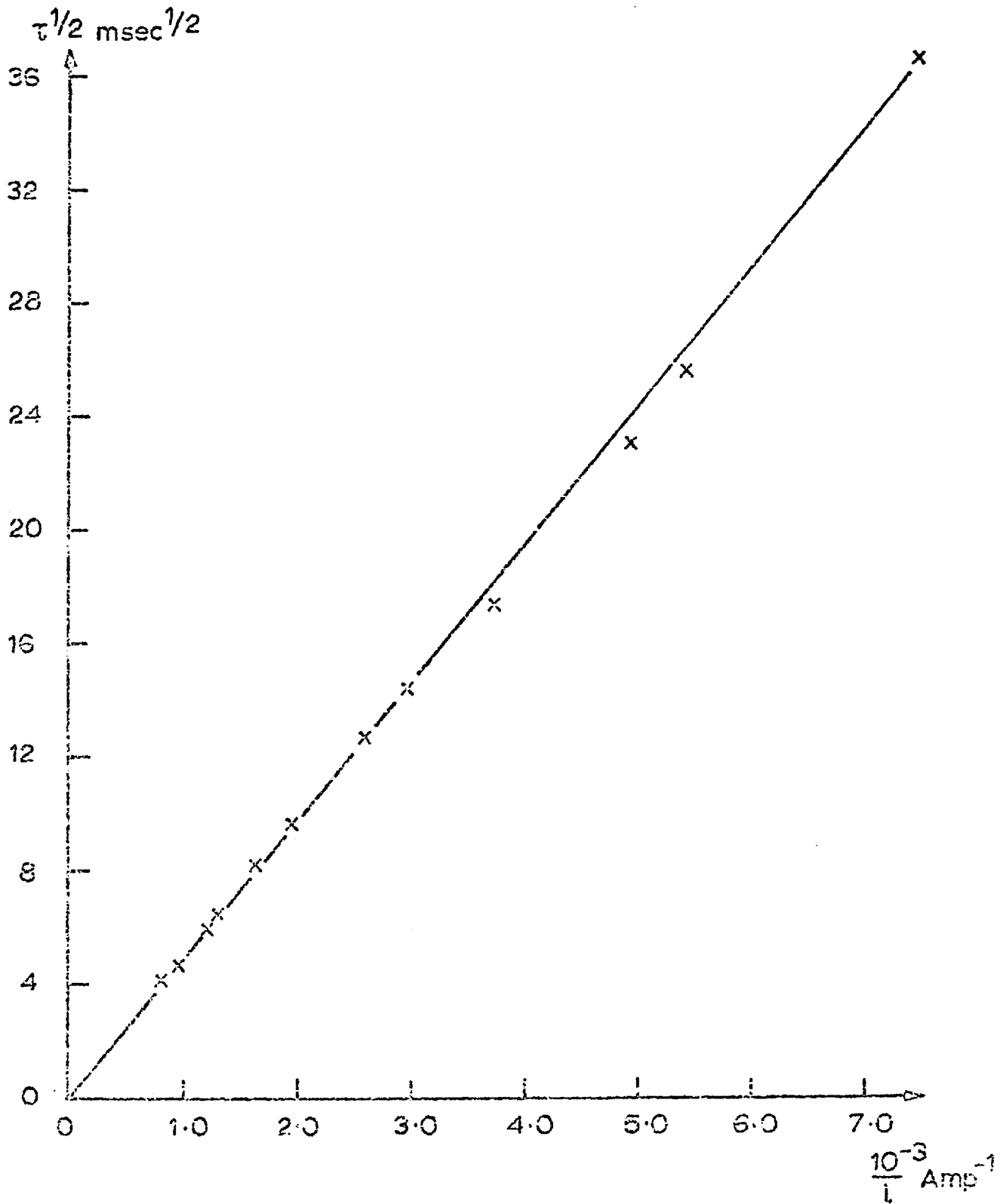
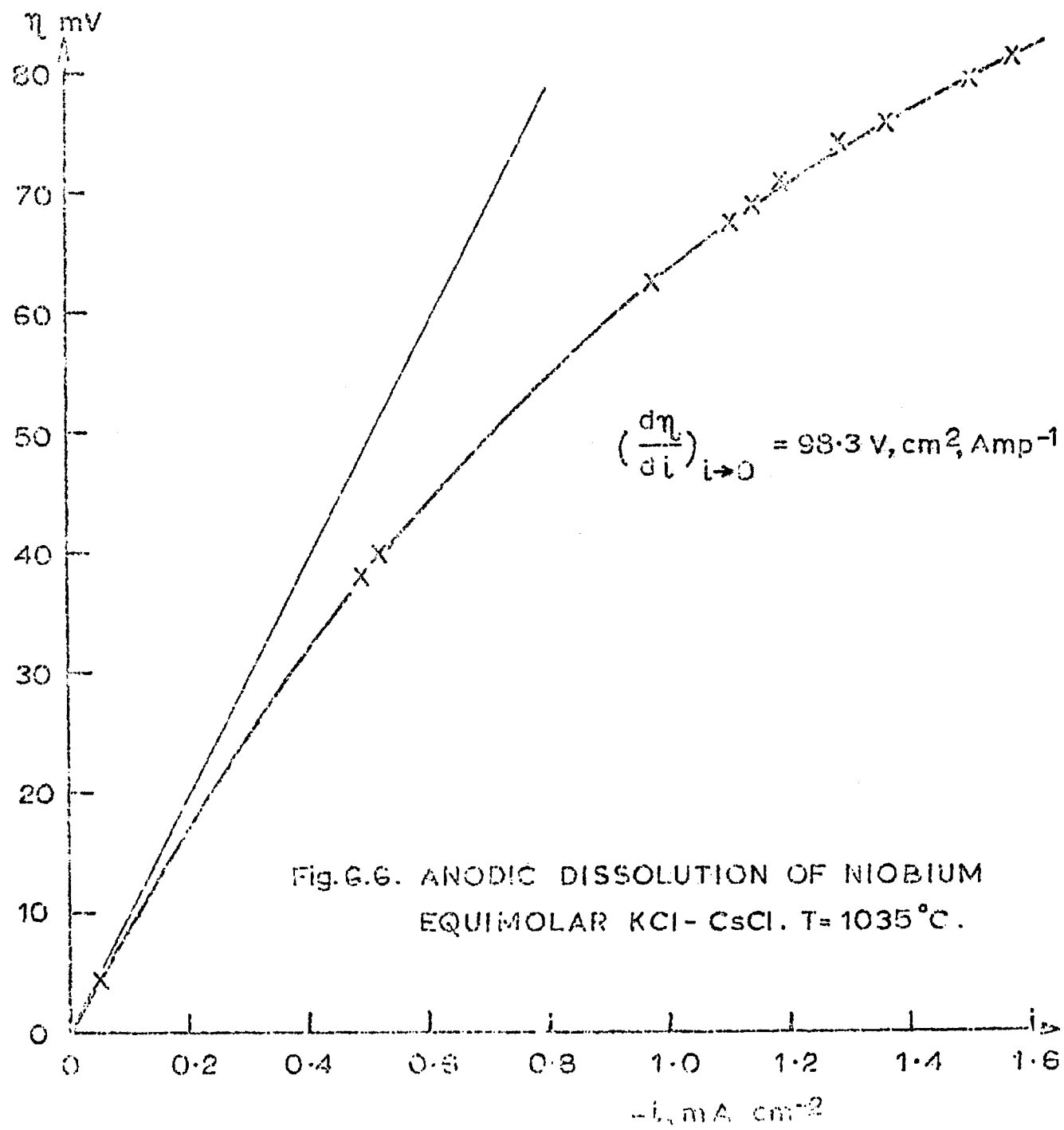Fig. 6.3   NIOBIUM IONS IN EQUIMOLAR KCl - CsCl . 1032° K
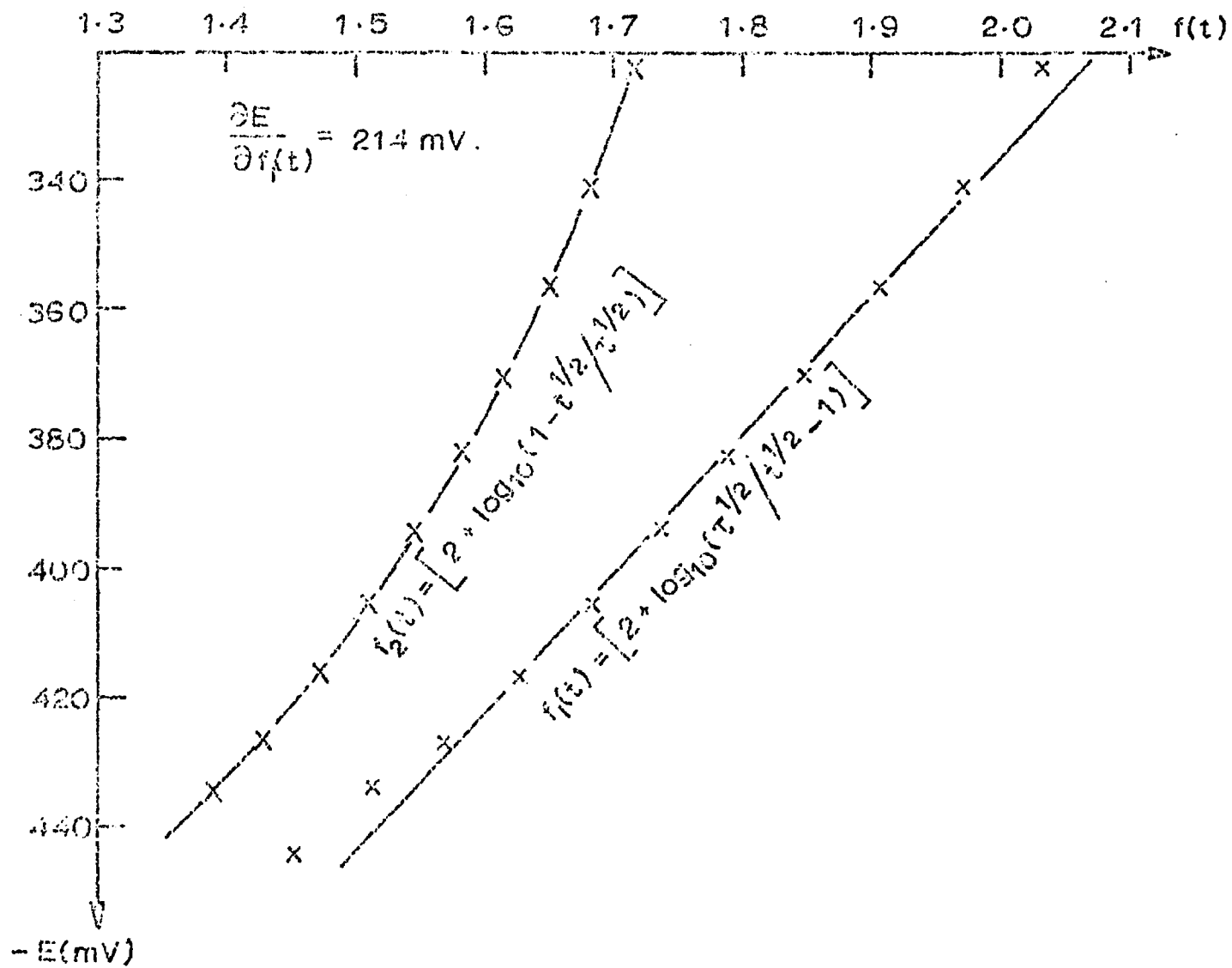
Fig.6.4 NIOBIUM IONS IN EQUIMOLAR KCl- CsCl AT 760°C

Fig. 6.5   ANODIC   DISSOLUTION   OF   NIOBIUM   IN
EQUIMOLAR   KCl- CsCl . T = 1035°K

$$\left(\frac{d\eta}{di}\right)_{i\to 0} = 98\cdot 3 \; V, cm^2, Amp^{-1}$$

Fig. 6.6. ANODIC DISSOLUTION OF NIOBIUM
EQUIMOLAR KCl – CsCl . T = 1035°C .

y-axis: η mV
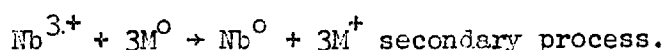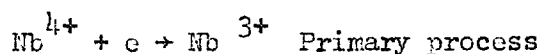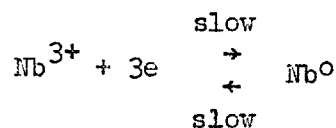
x-axis: $-i$, mA cm^{-2}
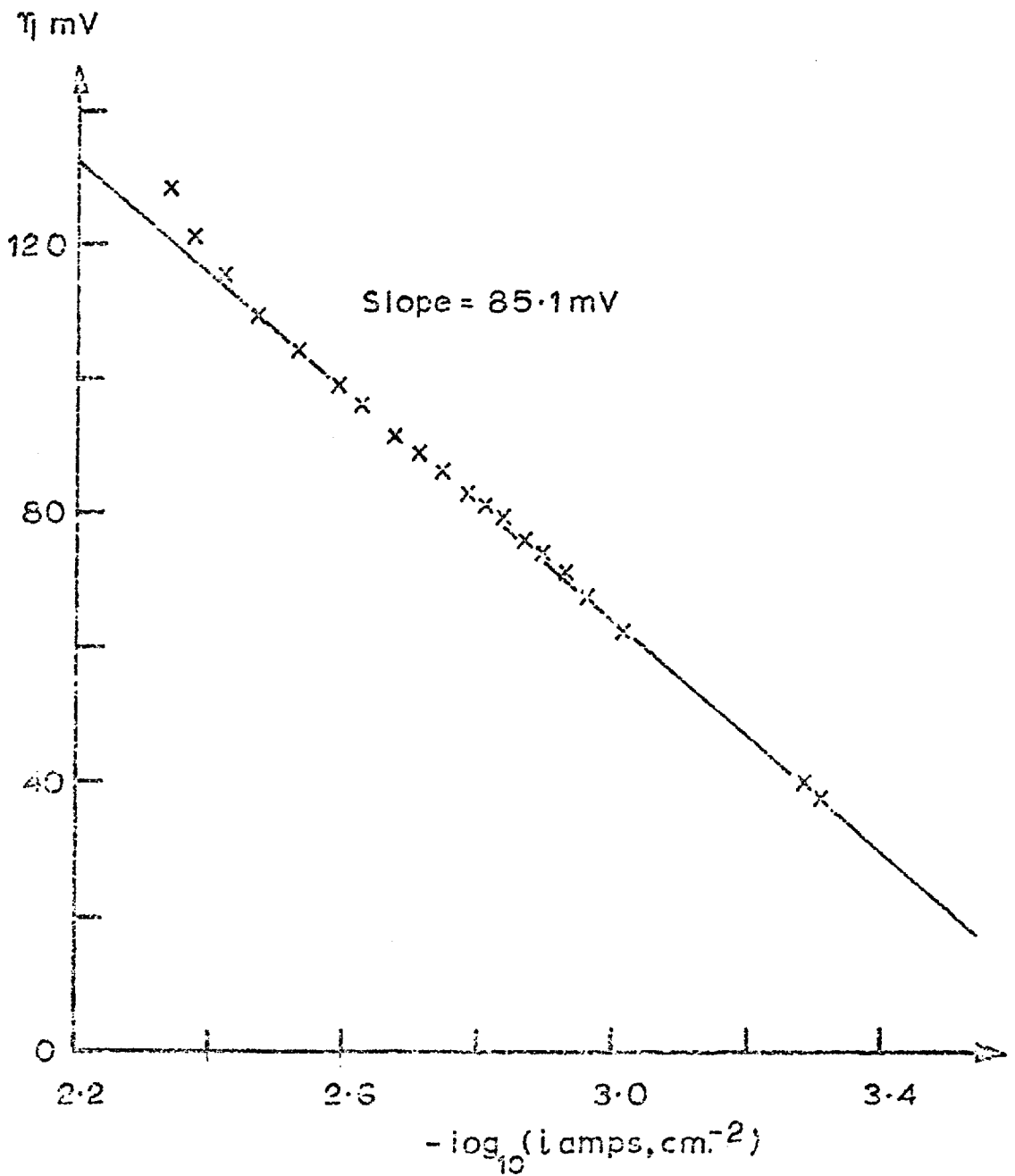
niobium (III) species. No chronopotentiometric wave was observed for species produced by low dissolution current densities. It can be concluded therefore that the reduction of the niobium (III) species, at the current densities employed by chronopotentiometry was irreversible and occurred by a secondary process following the deposition of alkali metal, c.f. Section 4.

$$M^+ + e \rightarrow M^o \quad (M = \text{alkali metal})$$
$$Nb^{3+} + 3M^o \rightarrow Nb^o + 3M^+$$
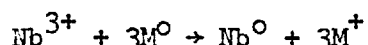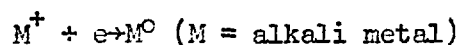
The steady state anode current density - anode potential measurements support an irreversible process for the anodic dissolution of niobium. The Tafel plot gave an exchange current density of 1.74×10^{-4} Amp cm^{-2} and a value for $(1-\alpha)$ n of 2.4. If this exchange current density is compared with that obtained from the low overpotential plot, i.e.

$i_o = 3.02 \times 10^{-4}$ and 2.27×10^{-4} Amp cm^{-2} when n = 3 and 4 respectively, it can be seen that they are all very close. The accuracy in determining the limiting slope from the applied current density tending to zero makes it impossible to differentiate between n = 3 or 4. Earlier work (166,169) suggests than n = 3, and in this case $\alpha = 0.2$. It cannot be said for certain whether the instability of the niobium species produced by dissolution at high current densities was a result of high volatility or chemical instability. The species though was stabilised by increasing the mean ionic radius of the solvent cations, and in the equimolar potassium chloride-caesium chloride, the higher valence species were stable. Linear plots for the "E" versus $\log_{10} (\tau^{\frac{1}{2}}/t^{\frac{1}{2}}-1)$ relationship in all the electrolytes supports a reversible charge-transfer, diffusion controlled reduction step, in

which the reduced species is soluble. The slopes for these plots indicate the process involves the transfer of a simple electron. The constant value for the product $i\tau^{\frac{1}{2}}$ supports the fact that in the caesium containing melt the process ·is diffusion controlled. The fact that the melts were blue in colour indicated that the electroactive species present was niobium (IV) (166). The chronopotentiometric wave can then be interpreted in terms of the reduction of niobium (IV) to niobium (III). The precipitate found in all cases could be ascribed to partially soluble niobium (III) as reported by Dartnell et alia (166).

Hence the probable process occurring in all the electrolytes may be summarised as follows:-

$$Nb^{3+} + 3e \underset{\text{slow}}{\overset{\text{slow}}{\rightleftharpoons}} Nb^{0}$$

$$Nb^{4+} + e \rightarrow Nb^{3+} \quad \text{Primary process}$$

$$Nb^{3+} + 3M^{0} \rightarrow Nb^{0} + 3M^{+} \quad \text{secondary process.}$$

## 6.2. Molybdenum ions in sodium chloride-potassium chloride.

6.2.1. Results.

Attempts to obtain measurements in the equimolar sodium chloride-potassium chloride electrolyte at $765^{\circ}C$ had to be abandoned. The molybdenum species produced by anodic dissolution were far too volatile to obtain satisfactory results.
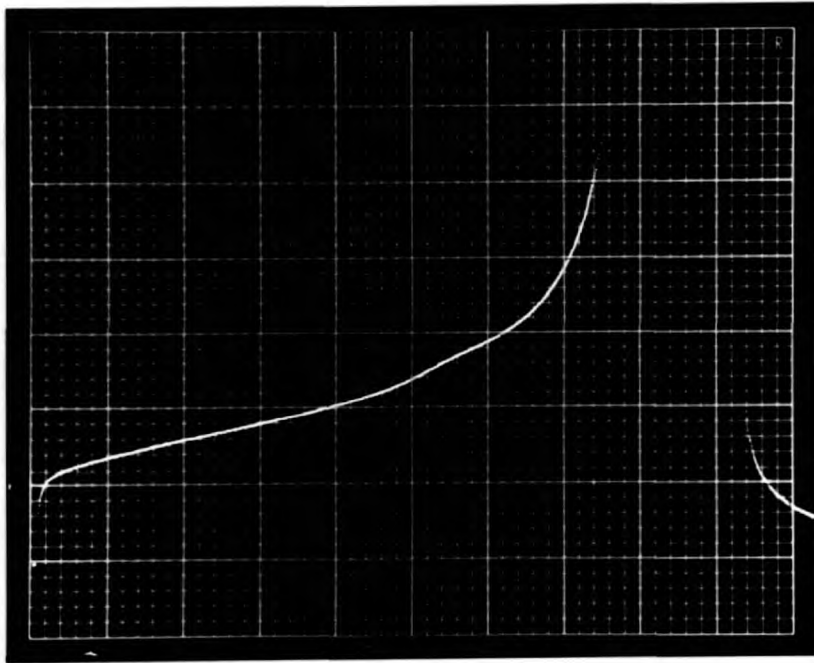
The stability of the molybdenum species in the sodium chloride 20 mole % - potassium chloride 80 mole % at $765^{\circ}C$ was sufficiently increased to allow measurements to be carried out. It must be pointed out though that the molybdenum
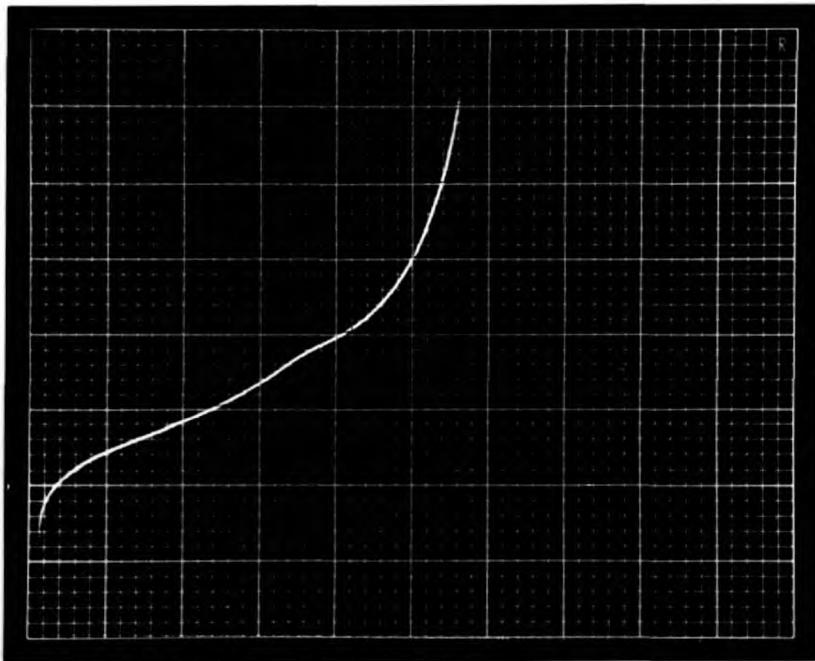
Photograph 6.2.
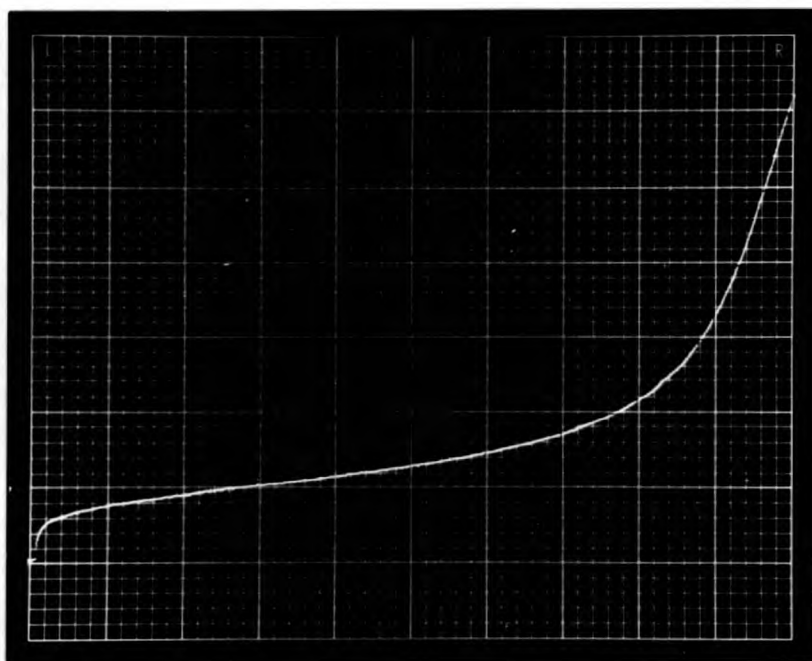
(a) Mo (III) in NaCl - KCl
    $y = 0.1v, cm^{-1}$. $x = 50\,msec, cm^{-1}$.
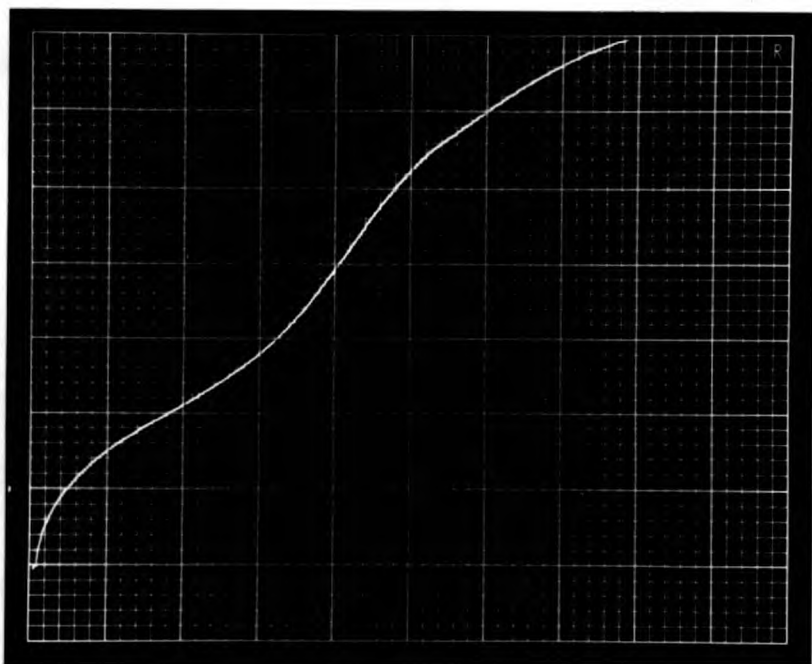
(b) Mo (III) in NaCl - KCl + 0.04 mole % F$^-$
    $y = 0.1\ v, cm^{-1}$ $x = 0.1\ sec, cm^{-1}$.
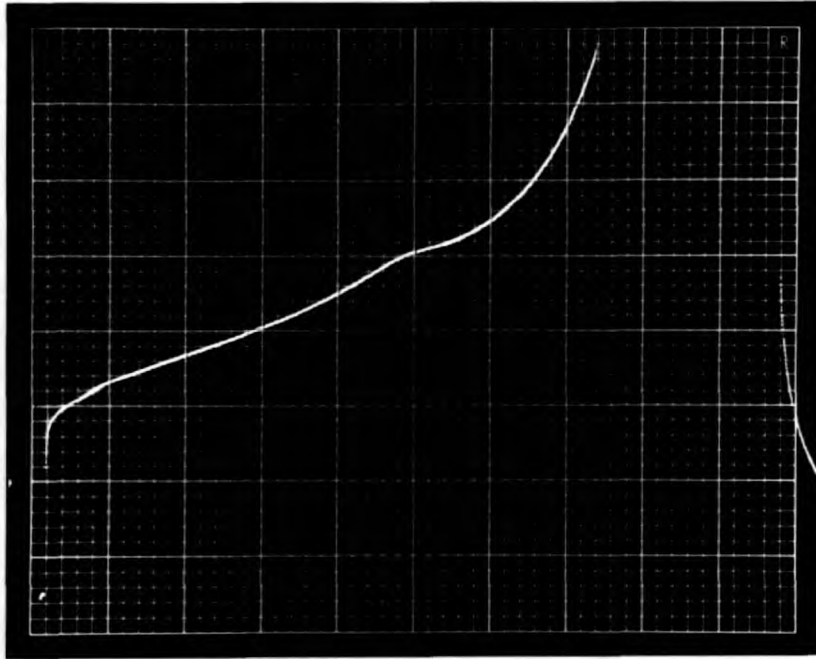
Photograph 6.3.

(a) Mo (III) ions in NaCl-KCl, C ≃ 3 x 10^{-2}M
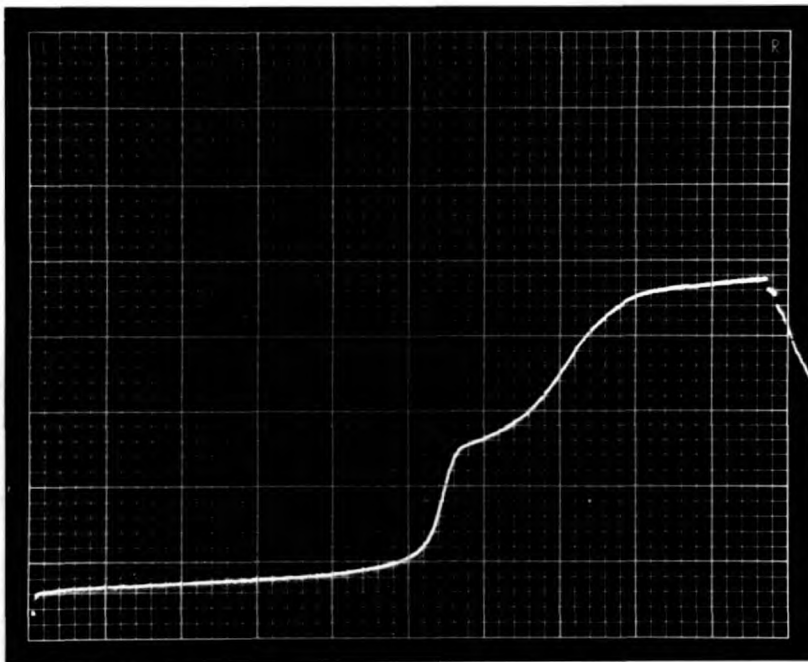y = 0.1 V, cm^{-1} x = 0.1 sec, cm^{-1}.

(b) M$_o$ (III) in NaCl - KCl, C≈6 x 10^{-2}M.
y = 0.05 V, cm^{-1}. x = 0.2 sec, cm^{-1}

Photograph 6.3.

(C) Mo (III) in NaCl - KCl C $\approx$ 7 x 10^{-2} M
y = 0.05 v,cm^{-1}. x = 0.1 sec, cm^{-1}.

(d) M_o (III) in NaCl-KCl C $\approx$ 7 x 10^{-1}M
y = 0.5 V_1cm^{-1} x = 0.1 sec, cm^{-1}.

species was still volatile, and hence only approximate estimates
could be made of the concentration of the species. The molybdenum
was anodically dissolved at a current density of 5 m A, cm^{-2}
At these current densities it was assumed that the molybdenum went
into solution as molybdenum (III). The assumption was based on
the findings of Selis (174) Suzuki (171) and Smirnov and Ryzhik
(175). The density of the melt calculated using equation (5.2),
was 1.54 g cm^{-3} at 765°C. The values for the densities of
sodium chloride and potassium chloride were estimated by
extrapolation to 1038°K the densities calculated from molar
volume values (186).

Molar volume NaCl 1073°K   37.5 cm^3

1189°R   39.2 cm^3

Molar volume KCl 1043°K   48.8 cm^3

1133°K   50.6 cm^3

A single chronopotentiometric reduction wave was observed for
molybdenum (III) concentrations of less than about 2.2 x 10^{-2} M
(See photograph 6.2(a)). Above this concentration a second wave
appeared at a more cathodic potential. At low concentrations the
second wave appeared as a "hump" at the end of the first
original wave but as the concentration was increased, the length
length of the second wave and the potential separation between the
two waves increased (see photograph 6.3(a) to (d)). At
concentrations of above about 2 x 10^{-2}M losses of molybdenum (III)
from the melt were not too significant over the time required
for a set of measurements. Significant losses through
were incurred in between sets of measurements. Examples of values
for the transition time "τ" and the product i $\tau^{\frac{1}{2}}$ are listed in
tables 6.4 for the concentration 1.7 x 10^{-3}M and 6.5 for the

Table 6.4

Molybdenum (III) ions in NaCl 20 mole % - KCl 80 mole %

Concentration = 1.7×10^{-3}M. Electrode area = 3.14 mm^2.

i,mA	τ,msec	$i\,\tau^{\frac{1}{2}}10,^{3}$A.msec$^{\frac{1}{2}}$
0.2681	25.9	1.44
0.2020	45.2	1.36
0.1831	54.1	1.35
0.1330	96.2	1.31
0.1266	102	1.28
0.1150	117	1.24
0.1122	118	1.22
0.09540	142	1.14
0.07619	234	1.17
0.05920	362	1.13
0.04585	555	1.08
0.03999	766	1.11

Table 6.6

Molybdenum (III) ions in Na Cl 20 mole % - KCl 80 mole %.

Concentration = 3.3×10^{-2} M   Electrode area = 3.14 mm^2

i,mA	τ_1,sec.	τ_2,sec.
0.8136	0.687	0.447
1.044	0.496	0.333
1.237	0.392	0.251
1.192	0.422	0.302
1.408	0.348	0.239
1.692	0.275	0.219
2.109	0.224	0.159

Table 6.7

Molybdenum (III) ions in NaCl 20 mole % - KCl 80 mole %

Concentration = 6.8×10^{-2}M   Electrode area = 3.14mm^2

i,mA	$\tau_1$sec	$\tau_2$sec
1.408	0.596	0.346
1.692	0.399	0.250
2.109	0.255	0.165
2.782	0.150	0.0932
3.541	0.0927	0.0614
4.390	0.0631	0.0404
4.930	0.0492	0.0286
6.103	0.0328	0.0155
7.357	0.0232	0.0097

concentration 1.7×10^{-2}M. There is a small but significant loss from the melt at the low concentration, i.e. $i\tau^{\frac{1}{2}}$ decreasing down the table. The values for $i\tau^{\frac{1}{2}}/c$ were at the low concentration 8.6×10^{-4} amp, $sec^{\frac{1}{2}}$ cm $mole^{-1}$ and at the high concentration was 6.6×10^{-4} amp, $sec^{\frac{1}{2}}$, cm, $mole^{-1}$, assuming a correct estimate was made for the concentration. Within the limits of the measurements it is possible to say Sand's equation is obeyed when only one reduction wave is present. The diffusion coefficient estimated from Sand's equation was 6×10^{-6} cm^{2}, sec^{-1}.

Plots of the micro electrode potential "E" versus log_{10} $(\tau^{\frac{1}{2}}/t^{\frac{1}{2}}-1)$ were non-linear when only one wave was present. At low concentrations the beginning of these plots were linear with slopes between 67 and 68 in mV which correspond to a value for "n" of 3 (equation (2.60)). The plots of "E" versus log_{10} $(1-t^{\frac{1}{2}}/\tau^{\frac{1}{2}})$ were linear with slopes varying between 160 mV and 220 mV, which corresponds to values of "n" between 1.3 and 0.94 (equation (2.69)). Examples of the potential-time plots are shown in figures 6.7 and 6.8. Plots of $E_{\tau/4}$ versus log_{10} i (when only one wave was present) were linear with slopes of between 45 and 49 m V (see figure 6.9).

Where fluoride ions were added (up to 0.04 mole %) to the melt of the shape of the single molybdenum (III) reduction wave was altered distinctly. Photograph 6.2 (b) shows a typical wave. The plot of micro electrode potential "E" versus log_{10} $(\tau^{\frac{1}{2}}/t^{\frac{1}{2}}-1)$ approached linearity, with slopes of about 150 mV, i.e. n; 1.4. Plots of "E" versus log_{10} $(1-t^{\frac{1}{2}}/t^{\frac{1}{2}})$ were non-linear. Examples of these plots are shown in figure 6.10.
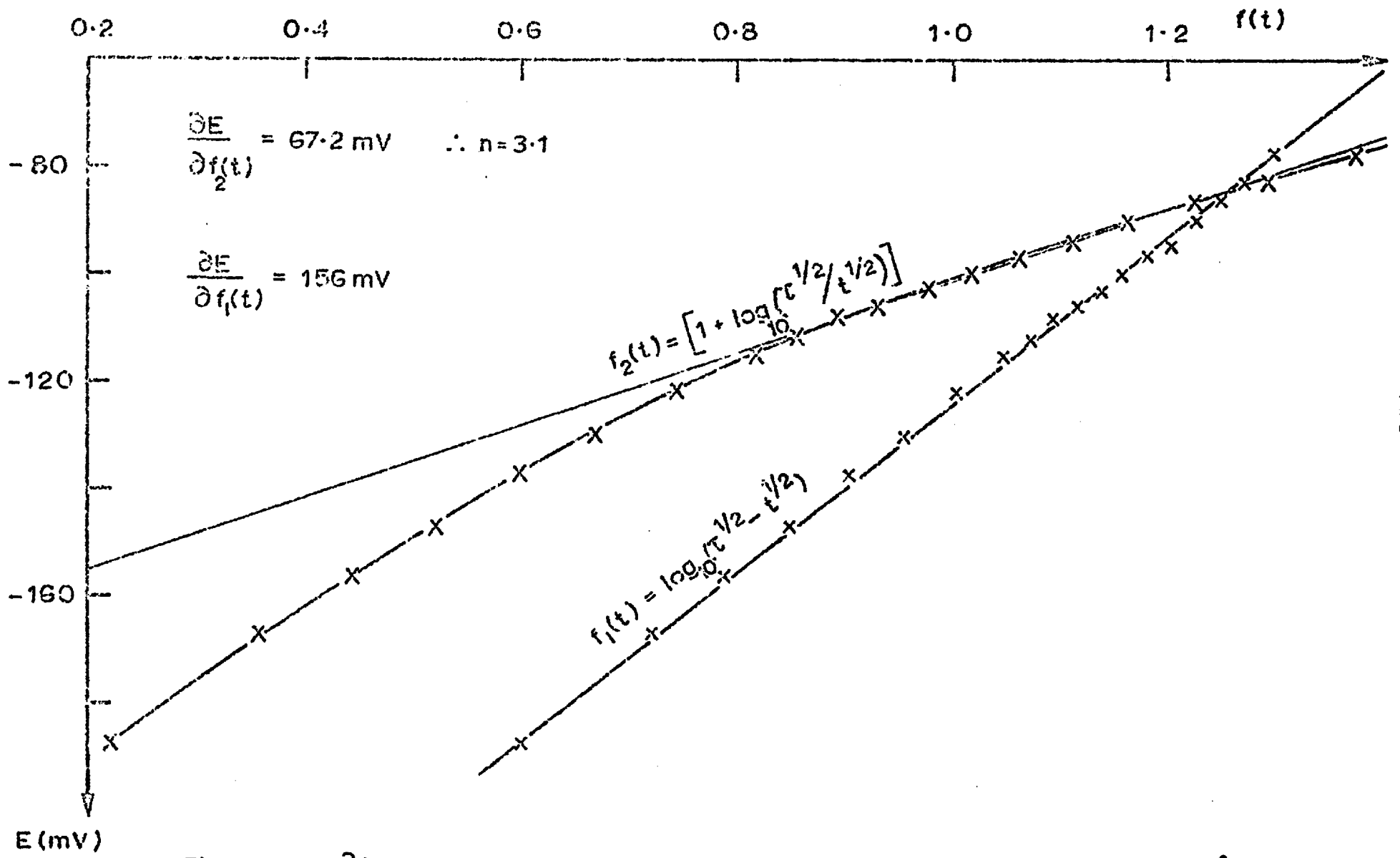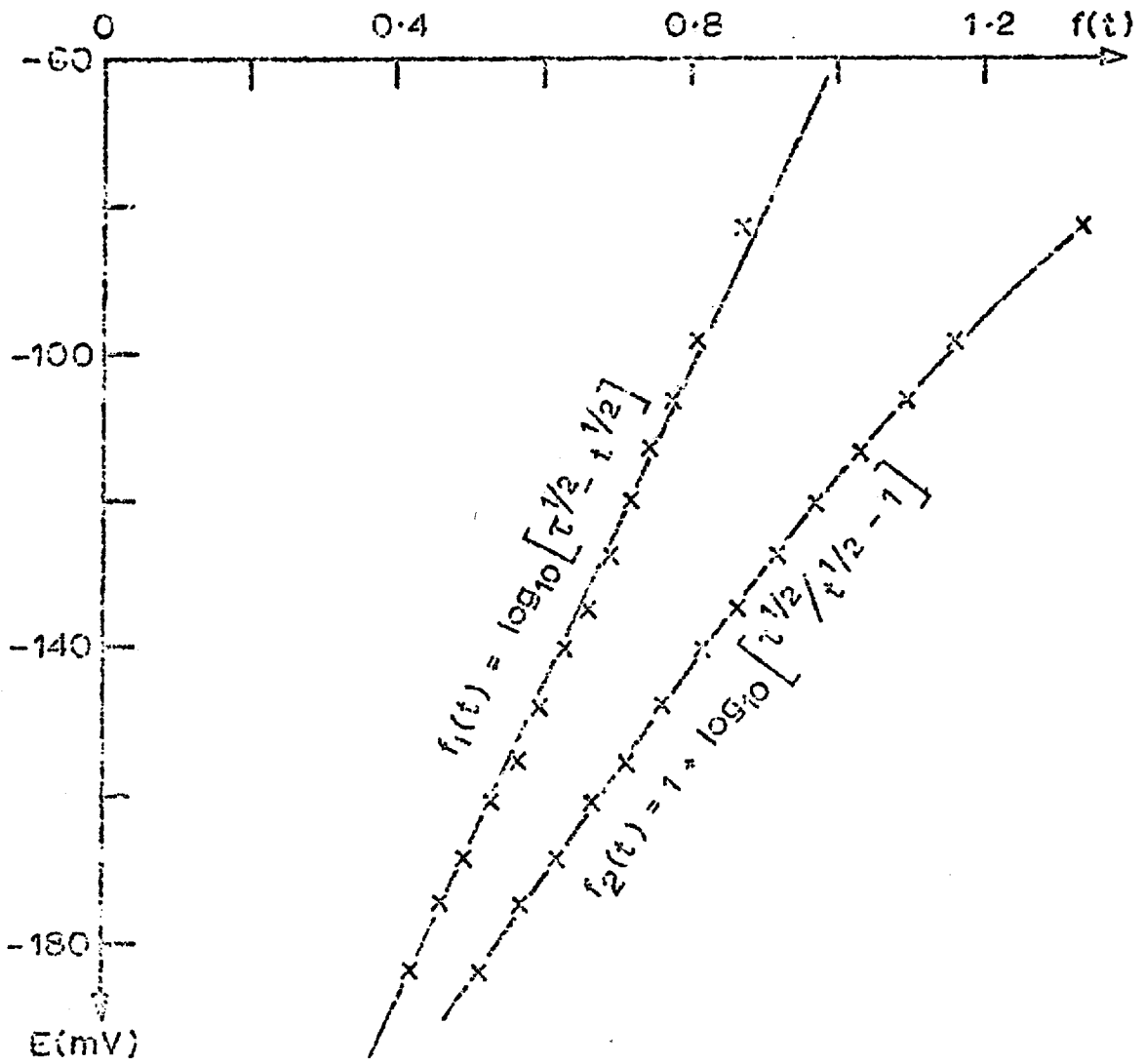
Fig.6.7 Mo^{3+} IN NaCl 20 mole% - KCl 80 mole% $\tau = 80.2$ msec. T = 1035°K

$$\frac{\partial E}{\partial f_2(t)} = 67.2 \text{ mV} \qquad \therefore n = 3.1$$

$$\frac{\partial E}{\partial f_1(t)} = 156 \text{ mV}$$

$$f_2(t) = \left[1 + \log_{10}\left(\tau^{1/2}/t^{1/2} \right) \right]$$

$$f_1(t) = \log_{10}\left(\tau^{1/2} - t^{1/2} \right)$$

E(mV)

f(t)

Fig.6.8 Mo^{3+} IN NaCl 20 mole% - KCl 80 mole% .

$\tau = 118$ m sec.

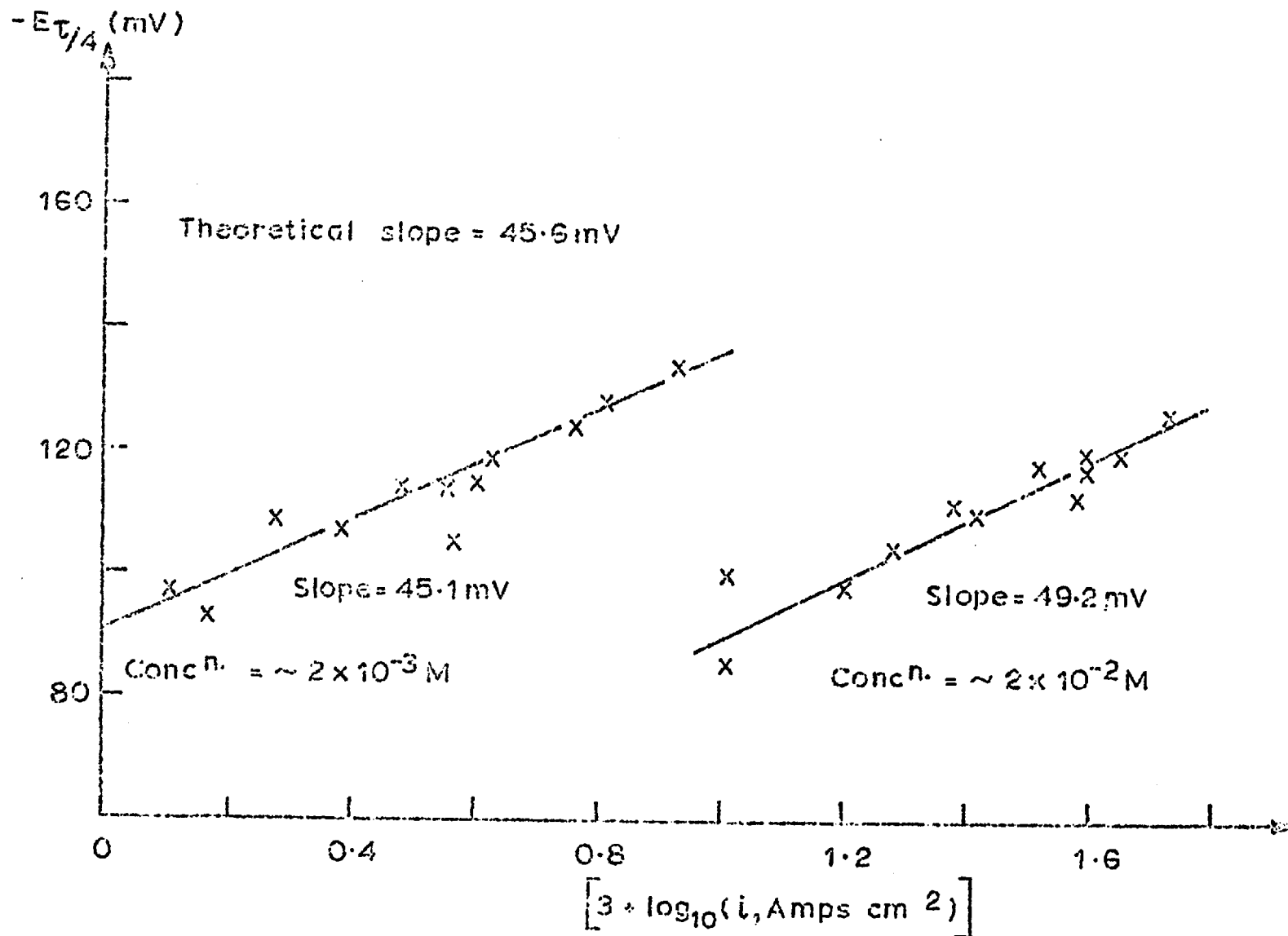$T = 1036°K$

$\dfrac{\partial E}{\partial f_i(t)} = 0.213$ mV
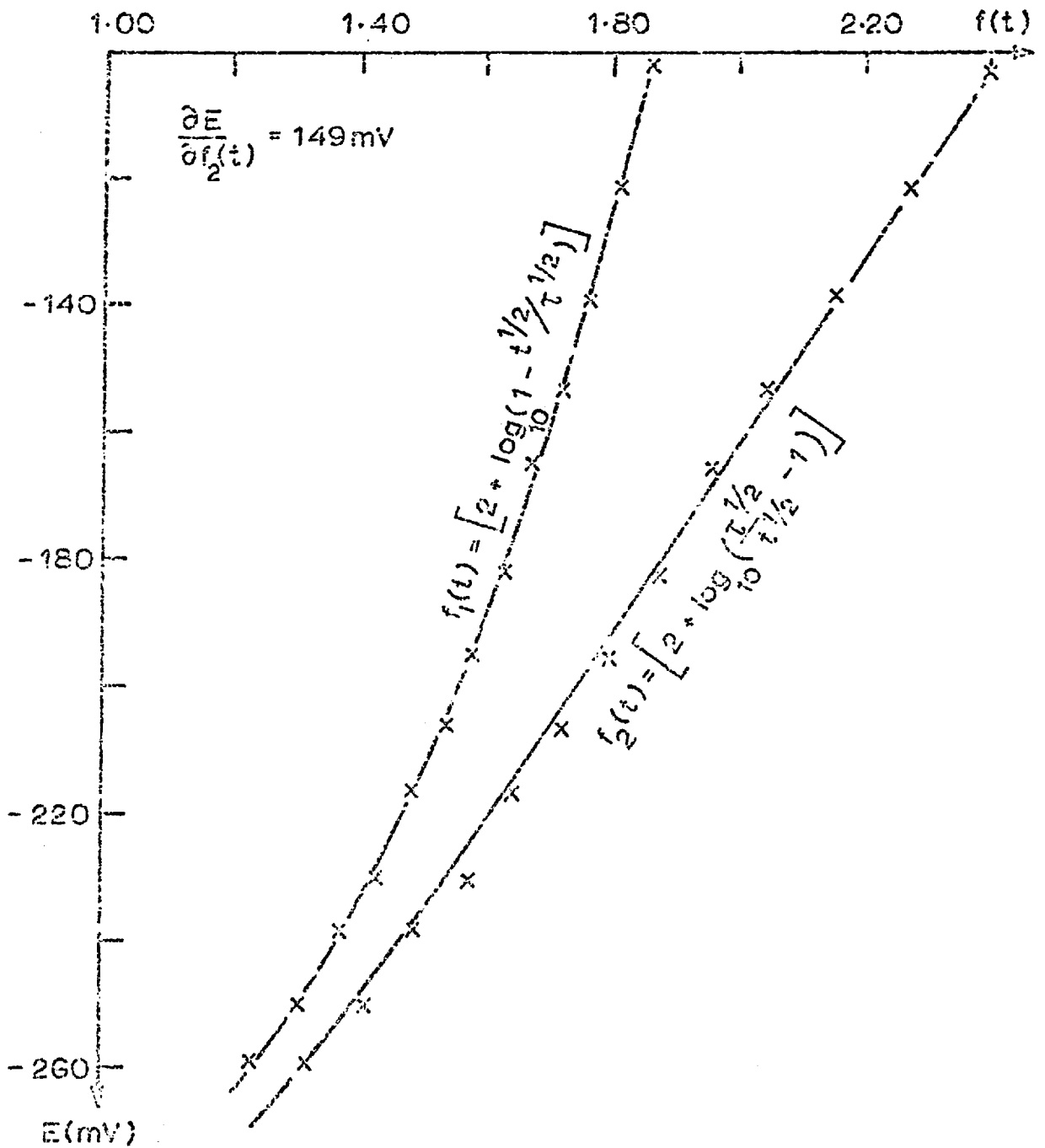
Fig.6.9   Mo^{3+} IN NaCl 20mole% - KCl 80mole%   T = 1034 °K

Fig.6.10 Mo^{3+} IN NaCl 20 mole % + KCl 80 mole %
+ 0·04 mole % F$^-$.

T = 1029 °K τ = 39·2 m sec.

$\dfrac{\partial E}{\partial f_2(t)} = 149\,mV$

$f_1(t) = \left[2 + \log_{10}(1 - t^{1/2}/\tau^{1/2})\right]$

$f_2(t) = \left[2 + \log_{10}\left(\dfrac{\tau^{1/2}}{t^{1/2}} - 1\right)\right]$

Plots for potential-time relationships for the first wave, when two waves were present in the pure chloride, were the same as for the single wave, except "n" varied between 1.0 and 1.5. Examples for the values of the two transition times are given in tables 6.6 and 6.7.

6.2.2. Discussion

The appearance of a second wave, which was more cathodic than the first wave, at higher concentrations is not consistent with the reduction of another oxidation state of molybdenum. Firstly if a higher oxidation state were produced by anodic dissolution at high concentrations, the new wave would appear before the original wave, i.e. at more anodic potentials. If the second wave were the result of the reduction of a lower oxidation state, i.e. the reduction went in two steps the second wave would also be present at low concentrations. It has been shown that the second wave was due to a molybdenum-containing species, since it was enhanced on the addition of more molybdenum. It is apparent therefore the second wave must result from the reduction of a species containing molybdenum in the same oxidation state as the first wave. The only way this could be possible, in a binary melt, is for a multinuclear species to exist, e.g. a dinuclear molybdenum (III) species. In this case the first wave would be due to the mononuclear molybdenum (III) species. Further evidence for the existence of such a large species is the very low diffusion coefficient for molybdenum (III), 6×10^{-6} cm^2 sec^{-1}.

Considering the first wave, the linearity in the plots of microelectrode potential "E" versus $\log_{10}$ $(1-t^{\frac{1}{2}}/\tau^{\frac{1}{2}})$ and the non-integral values for "n" obtained from their slopes indicate

the reduction of molybdenum (III) is irreversible. If the

irreversibility is due to the charge – transfer process the

charge transfer coefficient "n" would be between 0.3 and 0.5

which is not an unreasonable value. The linearity at the start

of the plots of "E" versus log ($\tau^{\frac{1}{2}}/t^{\frac{1}{2}}-1$) and a slope equivalent

to $\eta = 3$, is curious. It suggests that at the start of the

electrolysis at low concentrations, charge transfer would

take place via a reversible three electron step. This would

be expected if the slow step were a chemical step producing

molybdenum (III) ions. The initial part of the chronopotentiometric

wave would then involve the depletion of the free molybdenum (III)

ions present at the start of the electrolysis. If the first wave

were a reduction process involving an irreversible charge transfer

step, then the plot of $E_{\tau/4}$ versus $\log_{10} i$, would have the same

slope as the plots of "E" versus $\log_{10}$ ($1-t^{\frac{1}{2}}/\tau^{\frac{1}{2}}$) c.f. section

2.1.9.2. that is 160 – 220 mV. The slopes though were in the

range 45 – 49 mV, when only one wave was present. If the

process were considered in terms of a homogeneous chemical step i.e.

$$B \xrightarrow[\leftarrow]{\text{slow}} PO \qquad O + ne \xrightarrow{\text{fast}} R$$
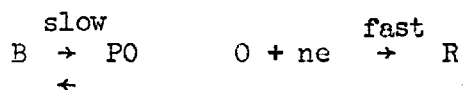
the slope could be considered to be 2.303 X 2 ν RT/$(\rho+1)$nF

c.f. section 2.2.2.3. A slope of 45.6 mV corresponds to

a 3 electron transfer process assuming $p = 2$ and $\nu = 1$.

The slopes for the $E_{\tau/4}$ versus $\log_{10}$ (i) plots support the

rest of the evidence for a slow chemical step, and the involvement

of a dinuclear species, viz

$$Mo_2^{6+} \text{(complex)} \xrightarrow[\leftarrow]{\text{slow}} 2Mo^{3+}$$

$$Mo^{3+} + 3e \rightarrow Mo^{0}.$$
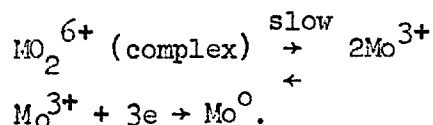
If the diffusion coefficients of the two species were

assumed to be equal, and it was assumed that the current density was high enough to ensure that the dissociation of the complex species species was insignificant, it was possible to gain an estimate for the value of the equilibrium constant. The concentration of the uncomplexed species was estimated from the first wave using Sand's equation, and the concentration for the complexed species was obtained from the second wave using the treatment for the reduction of two different species, c.f. section.

2.1.4. Hence

$$K = \frac{\{ M_o^{3+} \}^2}{\{ M_{o_2}^{6+} \}} \simeq 10^{-6} \text{ mole, litre}^{-1}$$

It must be pointed out that there is no real justification for the assumptions made above, and therefore no great reliance can be placed on the value for the equilibium constant.

The addition of fluoride ions of up to 0.04 mole % changed the shape of the reduction wave markedly. The change was represented by the reversible plot E versus $\log_{10} (\tau^{\frac{1}{2}}/t^{\frac{1}{2}}-1)$ becoming linear, but with a non integral "n" value. This can be interpreted in terms of a decrease in irreversibility of the reduction process even though the value of "n" is not 3. If the multinuclear complex of molybdenum (III) involved chloride liquid bridges as found in the solid state c.f. section 3.4.2. then it is feasible to consider that the fluoride ions would tend to break up the liquid bridges. The breaking up of the liquid bridges would then lead to a greater instability of the multinuclear species, and a decrease in the irreversibility of the reduction process.

## 6.3. Molybdenum ions in lithium chloride-potassium chloride

6.3.1. Results

The molybdenum was anodically dissolved in the eutectic

melt at $567^{\circ}C$, using current densities of 5mA, cm^{-2}. The

density of the melt, given by equation (5.1), was 1.59 g, cm^{-3}.

A single chronopotentiometric reduction wave was observed over the

concentration range of $4.87 \times 10^{-3}M$ to $3.31 \times 10^{-2}M$. An

example of the wave is shown in photograph 6.4(a). The wave

was found to be stable with time and reasonably reproducible.

The product $i\tau^{\frac{1}{2}}$ was found to decrease with applied current

density "i", i.e. a plot of $\tau^{\frac{1}{2}}$ versus 1/i had a negative

intercept at 1/i equal to zero. An example of such a plot is

shown in figure 6.11. The values of the product $i\tau^{\frac{1}{2}}$ and

applied current density "i" could be fitted to the equation

$$i\tau^{\frac{1}{2}} 10^3 = a - b.10^3.i \qquad (6.1)$$

The values for "a" and "b" together with concentration are

listed in table 6.8. It was considered that the scatter of

results did not justify fittings the data to a more complex

relationship i.e. $i\tau^{\frac{1}{2}}$ as a function of $i^{\frac{1}{2}}$ on $i^{4/3}$ for complex

kinetic schemes discussed in 2.1.6.4. The diffusion coefficient

was calculated from the intercept "a", when the applied

current density tends to zero (section 2.1.6).

Values for the diffusion coefficient at different concentrations

are listed in table 6.9. The diffusion coefficient increases

from $(4.4 \pm 0.6) \times 10^{-6}$ cm^2 sec^{-1} to $(7.4 \pm 1.3) \times 10^{-6}$ cm^2 sec^{-1}

for a concentration change of $4.87 \times 10^{-3}M$ to $3.31 \times 10^{-2}M$.

Plots of the micro electrode potential "E" versus

$\log_{10} (\tau^{\frac{1}{2}}/t^{\frac{1}{2}}-1)$ and $\log_{10} (1-t^{\frac{1}{2}}/\tau^{\frac{1}{2}})$ were both non-linear at

long transition times i.e. greater than 500 m sec (Figure 6.12).

At shorter times i.e. about 10 m sec, plots of "E" versus

Photographs 6.4.
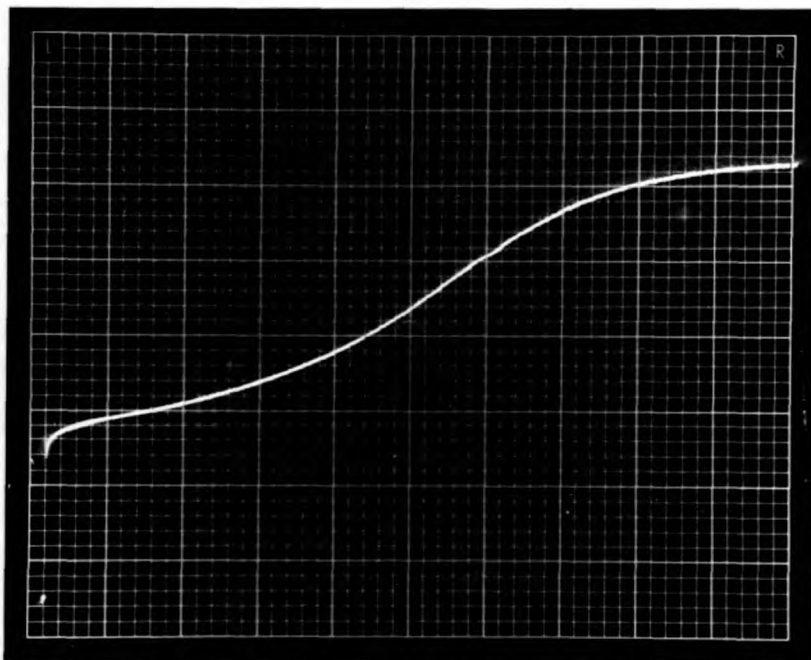
(a) M_o (III) in LiCl - KCl eutectic.
   $y = 0.1V, cm^{-1}$. $x = 0.1$ sec, cm^{-1}.
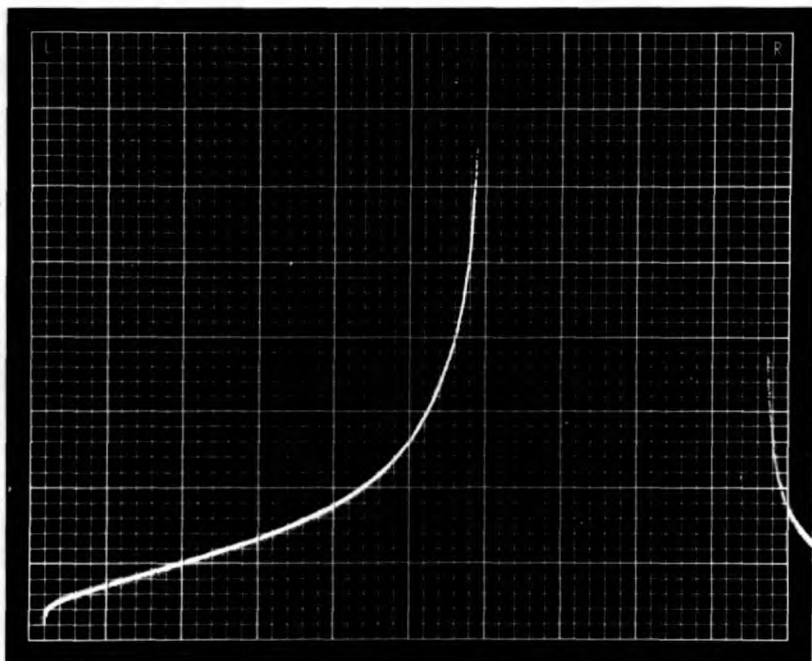
(b) Pt (II) in LiCl - KCl eutectic.
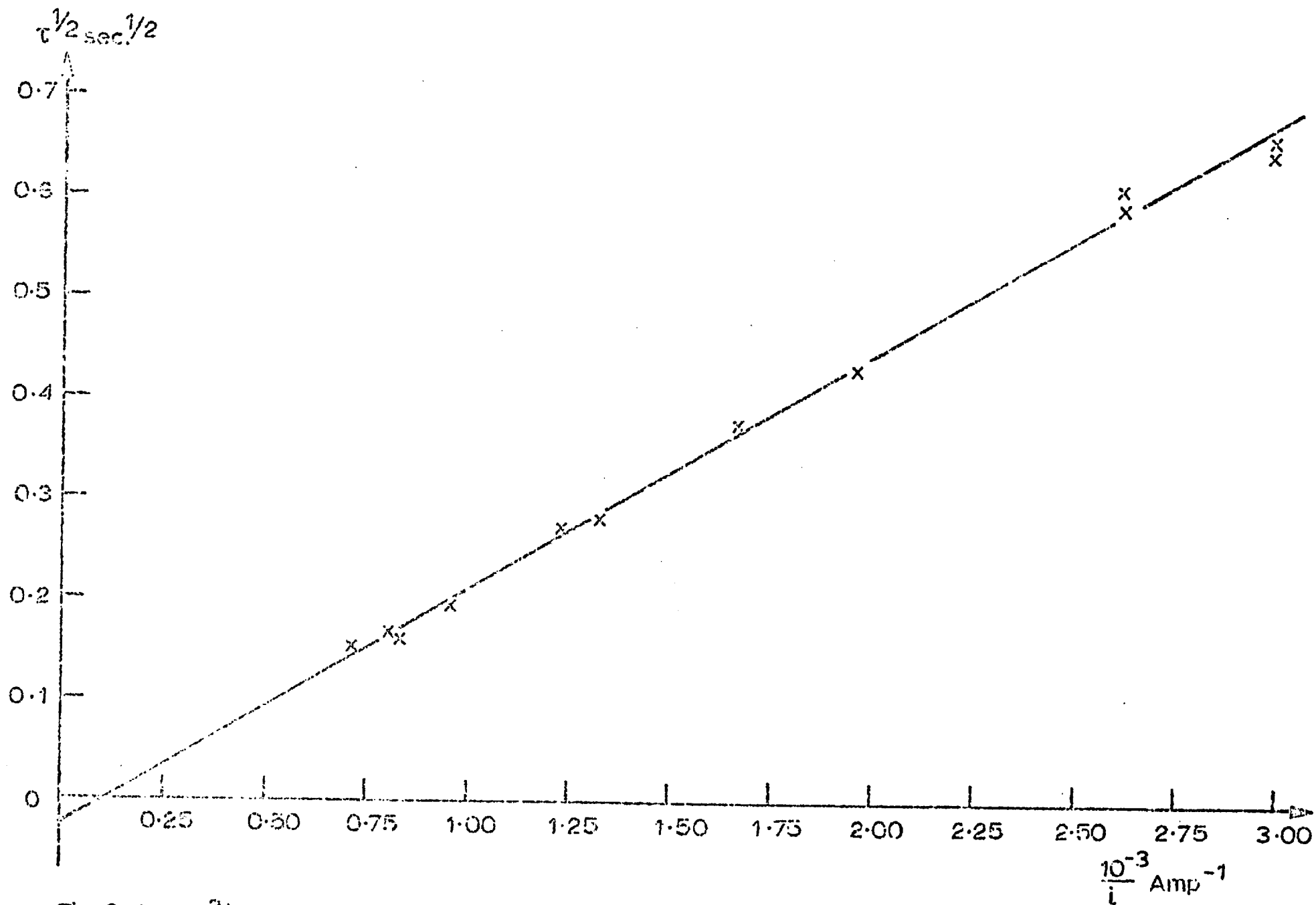 $y = 0.05$ V, cm^{-1}. $x = 0.2$ sec, cm^{-1}.

Fig. 6.11 Mo^{3+} IN LiCl-KCl EUTECTIC T= 839°K. Micro electrode area = 4·52 mm^2.

Mo^{3+} Concn.= 8·77 × 10^{-3} M

Table 6.8

Molybdenum (III) ions in LiCl-KCl eutectic.

Electrode area = A Cm^2

$i\tau^{\frac{1}{2}}.10^3 = a - b.i.10^3$

i = Amps τ = sec.

Conc^n	a/A	b/A
$4.87 \times 10^{-3}M$	2.63	0.199
$6.82 \times 10^{-3}M$	3.83	0.247
$8.77 \times 10^{-3}M$	5.13	0.498
$9.73 \times 10^{-3}M$	5.90	1.03
$3.31 \times 10^{-2}M$	23.0	0.579

Table 6.9

Molybdenum (III) ions in LiCl - KCl eutectic.

Concentration	Diffusion coefficient
4.87×10^{-3}M	$(4.4 \pm 0.6) \times 10^{-6}$,cm^{2}sec^{-1}
6.82×10^{-3}M	$(4.8 \pm 0.7) \times 10^{-6}$,cm^{2}sec^{-1}
8.77×10^{-3}M	$(5.2 \pm 0.5) \times 10^{-6}$ cm^2 sec^{-1}
9.73×10^{-3}M	$(5.6 \pm 0.8) \times 10^{-6}$ cm^2 sec^{-1}
3.31×10^{-2}M	$(7.4 \pm 1.3) \times 10^{-6}$ cm^2 sec^{-1}
3.31×10^{-2}M + 4.44×10^{-2}M, F$^-$	$(5.8 \pm 1.7) \times 10^{-6}$ cm^2 sec^{-1}
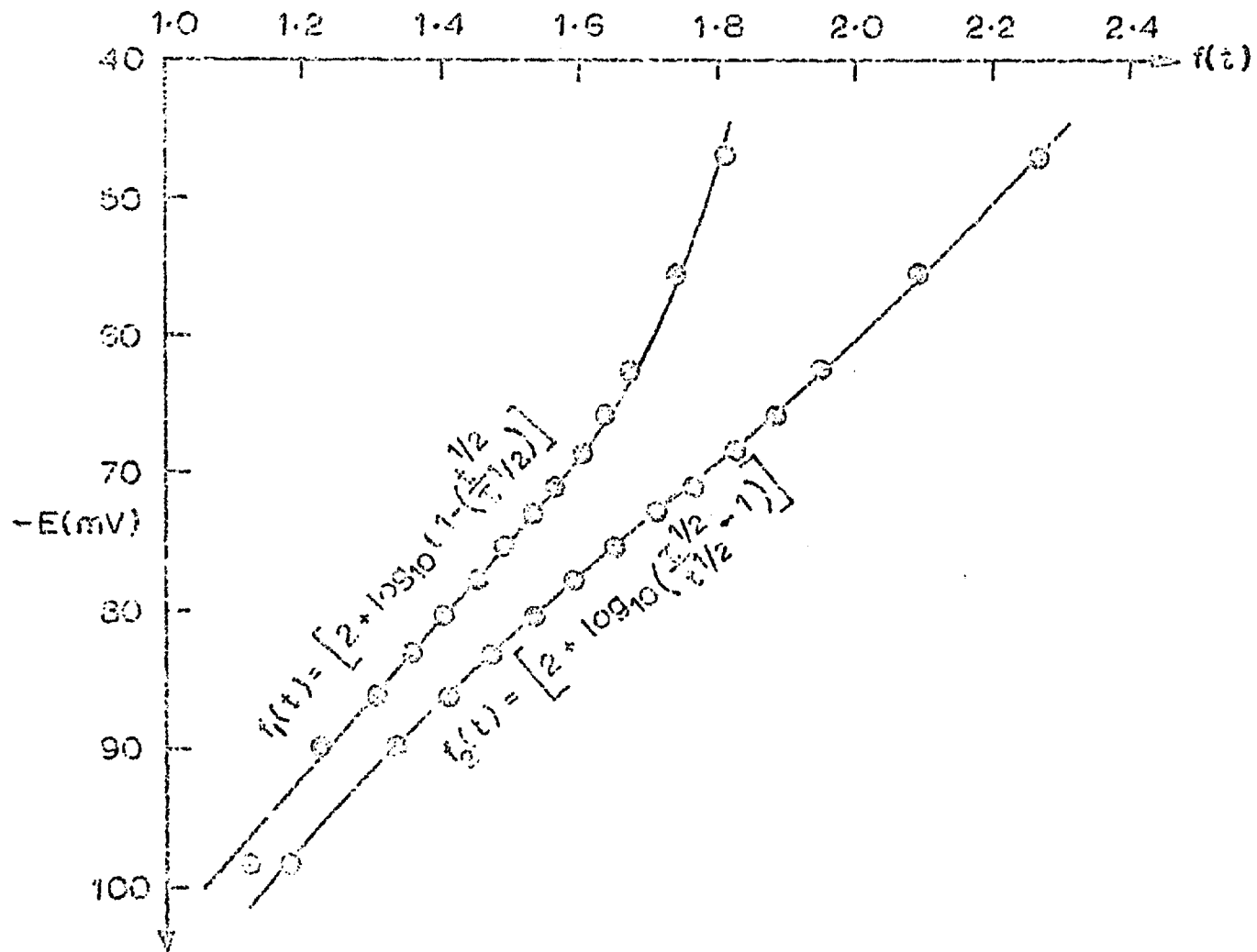
Fig. 6.12   Mo^{3+} IN LiCl-KCl AT 565°C. τ = 19 msec.

$$\frac{\partial E}{\partial f_i(t)} = 132\,mV$$

$$f(t) = \left[2 * \log_{10}\left(1 - t^{1/2}/\tau^{1/2}\right)\right]$$

$$f(t) = \left[2 * \log_{10}\left(\tau^{1/2}/t^{1/2} - 1\right)\right]$$
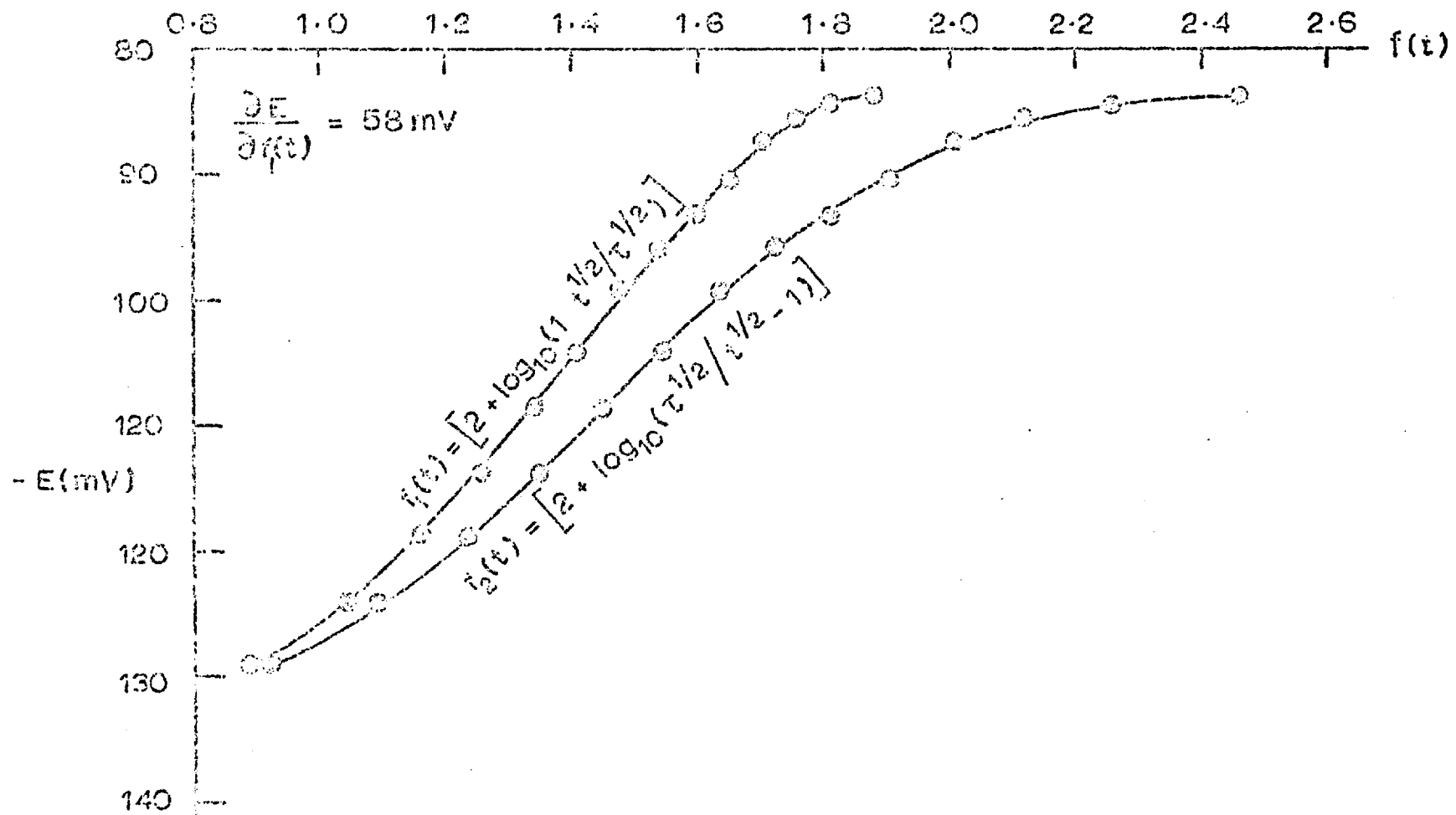
Fig. 6.13 Mo^{3+} in LiCl-KCl at 693°C
$\tau = 505$ msec.
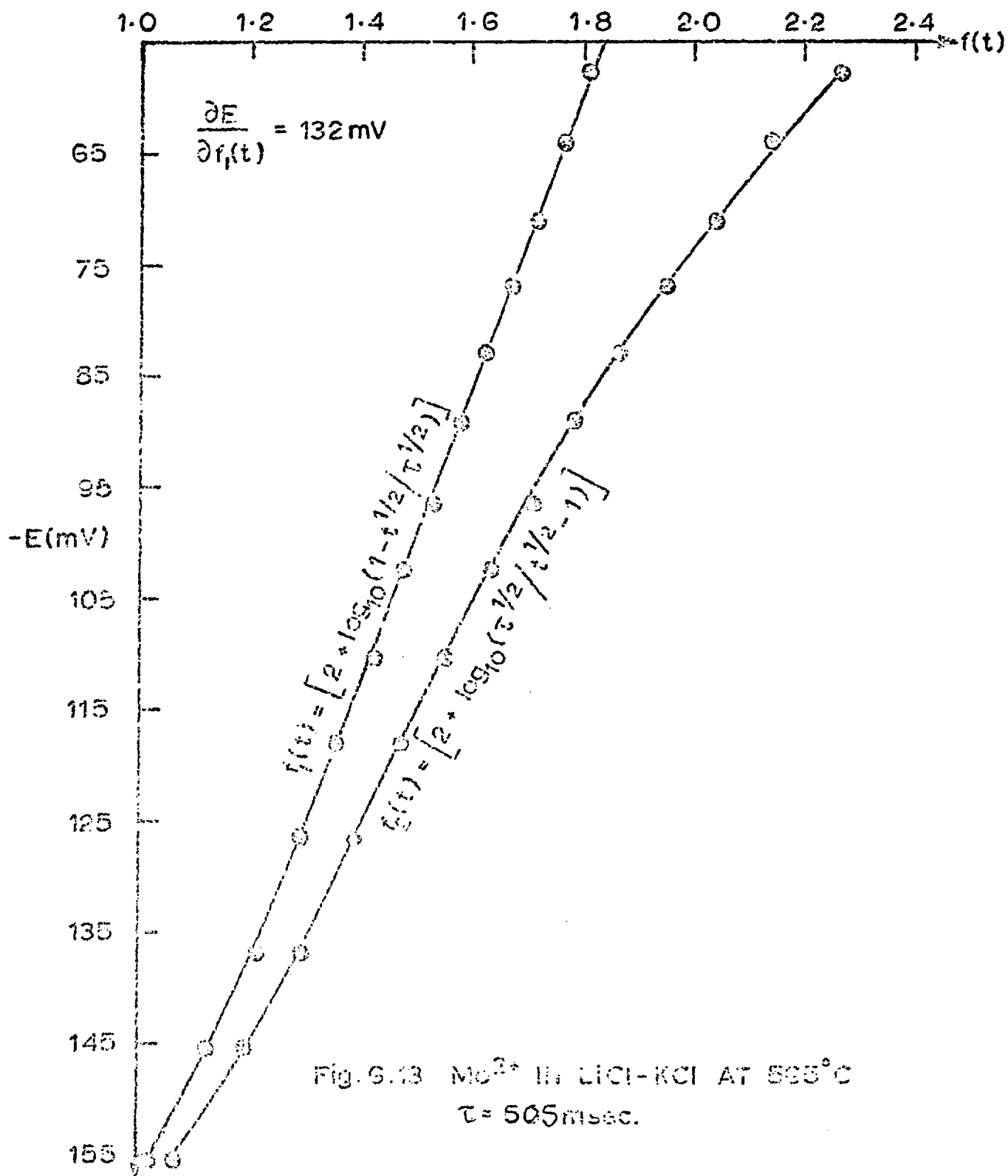
Fig.6.14   Mo³⁺ IN LiCl-KCl AT 565°C +FLUORIDE τ = 330 msec.
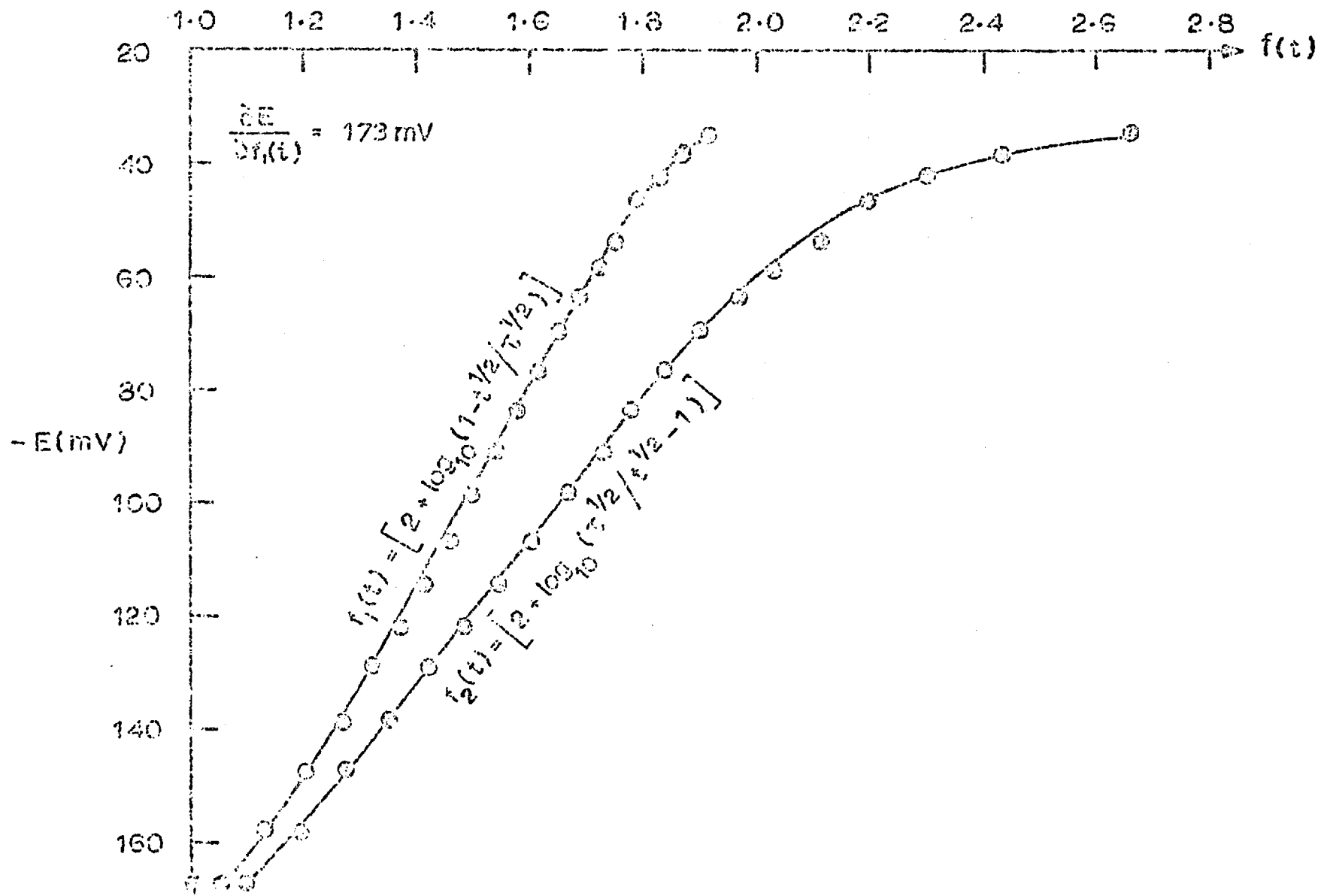
Fig. 6.15 Mo^{3+} IN LiCl-KCl AT 565°C + FLUORIDE $\tau = 10.0$ msec.

$\log_{10} (1-t^{\frac{1}{2}}/\tau^{\frac{1}{2}})$ became linear with slopes of about 130 mV

which corresponds to a value for "αn" of about 1.3.

(Figure 6.13) The addition of fluoride ions to a solution of

3.31×10^{-3} M molybdenum (III) (fluoride concentration of 4.44×10^{-2}M)

did not alter the shape of the curve significantly. The product

$i\tau^{\frac{1}{2}}$ became independant of applied current density, that is it

obeyed Sand's equation. The diffusion coefficient decreased from

$(7.5 \pm 1.3) \times 10^{-6}$ cm^2 sec^{-1} in the pure chloride to (5.3 ± 1.5)

$\times 10^{-6}$ cm^2, sec^{-1}. For a wave of 330 m sec the plot of "E" versus

$\log_{10} (1-t^{\frac{1}{2}}/\tau^{\frac{1}{2}})$ was almost linear with a slope of 58 mV, i.e.

n = 2.9 (Figure 6.14). For a wave of 10 m sec the plot of "E"

versus $\log_{10} (1-t^{\frac{1}{2}}/\tau^{\frac{1}{2}})$ was again almost linear but its slope was

173 mV which gives "αn" = 0.96.

6.3.2. Discussion

The work of Selis (174) Suzuki (171) and Smirnov and

Ryzhik (175) show that molybdenum at low current densities

dissolves as the trivalent ion. The single chronopotentiometric

wave observed was therefore ascribed to the reduction of

molybdenum (III). The decrease of $i\tau^{\frac{1}{2}}$ with increasing current

density is diagnostic of an intervening slow chemical reaction.

If the electrode process were a purely chemical kinetic

controlled reaction the value for "b" would be constant, and

"a" would fit a pure diffusion controlled process (section 2.1.6).

The calculation of the diffusion coefficient from "a" should

give a value independant of concentration "c". This was

not found to be the case. The diffusion coefficient for

molybdenum (III) in pure chloride melt increased with increasing

concentration i.e. "a/c" increased with concentration. The

slope "b" also increased with increasing concentration. These

results indicate that the chemical step is complicated by
another process, which could perhaps be adsorption. Adsorption
would also account for the scatter found for the values of the
transition time.

An intervening chemical step in a binary melt can only
be explained in terms of the slow dissociation of a multi —
nuclear complex species e.g. (molybdenum (III))$_2$. The very
low values obtained for the diffusion coefficient would support
the concept of a large multinuclear species. The low diffusion
coefficient is in agreement with the low diffusion coefficients

observed by Mellors and Senderoff (176) in the same melt at
higher temperatures.

The addition of fluoride ions to the melt lead to the
disappearance of the kinetic effect. At longer transition
times i.e. lower current densities the slopes of the plots of
"E" versus log $(1-t^{\frac{1}{2}}/ \tau^{\frac{1}{2}})$ were equivalent to an "n" value of
virtually three. At high current densities the plot reverted
to that for the wave in pure chloride. The integral value
of an "n" at low current densities fits a reversible process
in which the product of the reduction is insoluble.
Hence it appears that at low current densities the process is
reversible, but not at high current densities.

If the multinuclear complex of molybdenum (III)
involved chloride briding ligands, as found in the solid state,
cf. section 3.4.2. then the inclusion of the small fluoride
ion would tend to break up the ligand bridges.

Hence it would be expected that the addition of fluoride ions would at least reduce the chemical kinetic effect and produce a more reversible electro-reduction process.

There is, however, though one apparent anomaly in the data and that is the decrease in the diffusion coefficient on the addition of fluoride ions. Since the breakdown of the multinuclear species by fluoride ions should lead to smaller species and therefore a larger diffusion coefficient. If, however, the diffusion coefficient measurements in the pure chloride solvent is an apparent value enhanced by adsorption, then such results would be expected. The addition of the strongly complexing fluoride ion would increase the stability of the molybdenum (III) species in solution and hence decrease the adsorption. The reduction in the adsorption of the molybdenum (III) would mean a reduction in the value of $i\tau^{\frac{1}{2}}$ and hence a reduction in the measured diffusion coefficient.

The results fit an electroreduction process of molybdenum (III) which involves a slow chemical step. The slow step can be ascribed to the dissociation of a multinuclear species containing molybdenum (III). However, there is no real evidence to indicate whether the process is homogeneous, or heterogeneous in nature. There is some indication that adsorption could play a part in the electro-reduction process. If this is the case it would suggest that the slow stage is at least in part heterogeneous.

6.4. Platinum ions in lithium chloride-potassium chloride

6.4.1. Results

The platinum ions were anodically dissolved at a current

density of 5mA, cm^{-2} into the eutectic melt at $480°C$.

The Nernst plot of the potential of the platinum counter

electrode versus the logarithm of the concentration of the

platinum ions is shown in figure 6.16. The platinum was

assumed to be present in the divalent state. The potential

of the platinum electrode was measured against the silver-silver

(I) reference electrode. The slope of the Nernst plot was

80.5 mV, which corresponded to an "n" value of 1.9. This

confirms that the anodic dissolution of platinum at current

densities of 5mA, cm^{-2} produces platinum (II) ions. The

equation describing the plot was

$$E = 1.06 + 0.0806 \log C \quad (6.2)$$

Hence the standard electrode potential for the couple platinum -

platinum (II) at $480°C$ in lithium chloride-potassium chloride

eutectic would be 1.06 V (against Ag/Ag^+ $1.18 \times 10^{-2}M$).

Only one reduction wave was observed on chronopotentiograms

for platinum (II). Measurements were carried out in the

concentration range $3.06 \times 10^{-3}M$ to $2.76 \times 10^{-2}M$. The product

$i\tau^{\frac{1}{2}}$ increased slightly with increasing current density, and the

plot of $\tau^{\frac{1}{2}}$ versus $1/i$ exhibited a small positive intercept at

$1/i = 0$ (Figure 6.17). The positive intercept can be

considered in terms of adsorption. Values for the diffusion

coefficient and surface excess calculated from the SAR model

are given in table 6.10 and the same values for the AR.SR model

are given in table 6.11. The adsorption models are discussed

in Chapter 2. Typical plots for the SAR and AR.SR models are

given in figures 6.18 and 6.19 respectively. The shape of a

typical chronopotentiogram is shown in photograph 6.4 (b).

Since the electroreduction of platinum was carried out on platinum

electrodes only, the irreversible model and the
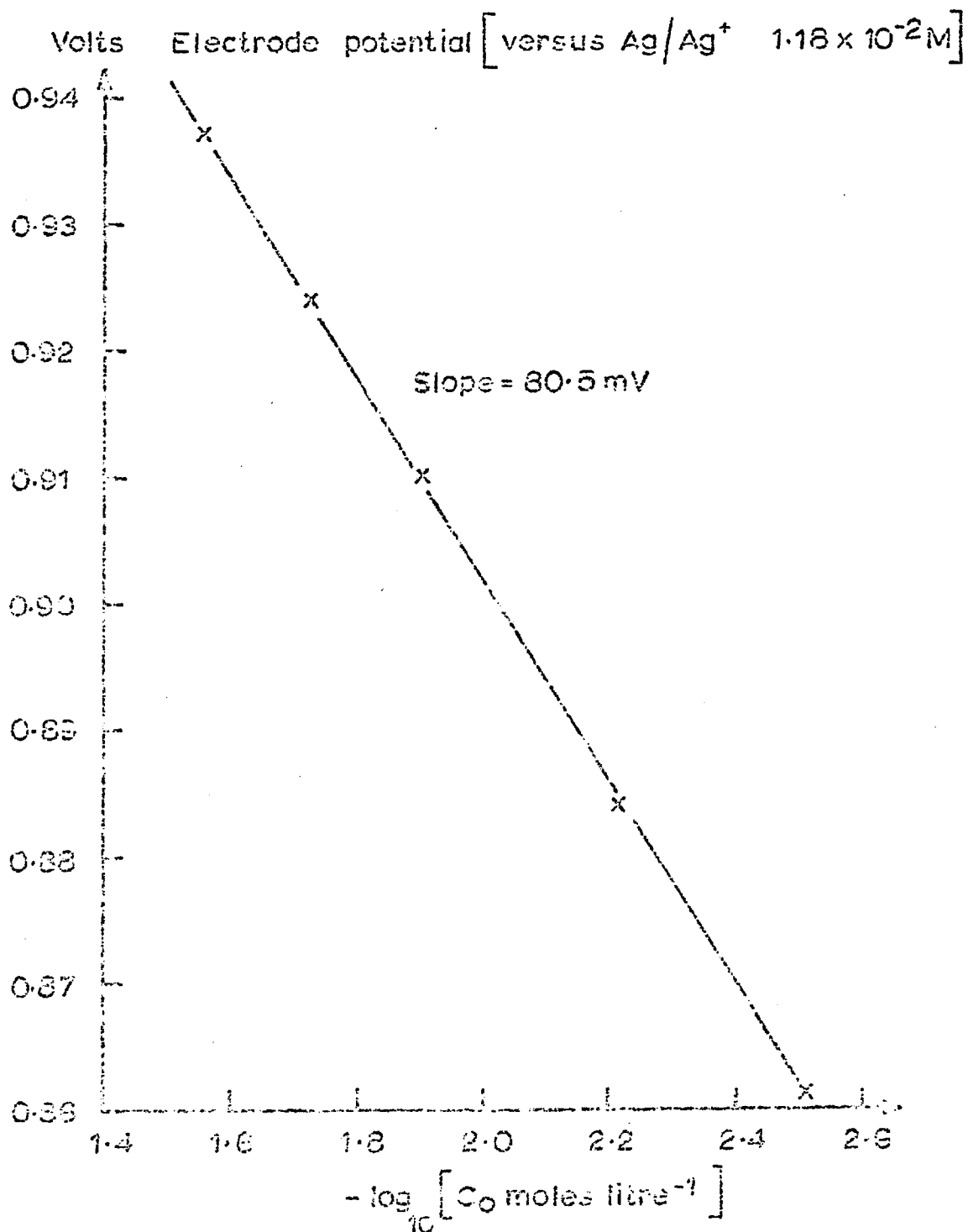
model for electro-deposition at a

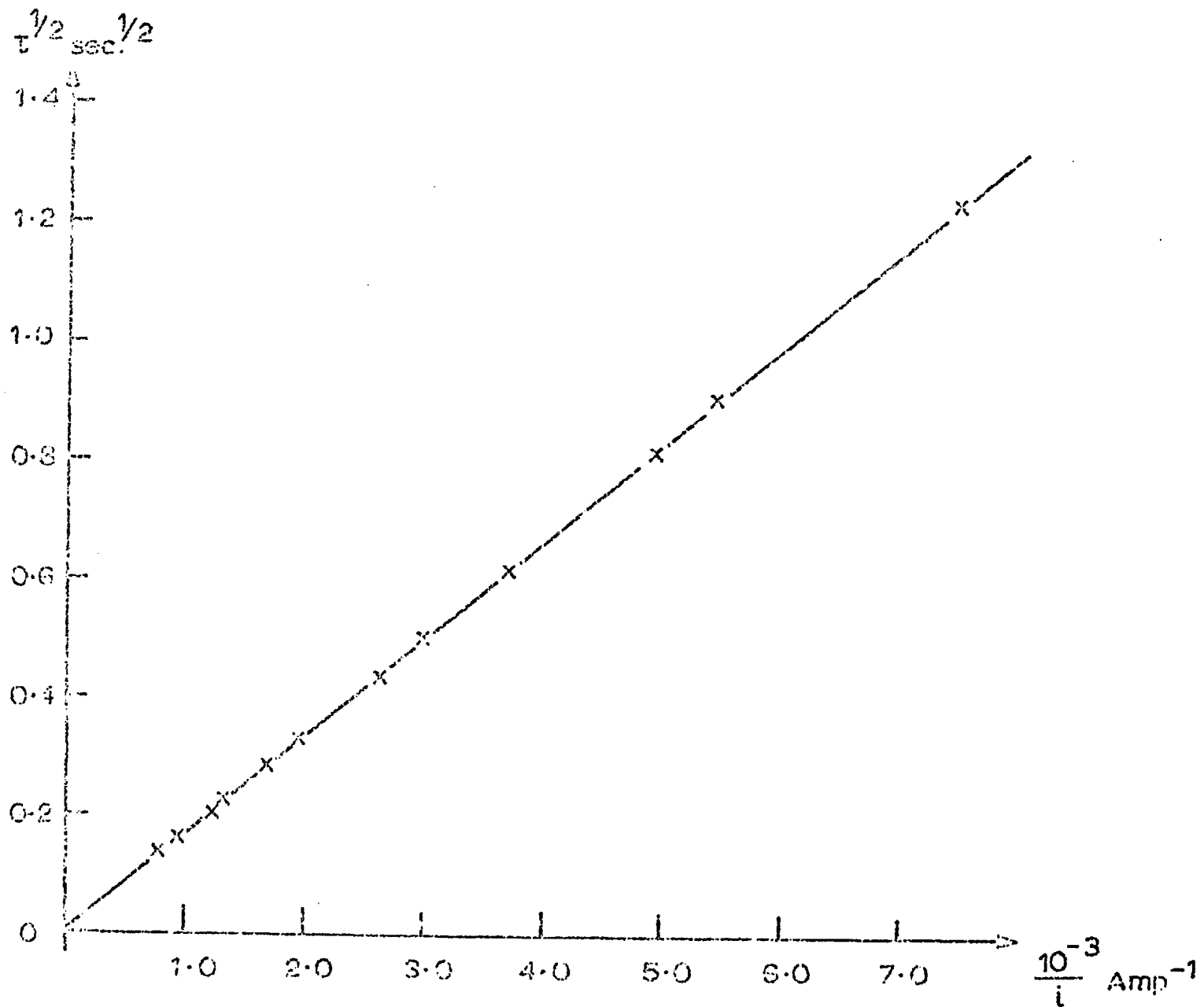Fig.6.16. Pt^{2+} IONS IN LICI-KCI EUTECTIC AT 480°C

Fig.6.17   Pt^{2+} IONS IN LiCl-KCl EUTECTIC AT 480°C. Micro electrode area=3·43mm^2.
Pt^{2+} conc^n. = 6·13 x 10^{-3}M

Table 6.10

Platinum (II) ions in LiCl-KCl eutectic at 480°C

SAR adsorption model.

Concentration moles litre^{-1}.	Diffusion coefficient cm^2 sec^{-1}	surface excess Moles cm^{-2}
3.06×10^{-3}	$(2.08 \pm 0.20) \times 10^{-5}$	1.6×10^{-10}
6.13×10^{-3}	$(2.08 \pm 0.03) \times 10^{-5}$	2.2×10^{-10}
1.23×10^{-2}	$(2.32 \pm 0.05) \times 10^{-5}$	3.2×10^{-10}
1.84×10^{-2}	$(2.46 \pm 0.06) \times 10^{-5}$	1.8×10^{-10}
2.76×10^{-2}	$(2.72 \pm 0.17) \times 10^{-5}$	7.5×10^{-10}

Table 6.11

Platinum (II) ions in LiCl - KCl eutectic at 480°C

AR.SR. adsorption model

Concentration moles litre^{-1}	Diffusion coefficient cm^2 sec^{-1}	Surface excess Moles cm^{-2}
3.06×10^{-3}	$(2.05 \pm 0.20) \times 10^{-5}$	3.9×10^{-10}
6.13×10^{-3}	$(2.08 \pm 0.02) \times 10^{-5}$	4.3×10^{-10}
1.23×10^{-2}	$(2.32 \pm 0.05) \times 10^{-5}$)	6.4×10^{-10}
1.84×10^{-2}	$(2.46 \pm 0.06) \times 10^{-5}$.	3.7×10^{-10}
2.76×10^{-2}	$(2.54 \pm 0.15) \times 10^{-5}$	1.6×10^{-9}

Fig. 6.18 Pt^{2+} IONS IN LiCl-KCl EUTECTIC AT
480°C. PLOT FOR SAR MODEL.
Electrode area = 3.43mm^2
Pt^{2+} concn. = 6.13 x 10^{-3}M

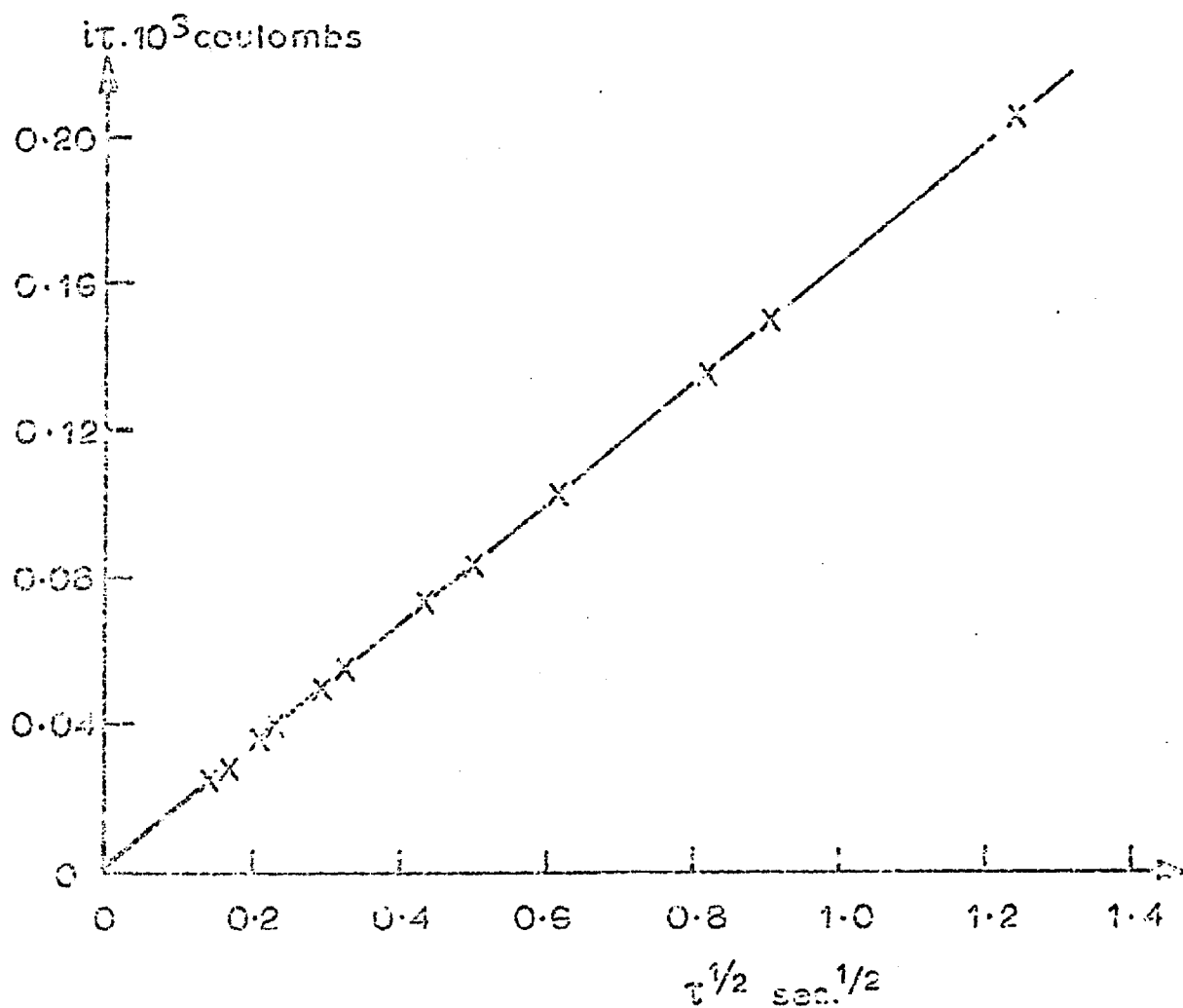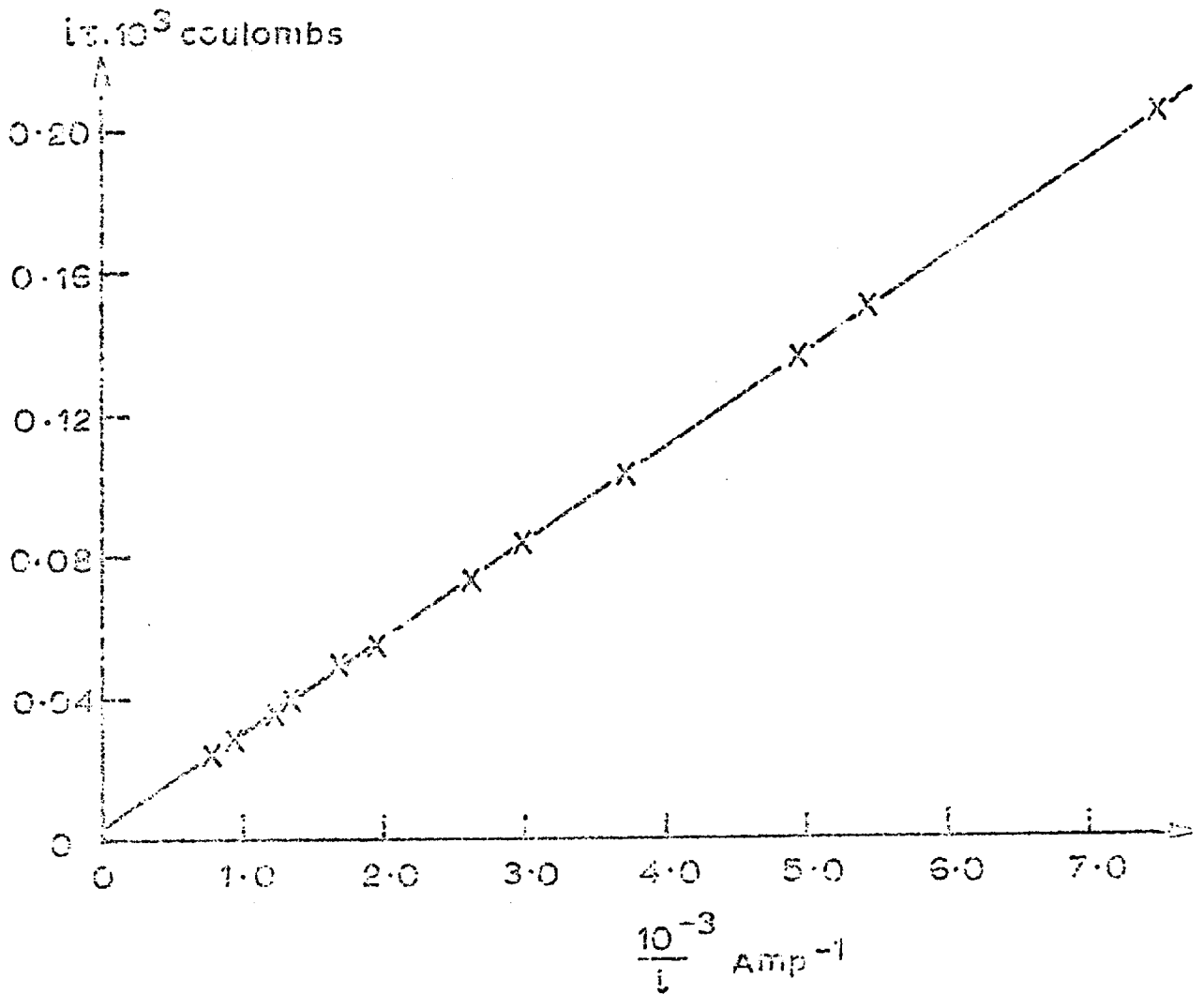Fig. 6.19 Pt^{2+} IONS IN LiCl-KCl EUTECTIC AT 480°C.
PLOT FOR AR.SR MODEL. Electrode area = 3·43mm^2
Pt^{2+} conc^n· = 6·13 × 10^{-3}M

unit activity were applicable, when considering the micro

electrode potential - time relationships c.f. equations (2.62)

and (2.69). Plots of "E" versus log $(1-t^{\frac{1}{2}}/\tau^{\frac{1}{2}})$ were linear

with slopes between 88 and 98 mV i.e. "αn" was between 1.5

and 1.7 a sample plot is given in diagram 6.20. The slopes

were the same, within the above limits, at both long and short

transition times (τ = 16 to 1,540 sec). Fluoride ions were

added to a solution containing 2.76×10^{-2} M platinum (II) ions.

The concentration of fluoride ions added were in the range of

4.65×10^{-2} M to 1.92×10^{-1}M. A small decrease of the product

$i\tau^{\frac{1}{2}}$ with increasing current density was observed e.g. see figure

6.21. This is diagnostic of a slow chemical step. The values

for "a" and "b" for equation (6.1) are listed in table 6.12.

Values for the diffusion coefficient were calculated from the

intercept "a", when the applied current density tends to

zero (section 2.1.6.). The values for the diffusion coefficient

are listed in table 6.13. for different fluoride ion

concentrations. The diffusion coefficient given by the SAR

model for a concentration of 2.76×10^{-2}M platinum (II)

in the absence of fluoride ions was $(2.72 \pm 0.17) \times 10^{-5}$ cm^2 sec^{-1}

This value decreased on the addition of fluoride ions to

$(2.21 \pm 0.10) \times 10^{-5}$ cm^2 sec^{-1} for a fluoride concentration

of 1.92×10^{-1}M. Plots of "E" versus log is $(1-t^{\frac{1}{2}}/\tau^{\frac{1}{2}})$ were

still linear after the addition of fluoride ions. Their slopes

were of the same value as those in the absence of fluoride ions.

Plots of "E" versus $\log_{10} \frac{}{t/4} |i|$ were not linear, see figure 6.22.

6.4.2. Discussion

The potentiometric data is consistent with anodic

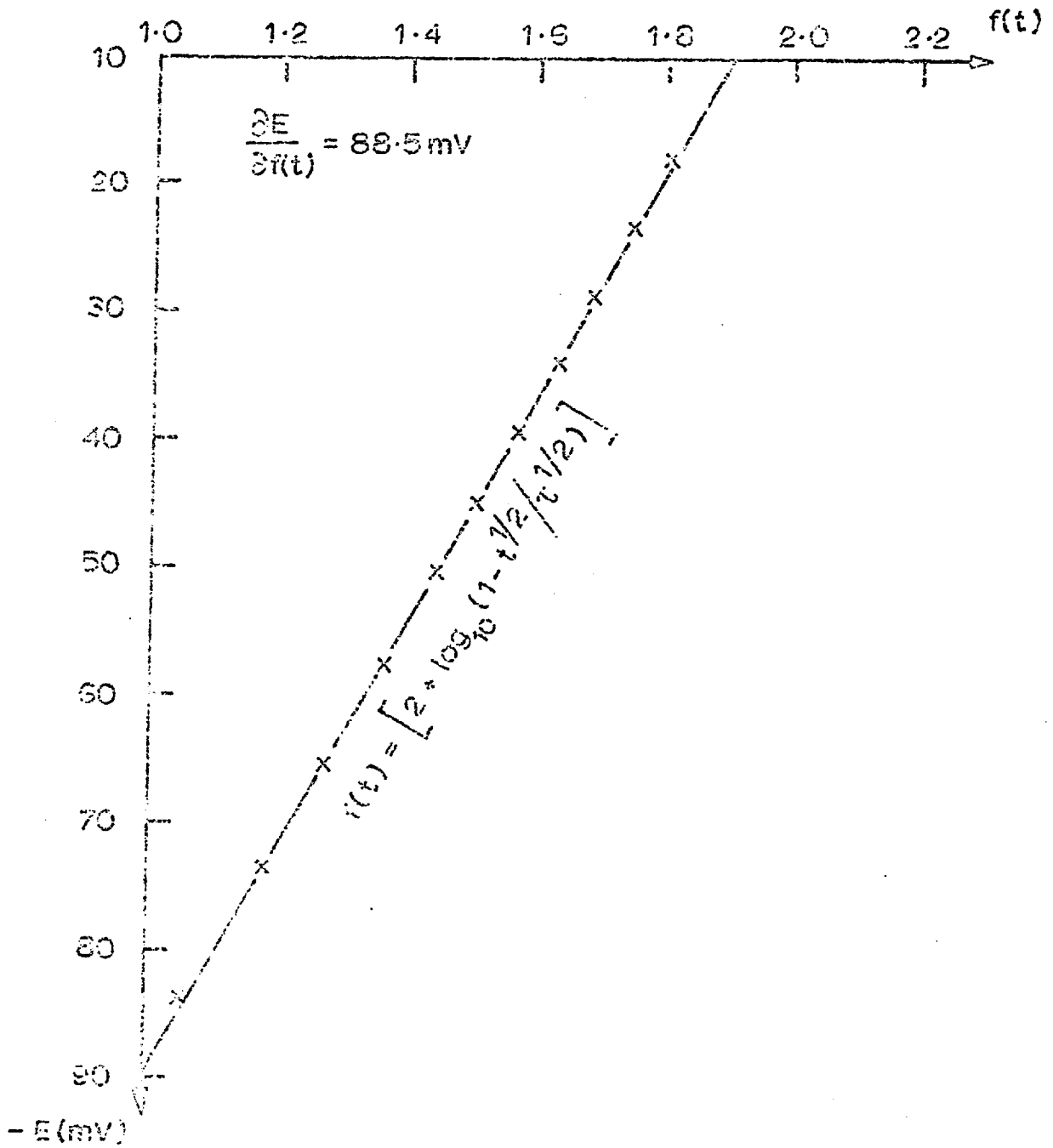dissolution at low current densities (5 m A, cm^{-2}) giving

divalent platinum ions.

Fig.6.20 Pt²⁺ IONS IN LiCl - KCl EUTECTIC AT 450°C
τ = 1220 m sec.

Fig. 6.21 Pt^{2+} IONS IN LiCl-KCl EUTECTIC AT 480°C.
Pt^{2+} conc^n. = 2·76 x 10^{-2} M . F^- conc^n. = 1·92 x 10^{-1} M.
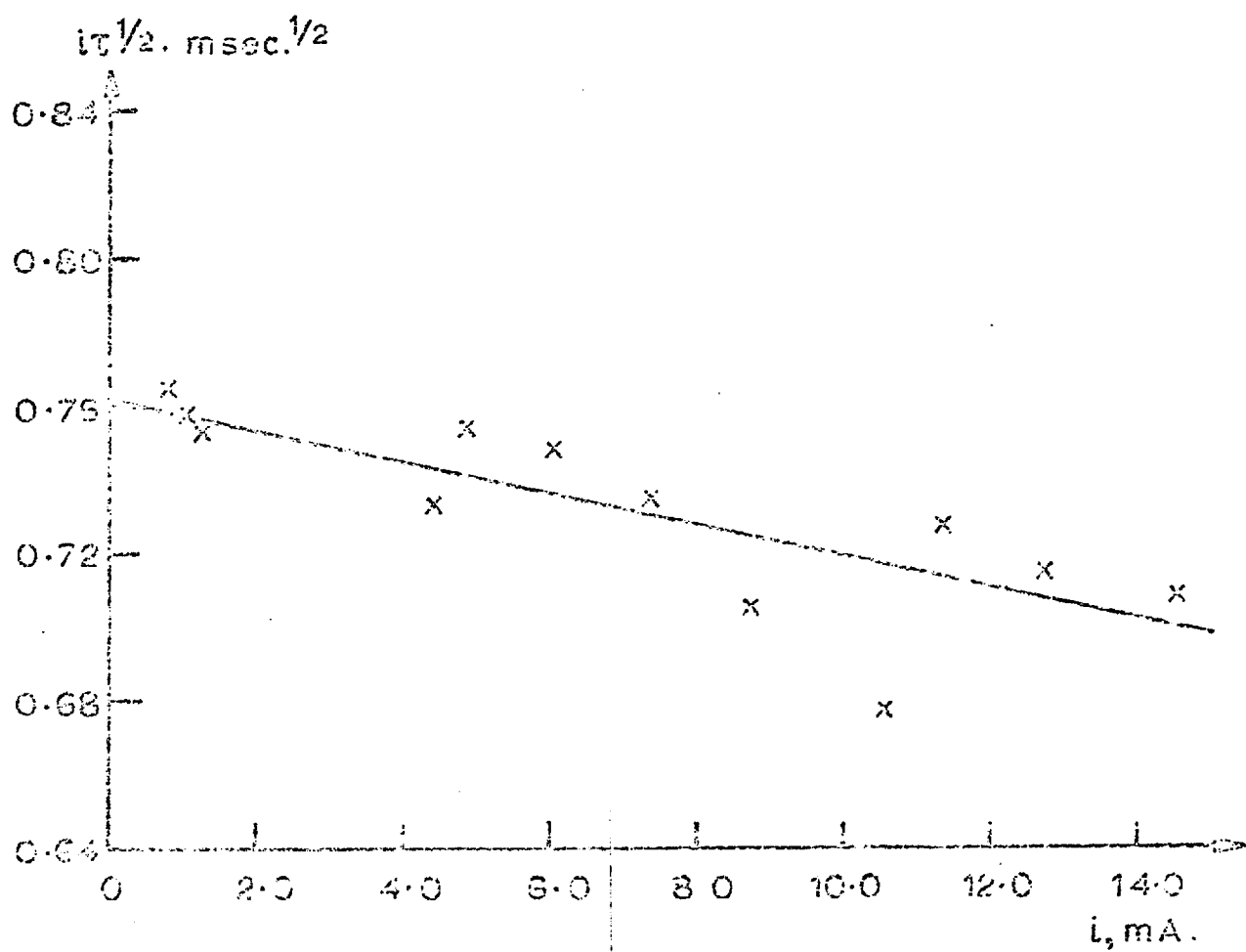Electrode area = 3·43mm^2

Table 6.12.

Platinum (II) ions in LiCl-KCl eutectic at 480°C

Electrode area = 3.43 mm^2

Conc of platinum (II) = 2.76 x 10^{-2}M

$$i\tau^{\frac{1}{2}} 10^3 = a - b.i.10^3$$

i = Amps τ = secs.

F⁻ conc^n	a	b
4.65 x 10^{-2}M	0.804	0.0008
9.15 x 10^{-2}M	0.791	0.0038
1.07 x 10^{-1}M	0.792	0.0019
1.33 x 10^{-1}M	0.790	0.0097
1.92 x 10^{-1}M	0.762	0.0043

Table 6.13

Platinum (II) ions in LiCl-KCl eutectic at $480°C$

Concentration of platinum (II) = $2.76 \times 10^{-2}M$

Conc of F^- ions added moles, litre^{-1}.	Diffusion coefficient cm^2 sec^{-1}.
0	$(2.72 \pm 0.17) \times 10^{-5}$
4.65×10^{-2}	$(2.47 \pm 0.07) \times 10^{-5}$
9.15×10^{-2}	$(2.39 \pm 0.13) \times 10^{-5}$
1.07×10^{-1}	$(2.39 \pm 0.05) \times 10^{-5}$
1.33×10^{-1}	$(2.38 \pm 0.05) \times 10^{-5}$
1.92×10^{-1}	$(2.21 \pm 0.10) \times 10^{-5}$

Fig. 6.22 Pt^{2+} IN LiCl-KCl EUTECTIC AT 480°C.

Conc^n. of Pt^{2+} = 2.76×10^{-2} M

Conc^n. of F^- = 1.92×10^{-1} M

$-E_{1/4}$

$-\log_{10}(i.A.cm^{-2})$
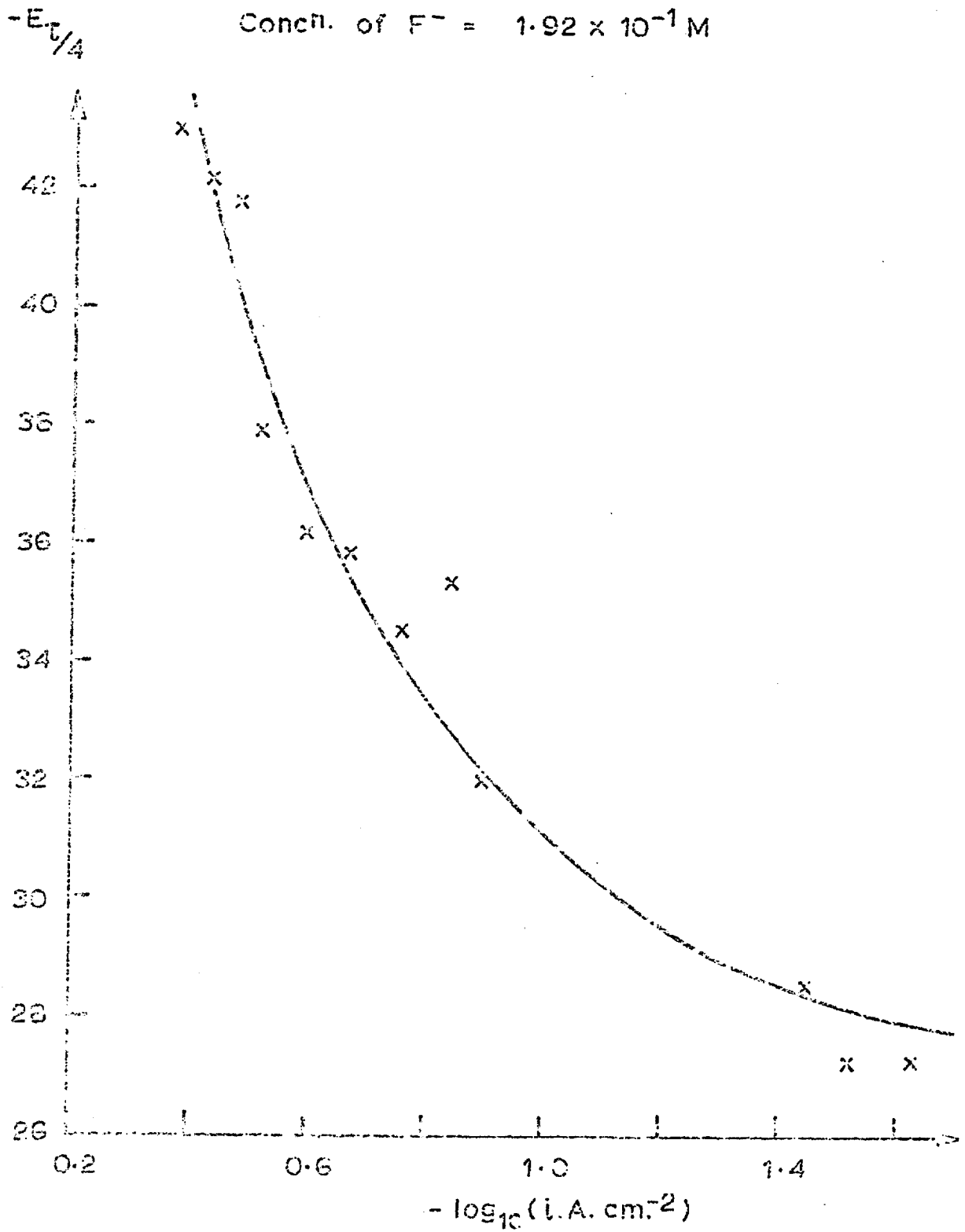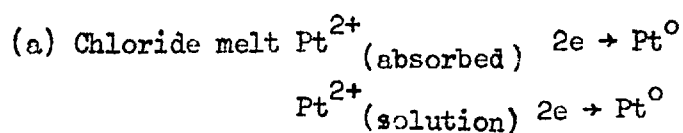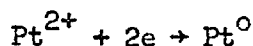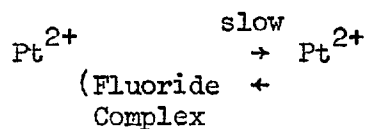
The chronopotentiometric data for the electro-reduction of platinum (II) ions in the pure chloride melt indicated the presence of adsorption of the platinum (II) ions. This is in agreement with the findings of Ukshe and Bukun (187) in their impedance measurement study on the same system at $450^{\circ}C$. The small increase in the diffusion coefficient, using the S.A.R. model (2.08 $\pm$ 0.20) x 10^{-5} cm^2 sec^{-1} to (2.7 2 $\pm$ 0.17) x $10^{-5}cm^2$ sec^{-1} can be explained in terms of an incomplete fit to the absorption model. Other workers (178) have determined the diffusion coefficient for platinum (II) in the same melt at $450^{\circ}C$. The polarographic technique used, gave a value of 1.49 x 10^{-5} cm^2 sec^{-1} which is within reasonable agreement with this value. They made no mention of the presence of adsorption.

The potential time relationships in both the pure chloride and the chloride plus fluoride systems indicate the electro-reduction process is to some degree irreversible with a charge transfer coefficient between 0.75 and 0.85. The value is rather high, one would expect the value to be closer to 0.5. The non-linearity of the plot of $E\tau/4$ versus log i supports the idea of a quasi reversible process.

The slow chemical kinetic effect observed on the addition of fluoride ions can be attributed to the slow dissociation of the platinum (II) - fluoride complex species. It can be considered as direct evidence of a long-lived complex species in a reciprocal salt melt. The proposed electrode process may be summarised as follows :-

(a) Chloride melt $Pt^{2+}_{(absorbed)}$ $2e \rightarrow Pt^{o}$

$Pt^{2+}_{(solution)}$ $2e \rightarrow Pt^{o}$

(b) Chloride plus fluoride melt

$$Pt^{2+} \xrightarrow{\text{slow}} Pt^{2+}$$
$$(\text{Fluoride} \leftarrow$$
$$\text{Complex}$$

$$Pt^{2+} + 2e \rightarrow Pt^{o}$$

The proposed process is not in agreement with the findings

of Inman et alia (188), who propose that the strength of

platinum (II) complexes in fused lithium chloride-potassium

eutectic fitted Ahrland's table (189). They found that the

bromide complex was stronger than the chloride complexes, and

hence it could be inferred that the fluoride complexes would be

weaker than the chloride complexes. If this were the case, then

a kinetic effect should not appear on the addition of fluoride

ions. The only alternative explanation is that the slow

chemical step was also present in the pure chloride melt, but it

was masked by adsorption. This could perhaps account for the

slight increase in the diffusion coefficient for platinum (II)

with increasing concentration of platinum (II) ions. The addition

of fluoride ions reduced the adsorption of platinum (II) ions,

but did not significantly alter the strength of the bulk

complexes. The quasi-reversibility of the reduction process

could then be attributed to a slow chemical step. There is

evidence from X-ray diffraction studies (190) that solid

platinum dichloride exists as $Pt_6 Cl_{12}$ clusters involving

chloride bridging type structures. The slow chemical

step could then be attributed to the dissociation of a

multinuclear complex species.

$$Pt_n^{2n+} \underset{\leftarrow}{\overset{\text{slow}}{\rightarrow}} nPt^{2+}$$

$$Pt^{2+} + 2e \rightarrow Pt^{o}$$
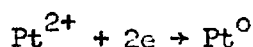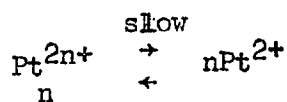
6.5. Tantalum ions in sodium fluoride-potassium fluoride

6.5.1. Results

Experiments were carried out in the molten sodium fluoride 40 mole % - potassium fluoride 60 mole % at $730^{\circ}C$. The density of the melt at this temperature is 2.01 g cm^{-3} (121). The tantalum (V) ions were added as the complex fluoride salt K_2TaF_7.

Great difficulty was experienced in obtaining results which were in any way reproducible. Too often the chronopotentiometric waves were almost totally coulombic i.e. not diffusion controlled, which would be expected for the discharge of oxide films on the electrode surface. The problems appeared to be associated with the presence of oxide in the melt. However, it was possible to obtain a set of data at onø concentration of tantalum (V) using a platinum and a tantalum micro electrode.

Two reduction waves were observed on the chronopotentiograms using the platinum micro electrode. The second, more cathodic, wave was so close to the melt decomposition voltage, that it merged with the melt decomposition wave (photograph 6.5(a). The product $i\tau^{\frac{1}{2}}$ for the first wave was independent of applied current density, and the plot of $\tau^{\frac{1}{2}}$ versus $1/i$ passed through the origin (Figure 6.23 and table 6.14). The plot of the micro electrode potential "E" versus $\log_{10}$ $(\tau^{\frac{1}{2}}/t^{\frac{1}{2}}-1)$ was virtually linear with slopes of the order of 73 mV which corresponds to $n = 2.7$. The plots of "E" versus $\log_{10}$ $(1-t^{\frac{1}{2}}/\tau^{\frac{1}{2}})$ were non-linear. Figure 6.24. Assuming the number of electrons "n" involved in the first wave was 3, the diffusion coefficient was calculated from Sand's equation.

$$D = (5.09 \pm 0.54) \times 10^{-5} \text{ cm}^2 \text{ sec}^{-1}.$$

Photograph 6.5.
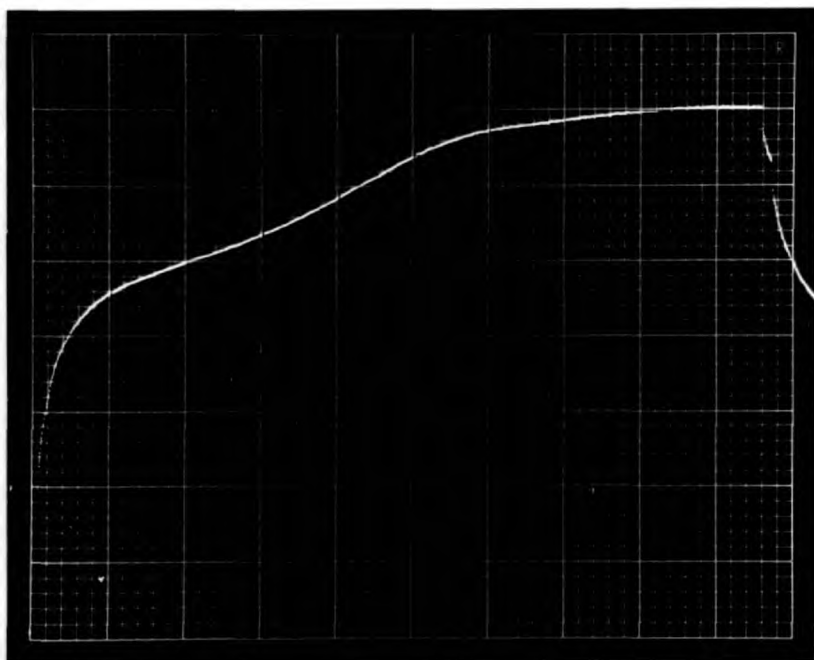
(a) Ta (V) in NaF-KF. Platinum micro electrode
    y = 0.1v, cm^{-1}.   x = 0.1 sec, cm^{-1}.
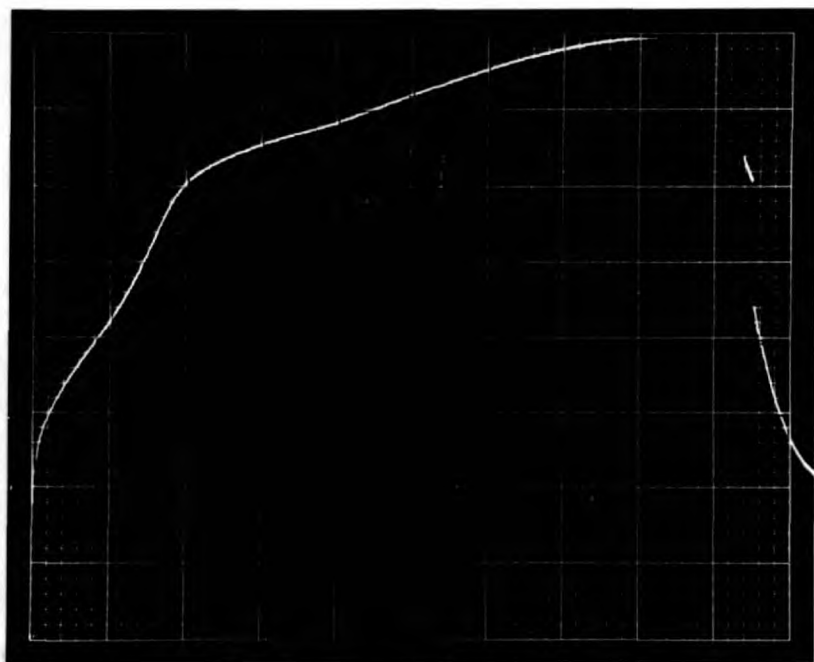
(b) Ta (V) in NaF - KF. Tantalum micro electrode.
    y = 0.1V, cm^{-1}.   x = 0.1 sec, cm-1
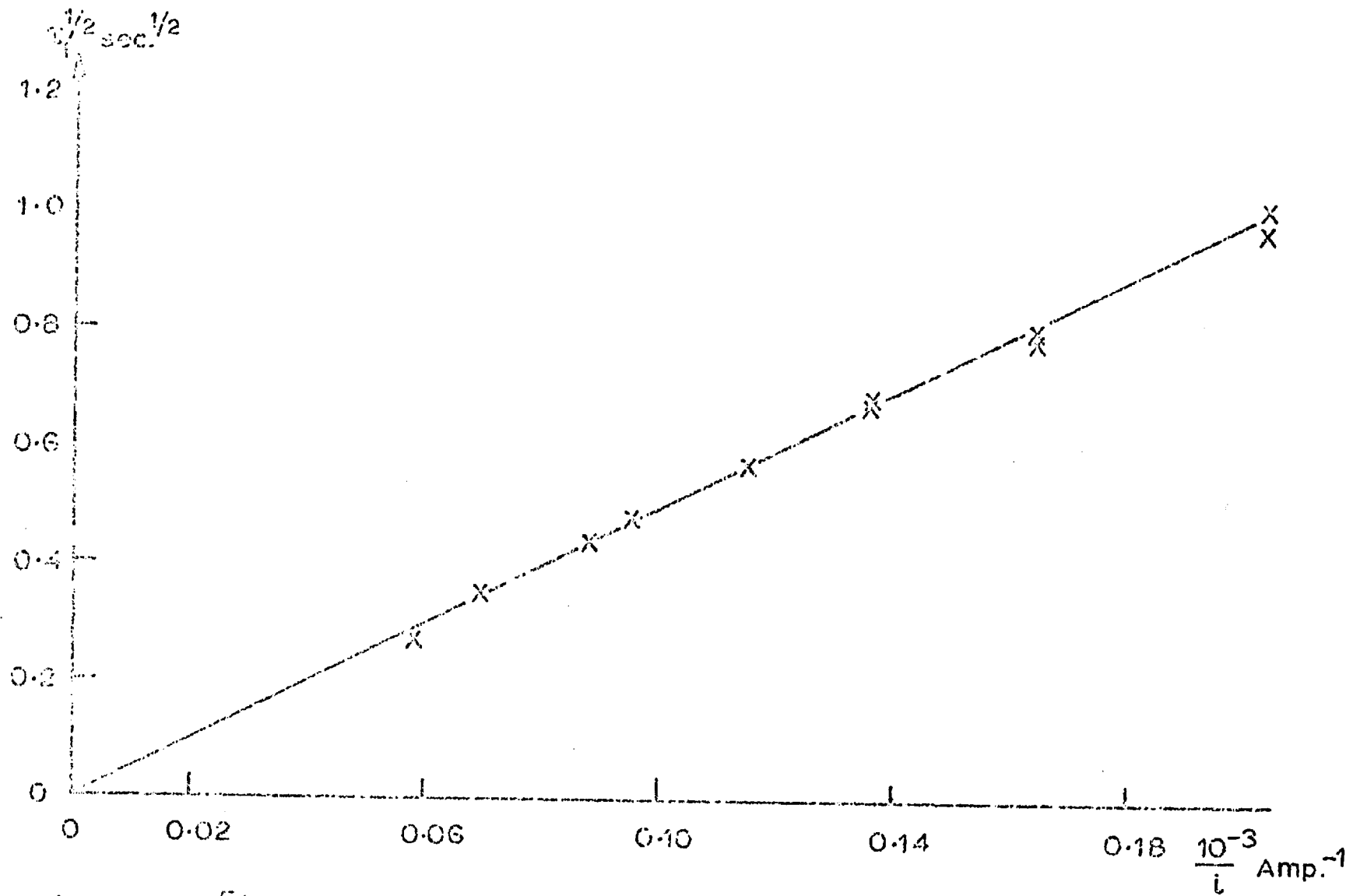
Fig.6.23 Ta^{5+} IN NaF 40mole% + KF 60mole%. Pt micro electrode area = 19.5mm2. Conc^n. Ta^{5+} = 1.37 × 10^{-2} M

Table 6.14

Tantalum (V) in NaF 40 mole% - KF60 mole %

Platinum mirco electrode area = 19.5 mm^2

Concentration of Ta(V) = 1.37 x $10^{-2}M$

i, mA	τ_1, sec	$i\,\tau_1^{\frac{1}{2}}10^3$, A. $sec^{\frac{1}{2}}$
4.930	1.04	5.02
6.103	0.619	4.80
7.357	0.477	5.08
8.710	0.324	4.96
10.51	0.228	5.02
11.37	0.197	5.04
14.52	0.125	5.13
17.15	0.0739	4.66
4.930	0.951	4.81
6.103	0.645	4.90
7.357	0.483	5.11

$\dfrac{\partial E}{\partial f(t)} = 73\,mV$

$f_2(t) = \left[2 * \log_{10}(1 - t^{1/2}/\tau^{1/2})\right]$
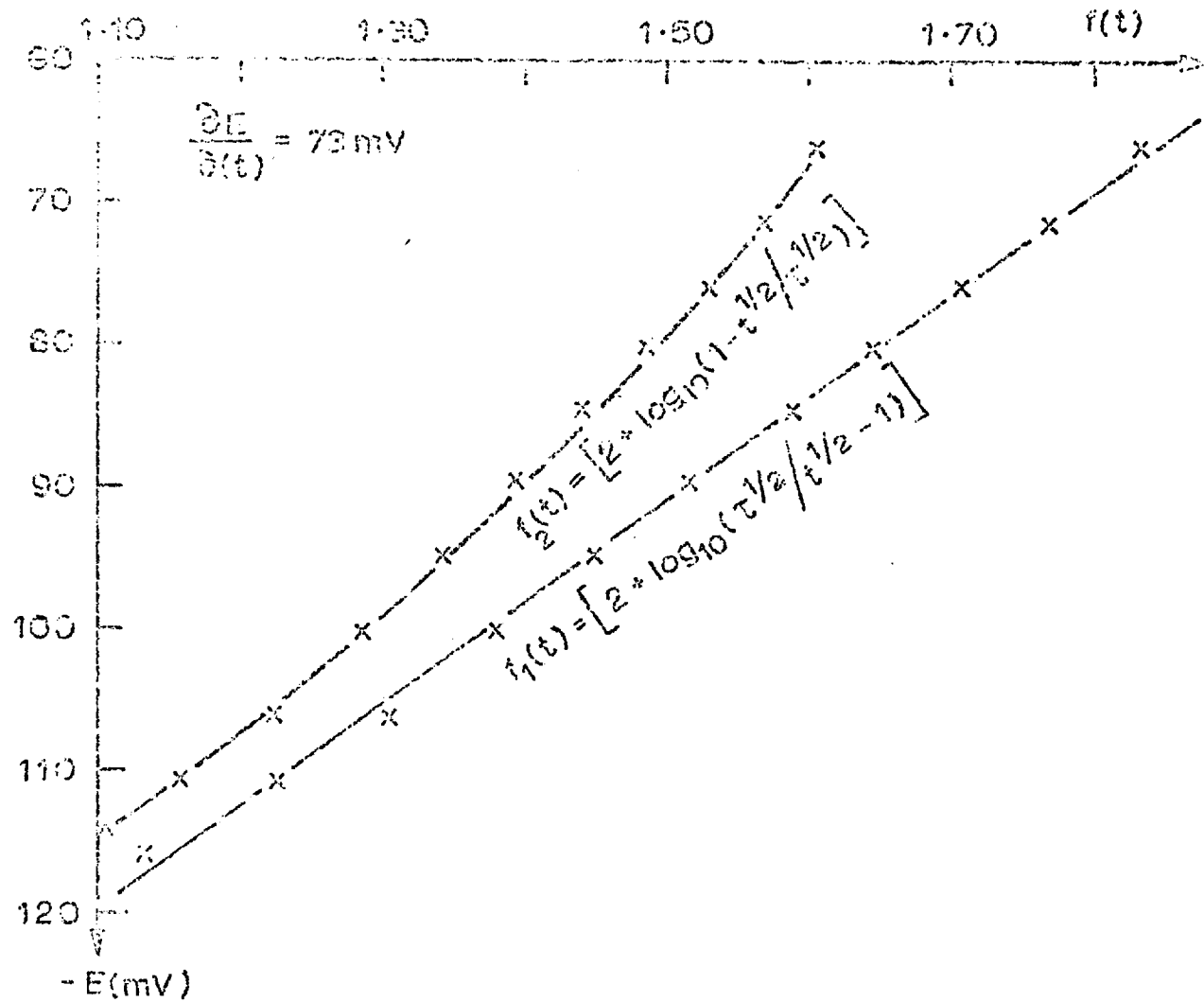
$f_1(t) = \left[2 * \log_{10}(\tau^{1/2}/t^{1/2} - 1)\right]$

f(t)

− E(mV)

Fig.6.24 Ta^{5+} IONS IN NaF 40mole% − KF 60mole%. T=1001°K.
τ = 477 msec. Platinum micro electrode

Chronopotentiograms obtained using the tantalum

micro electrode exhibited two clearly definable waves. The ratio

of the second transition time to first transition time τ_2/τ_1

was 1.69 $\pm$ 0.15. The product $i\tau^{\frac{1}{2}}$ increased markedly with

increasing concentration (see table 6.15).

Plots of $i\tau$ versus τ (SAR adsorption model) and $i\tau$ versus $1/i$

(AR.SR adsorption model) are shown in figures 6.25 and 6.26

respectively. The electrode area of the tantalum electrode was

calculated from the slope of the SAR plot using the value for

the diffusion coefficient obtained on the platinum electrode.

The surface excess "Γ" was then calculated for both the models.

$$\Gamma_{SAR} = (5.6 \pm 3.7) \times 10^{-8} \text{ moles cm}^{-2}$$

$$\Gamma_{ARSR} = (8.0 \pm 3.2) \times 10^{-8} \text{ moles cm}^{-2}$$

6.5.2. Discussion

Considering the chronopotentiograms on the platinum micro

electrodes, it can be said that the first wave fits the reduction

of tantalum (V) to tantalum (II) by an almost reversible step,

the tantalum (II), being soluble in the melt. The second wave

was only partially visible, could be associated with the

reduction of tantalum (II) to the metal. If this were the

case tantalum (II) would be reduced to the metal by two

processes. Firstly by primary electro-reduction and secondly

by secondary reduction by alkali metal.

$$Ta^{5+} + 3e \xrightarrow{Fast} Ta^{2+}$$

$$Ta^{2+} + 2e \to Ta^{o}$$

and $Ta^{2+} + 2M \to Ta^{o}$ (M = alkali metal)
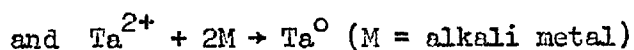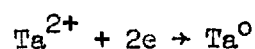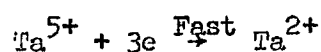
When a tantalum micro electrode was used two well defined waves

Table 6.15

Tantalum (V) in NaF40 mole% - KF 60 mole %

Tantalum micro electrode used.

Concentration of Ta(V) = 1.37×10^{-2} M

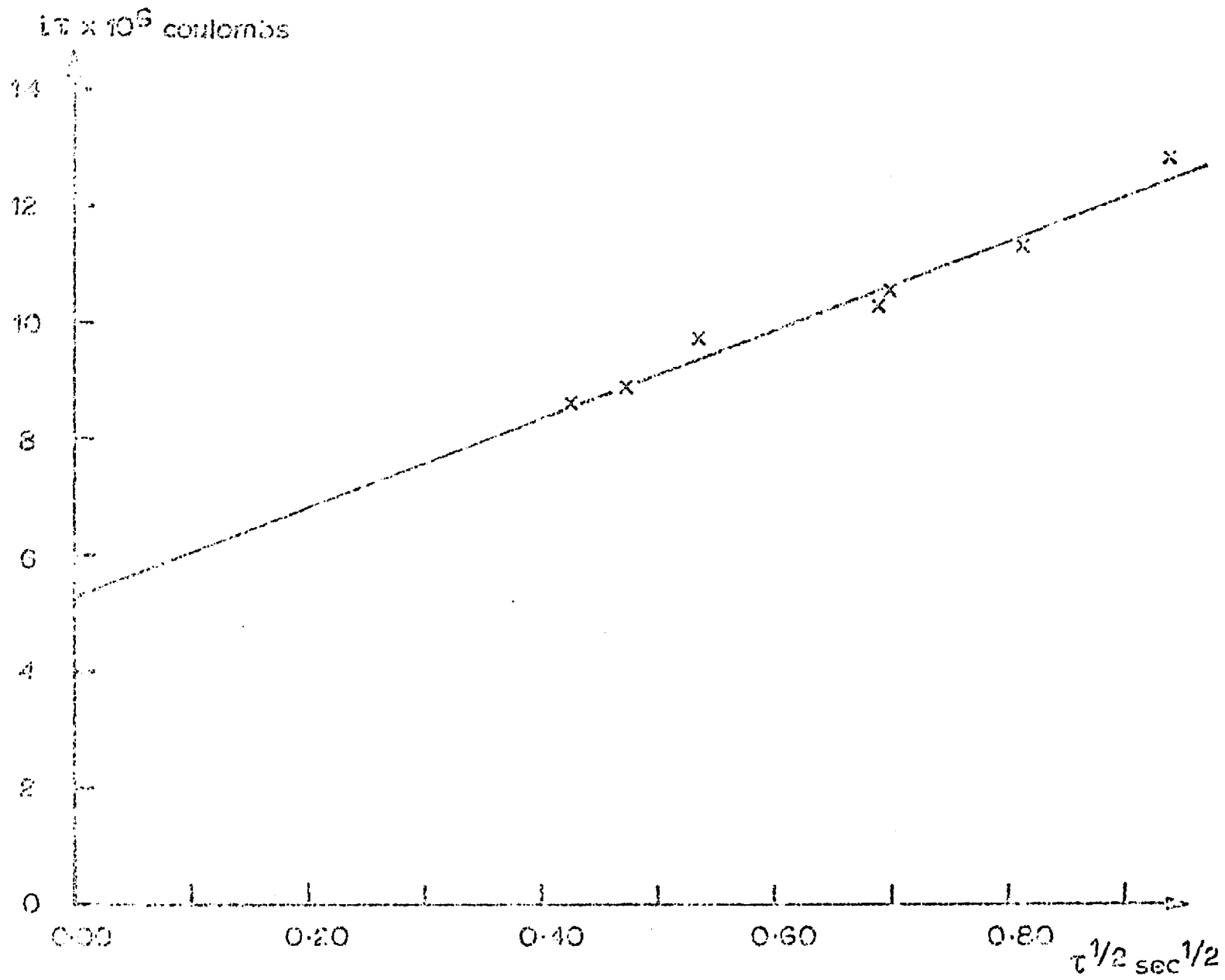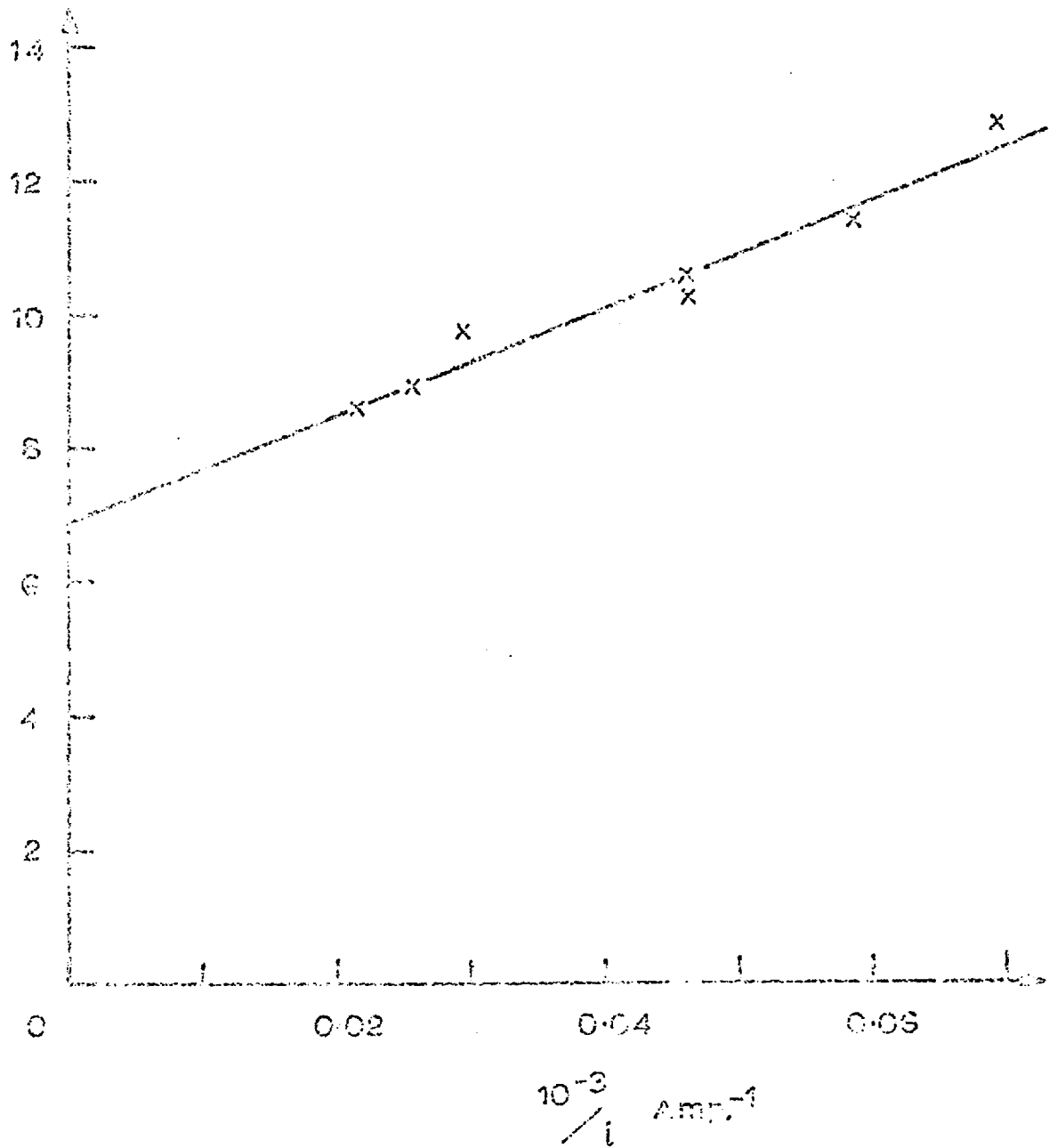| i,mA	τ_1,sec	$i\tau_1 10^3$, A.sec$^{\frac{1}{2}}$
14.52	0.885	12.9
17.15	0.661	11.3
21.53	0.477	10.3
21.53	0.490	10.5
34.11	0.286	9.76
39.29	0.226	8.88
47.20	0.183	8.62

Fig. 6.25   Ta^{3+} IN   NaF 40mole% - KF 60mole% AT 1000°K

Fig.6.26. Ta^{5+} IN NaF 40 mole % - KF 60 mole %

were observed. If the waves were assumed to represent the reduction of tantalum (V) to the metal then the total number of electrons involved would have to be 5; i.e. $(n_1 + n_2) = 5$. The ratio of τ_2/τ_1 when $n_1 = 3$ and $n_2 = 2$, would be 1.78. If $n_1 = 2$ and $n_2 = 3$ then $\tau_2/\tau_1 = 0.56$ (equation (2.15)). Even in the presence of adsorption the values for τ_2/τ_1 differ so widely that a ratio of 1.69 ± 0.15 can only be interpreted in terms of $n_1 = 3$ and $n_2 = 2$.

$$Ta^{5+} + 3e \rightarrow Ta^{2+}$$

$$Ta^{2+} + 2e \rightarrow Ta^{0}$$
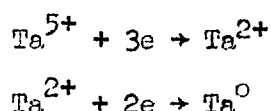
The very large value for the surface excess of $(5.6 \pm 3.7) \times 10^{-8}$ moles cm^{-2} (SAR model) when a mono layer will be of the order of $10^{-10} - 10^{-9}$ mole cm^{-2} could be explained in terms of a surface layer of oxide i.e. Ta_2O_5
If it was postulated that the oxide was more readily reduced than the chloride, then it would be expected that the second reduction step would occur at a less cathodic potential on the tantalum electrode than on platinum. The multiple reduction step postulated for tantalum (V) in the above electrolyte is identical to that proposed by other workers (173) in molten Flinak electrolyte.

C H A P T E R   7

C O N C L U S I O N S

7.1. Summary and general conclusions

The chronopotentiometric study of niobium (IV) ions in

fused chloride electrolytes can be interpreted in terms of a

one electron reduction step, which is reversible, followed by

reduction to the niobium metal via a secondary process. This

is in agreement with the findings of Dartnell et alia (166) in
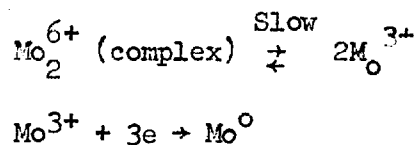
the fused equimolar sodium chloride - potassium chloride

electrolyte. Caton and Freund's (191) polarographic measurements

indicated niobium (IV) was reduced to niobium (III) which

was in turn reduced to the metal.

$$Nb^{4+} \;\; +e \;\; \rightarrow \; Nb^{3+}$$

$$Nb^{3+} \;\; + \; 3M^{\circ} \; \rightarrow \; Nb^{\circ} \;\; + \; 3M^{+} \quad (M = \text{alkali metal}).$$
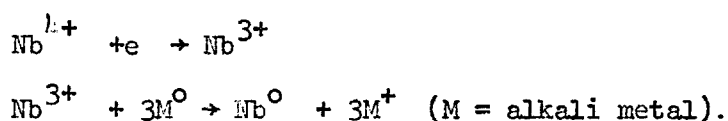
The chronopotentiometric study of molybdenum (III)

in fused sodium chloride 20 mole% - potassium chloride 80 mole %

was hampered by volatility problems. The data supported a

reduction process which involved the slow dissociation of a

multinuclear complex species. On the basis of the data it

was postulated that the complex species was a dinuclear species.

$$Mo_2^{6+} \; (\text{complex}) \; \underset{\leftarrow}{\overset{\text{Slow}}{\rightharpoonup}} \; 2Mo^{3+}$$

$$Mo^{3+} \; + \; 3e \; \rightarrow \; Mo^{\circ}$$

The complex species was found to be electro-active, which

would support a dinuclear species rather than some larger

species i.e. trinuclear upwards. The low diffusion

coefficient, $6 \times 10^{-6} \; cm^2 \; sec^{-1}$, also suggests the presence

of a large species. The addition of fluoride ions to the

electrolyte appeared to increase the reversibility of the
reduction step. The effect of fluoride ions on the stability
of the complex species could result from the replacement of
chloride ligand bridges by non-bridging fluoride ions.

The chronopotentiometric investigation of the electroduction
of molybdenum (III) in molten lithium chloride-potassium chloride
eutectic indicated the involvement of a slow chemical step.
It was suggested that the slow step resulted from the slow
dissociation of a multinuclear species containing molybdenum
(III). There was no evidence to suggest the complex-species was
electroactive, and hence it is possible that the complex species
could involve more than two molybdenum (III) nuclei. The
low value for the diffusion coefficient, of the order of
5×10^{-6} cm^2 sec^{-1}, is supported by the low values obtained
by other workers (176) in the same electrolyte at higher
temperatures. There is some evidence to suggest that adsorption
also plays some part in the reduction step.

$$Mo_n^{3n+} \text{ (complex)} \overset{slow}{\underset{\leftarrow}{\rightarrow}} nMo^{3+}$$

$$Mo^{3+} + 3e \rightarrow Mo^{o}$$
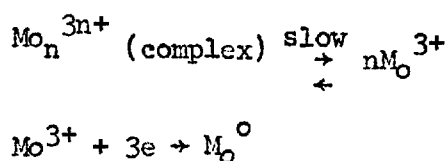
It was found that the presence of fluoride ions led to
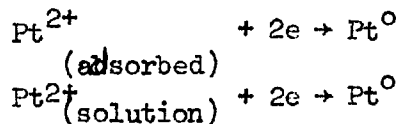an increase in the reversibility of the reduction process.
The effect was explained in terms of the replacement of
chloride liquid bridges in the complex species by non-bridging
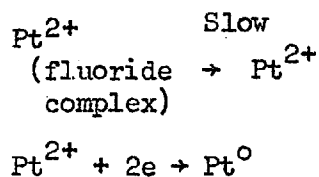fluoride liquids.

It was shown by potentiometric measurements that
platinum (II) ions were produced by the anodic dissolution
of platinum ($5m,A$, cm^{-2}) into fused lithium chloride-potassium

chloride eutectic. The standard electrode potential for
platinum (II) (in molar units) was 1.063 ± 0.007 volts versus
silver-silver (I) 1.18×10^{-2}M at 479°C. Chronopotentiometric
measurements on the reduction of platinum (II) in the same
electrolyte indicated that the process was quasi-reversible,
and that adsorption also played a role in the process. The
surface excesses were within 10^{-10} and 10^{-9} moles cm^{-2} which
is the range expected for a monolayer, (area of species
of 10-20 sq $\overset{o}{A}$). The data obtained from the addition of
fluoride ions indicated the appearance of a slow chemical
step. The presence of some adsorption made any quantitative
calculations impossible. The slow chemical step could be
accounted for by two postulations. The first explanation
ascribes the slow chemical step to the slow breakdown of
a fluoride complex species.

Chloride melt

$$Pt^{2+}_{(adsorbed)} + 2e \rightarrow Pt^{o}$$
$$Pt^{2+}_{(solution)} + 2e \rightarrow Pt^{o}$$

Chloride + fluoride melt

$$Pt^{2+}_{(fluoride\ complex)} \xrightarrow{Slow} Pt^{2+}$$

$$Pt^{2+} + 2e \rightarrow Pt^{o}$$

The second explanation, which in many ways is more
satisfactory, takes into account the findings of
Inman et alia (188). Their work suggested that fluoro -
complexes in the bulk would be less stable than the
chloro-complexes. It is assumed that the slow chemical
step is also present in the chloride melt, but is not
apparent because of the presence of adsorption. The effect
of the addition of fluoride ions is to reduce the adsorption

of platinum (II), and hence the slow chemical step becomes apparent. The slow chemical step can be ascribed to the slow dissociation of platinum (II) multinuclear species, c.f. reference (190).

$$Pt_n^{2n+} \xrightleftharpoons{\text{slow}} nPt^{2+}$$

$$Pt^{2+} + 2e \rightarrow Pt^o$$
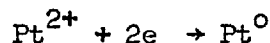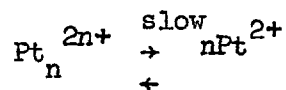
The study of tantalum (V) in sodium fluoride 40 mole % - potassium fluoride 60 mole %, gave similar results to those obtained by other workers in molten Flinak (173). The reduction proceded by a two step process
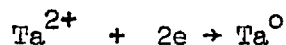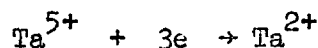
$$Ta^{5+} + 3e \rightarrow Ta^{2+}$$
$$Ta^{2+} + 2e \rightarrow Ta^o$$

The first step was reversible with a soluble product. The second step occurred by two processes, that is primary electroreduction and secondary reduction by deposited alkali metals. The diffusion coefficient for tantalum (V) was estimated to be $(5.09 \pm 0.54) \times 10^{-5}$ cm^2 sec^{-1}. which appears to be reasonable. There is evidence to indicate that the formation of tantalum (V) oxide (Ta_2O_5) on the electrode reduces the deposition potential of tantalum, such that the reduction of tantalum (II) proceeds via a primary process.

It was mentioned in Chapter 4 that there is evidence from the studies of other workers for a slow chemical step intervening in the electro-reduction process of refractory metals in pure fused chloride and fluoride melts.
The solid state chemistry of the halides of refractory metals is dominated by the formation metal cluster compounds involving

halide bridges. Hence it is not unreasonable to speculate that these multinuclear species play a part in the slow chemical step. Other evidence for such metal cluster compounds is the increase in reversibility of molybdenum (III) reduction on the addition of fluoride ions.

7.2. Significance of the study to industrial processes

The concepts of the effects reversibility of electro-reduction processes on the type of electro deposit obtained have been discussed in Chapter 4. From the discussion it is apparent that the design of a plating bath involves choosing a system, which has the right kinetics. In the case of irreversibility due to a slow chemical step, it would require the choice of a system containing complex species of a certain stability. One method of controlling the stability of the complex species is by altering the size and charge of the solvent cations, see chapter 3 and 4. Another method as has become apparent from the study of molybdenum (III) is the addition of fluoride ions, which appear to inhibit the formation of chloride bridges and it is possible that such concepts could be applied to other methods. It should be possible using a suitable mixture of alkali on alkaline earth halides, to obtain a plating bath to give coherent deposits of the refractory metals. The only proviso is that the overvoltage required to produce coherent deposits will not take the deposition potential more cathodic than the solvent cation deposition potential. This The use of mixed chloride-fluoride plating baths would allow lower operating temperatures, and the use of systems far less corrosive than pure fluorides.

7.3. Possible extensions to the study

The first and most obvious extension to the study is an investigation into the electro reduction of the lower valent refractory metal ions in pure fused fluorides and fused fluorides with additions of chlorides. Molybdenum (III) and tungsten (IV) ions have already been briefly examined in molten flinak (177) but they still require further examination. Other ions worth examining are tantalum and niobium in low oxidation states e.g. Ta^{2+} and Nb^{+}. It is possible that these ions could be produced by anodic dissolution. No quantitative data has been obtained for any of the refractory metal - fused halide - oxide systems. These systems are important in the field of electrowinning from oxides.

The study also needs extending to include other refractory metals in fused chloride electrolytes and fused chloride electrolytes with added fluoride ions.

Diagnostic evidence is required for the existence of multinuclear complexes in the binary systems. Such evidence could be supplied by magnetic susceptibility measurement supported by spectroscopic data. Such measurements should supply evidence for metal metal bonding i.e. pairing of electrons.

B I B L I O G R A P H Y

1. T.E. Tietz and J.W. Wilson, "Behaviour and properties
    of refractory metals "(1965): Stanford Cal.
    (Stanford University Press).

2. "Rare metals handbook" edited by C.A. Hampel
    2nd edition (1961): London.
    (Chapman and Hall).

3. Miller, "Ind. Chem. Manuf", 102 (1953)

4. E. de Barry Barnett and C.L. Wilson, "Inorganic Chemistry",
    III, 2nd edition (1960): London. (Longmans)

5. G.W. Mellors and S. Senderoff, "Plating 51, 972 (1964)

6. S. Senderoff, "Metallurgical Reviews" II, 97 (1966).

7. S. Senderoff and A. Brenner, "J. Electrochem. Soc.",
    101, 16, 28,31 (1954).

8. D.E. Couch and S. Senderoff, "Trans. Met. Soc. A.I.M.E."
    212, 320 (1958).

9. S. Senderoff, "The Metal Molybdenum" (edited by
    J.J. Harwood) 206-211 (1958): Cleveland 0.
    (Amer. Soc. Metals).

10. M.S. Burton, "Applied Metallurgy for Engineers",
    387 (1956): New York (McGraw Hill).

11. G.L. Davis and C.H.R. Grentry, "Metallurgica"
    53, 3 (1956)

12. G.W. Mellors and S. Senderoff, Canadian Patent 688, 46
    (1964).

13. Barton and Bockris, "Proc. R. Soc.", A268,485, (1962)

14. D. Inman and S.H. White, "Ann Reports. Chem. Soc."
    62, 106 (1965)

15. C.J. Janz, "Bibliography of Molten Salts", 2nd edition (1961 (Rensselaer Polytechnic Inst).

16. H. Bloom, "Chemistry of Molten Salts" (1967), New York, Amsterdam (W.A. Benjamin, Inc.)

17. B.R. Sandheim (ed), "Fused Salts", (1964), New York. (McGraw Hill).

18. M. Blander (ed) ""Molten Salt Chemistry" (1964) New York (Inter science).

19. J. Lumsden "Thermodynamics of Molten Salt Mixtures," (1966) London (Academic Press).

20. C.J. Janz , "Molten Salts Handbook" (1967) (Academic Press).

21. J.O.M. Bockris, J.L. White and J.D. Mackenzie, "Physio-chemical measurements at high temperatures", (1959), London (Butterworths).

22. J.D. Corbett and F.R. Duke in "Techniques of Inorganic Chemistry" Ed. H.B. Jonassen. (1963) New York (Interscience)

23. R.A. Bailey and C.J. Janz "Experimental Techniques in the Study of Fused Salts" in "The Chemistry of Non-Aqueous Solvents" ed J.J. Lagowski, Vol 1 (1966) (Academic Press).

24. T.B. Reddy, "Electrochem Technol", 1,325 (1963)

25. Yu.K. Delimarskii and B.F. Markov, "Electrochemistry of Fused Salts" Trans (1961) New York (Sigma Press).

26. A.D. Graves, G.J. Hills and D. Inman in, "Advances in Electrochemistry and Electrochemical Engineerin Vol. 4, ed. P. Delahoy, (1966) New York (Inter science).

27. D. Inman, A.D. Graves and R.S. Sethi, "Special Repts. Chem. Soc." In print.

28. R.W. Murray and C.N. Reilley, "J. Electroanal Chem", 3 182 (1962).

29. H.B. Herman and A.J. Bard, "Anal. Chem", 35, 1121 (1963)

30. Y. Takemovi, T. Kambara, M. Senda and I. Tachi, "J. Phys. Chem" 61,968 (1957)

31. H.C. Gaur and H.L. Jindal, "J. Electroanal Chem", 14, 297 (1967)

32. H.F. Weber "Wied Ann Physik" 7,536, (1879).

33. H.J.S. Sand, "Phil Mag", 1 45, (1901)

34. J.A.V. Butler and G. Armstrong, "Proc. Royal Soc", (London), A139, 406 (1933)

35. J.A.V. Butler and G. Armstrong, "Trans. Faraday Soc", 30, 1173, (1934)

36. L. Gierst and A. Julliard, "Proceedings of the 2nd meeting of the International Committee on Electrochemic Thermodynamics and Kinetics". Tamburine, Milan, (1950).

37. L. Gierst and A. Julliard, "J. Phys Chem", 57 701, (1953)

38. P. Delahay, "New Instrumental Methods in Electrochemistry" (1954) New York (Interscience).

39. A. Fick, "Pogg. Ann.," 94 59, (1855)

40. T.R. Rosebrugh and W.L. Miller "J. Phys. Chem." 14, 6816, (1910).

41. Z. Karaoglanoff, "Z. Elektrochem", 12, 5, (1906)

42. T. Berzins and P. Delahay, "J. Am. Chem. Soc., "75, 4205, (1953).

43. W. Lorenz, "Z. Electrochem" 59,730, (1955).

44. W. Reinmuth, "Anal Chem", 33, 322, (1961)

45. H.A. Laitinen, "Anal Chem", 33, 1458, (1961)

46. H.A. Laitinen and L.M. Chambers, "Anal. Chem", 36, 5, (1964)

47. R.W. Murray and D.J. Gross, "Anal Chem", 38, 392, (1966)

48. F.C. Anson, "Anal Chem", 33 1123, (1961)

49. S.V. Tatwawadi and A.J. Bard, "Anal Chem", 36, 2, (1964)

50. P.J. Lingane, "Anal Chem" 39, 485, (1967)

51. E. Franks and D. Inman, "J. Electroanal. Chem",
    26, 13, (1970)

52. Hills and Broadhead "J. Electroanal Chem. 13, 354 (1967)

53. J. Bjerrum, "Chem Revs" 46, 381 (1950)

54. P. Delahay and T. Berzins, "J. Amer. Chem. Soc",
    75, 2486, (1953)

55. B.O. Pierce, "A Short Table of Integrals"
    116-120, 3rd edition (1929) Boston (Ginn).

56. J. Koutecky and V. Hanus, "Coll. Czech. Chem. Comm.
    "20, 124, (1955)

57. J. Kouteky and J. Cizek, "Coll. Czech. Chem. Comm",
    22, 914, (1957).

58. O. Fischer, O. Dracka and E. Fischerova, "Coll. Czech.
    Chem. Comm. "25, 323, (1960).

59. R. Brdicka and K. Wiesner, "Coll. Czech. Chem. Comm",
    12, 39, (1947).

60. A. Eucken, "Z. Physik. Chem" 64, 564, (1908)

61. K. Wiesner, "Z. Elektrochem", 49, 164 (1943)

62. P. Delahay, C.C. Mattax and T. Berzins, "Tech. Rept.
    Office of Naval Research, "Project NR 051-258,
    Rept No. 15. (1953).

63. P. Delahay, C.C. Mattax and T. Berzins, "J. Amer. Chem. Sec"
    76, 5319, (1954). /

64. H. Eyring, S. Glasstone and K.J. Laidler,
    "J. Phys. Chem", 7, 1053 (1939).

65. P. Delahay and C.C. Mattax, "J. Am. Chem. Soc"
    76, 874, (1954).

66. J.M. Coulson and J.F. Richardson "Chemical Engineering"
    Vol. 1, 220, (1964), Oxford (Pergamon).

67. M.D. Morris and J.J. Lingane, "J. Electroanal Chem".
    6,300, (1963).

68. G. Mamantov and P. Delahay, "J. Am. Chem. Soc",
    76, 5323, (1954).

69. D.G. Peters and J.J. Lingane, "J. Electroanal Chem"
    2, 1, (1961).

70. D.M. Evans, Thesis, Harvard University (1964).

71. H. Hurwitz, "J. Electranal Chem", 7, 368, (1964).

72. L. Gierst, Thesis, University of Brussels, (1952)

73. C. Wagner, "J. Electrochem Soc", 101, 225, (1954).

74. H. Gerischer and P. Delahay, "Anal. Chem. Acta," 18, 12, (1958)

75. J.J. McMullen and N. Hackerman, "J. Electrochem Soc",
    106, 341, (1959).

76. A.J. Bard, "Anal Chem", 33, 11, (1961)

77. W.M. Reinmuth, "Anal Chem", 33 485, (1961)

78. P. Delahay and C.T. Fike, "J. An. Chem Soc.", 80, 2628, (1958)

79. M. Kodana and R.W. Murray, "Anal Chem",
    37, 1938, (1965)

80. O. Fischer, O. Dracka and J. Stepanek, Coll. Czech.
    Chem.," 31, 1644, (1966)

81. D.C. Noonan, Thesis, Columbia University (1967).

82. J.D. Voorhies and N.H. Furman, "Anal Chem", 30, 1656,
    (1958).

83. C.P. Russell and J.M. Peterson, "J. Electroanal. Chem",
    5, 467, (1963)

84. P. Bos, "Chem. Weeklabd," 61, 535, (1965)

85. R.W. Laity and J.D.E. McIntyre, "J. Am. Chem. Soc",
    87, 3807, (1965)

86. R.T. Iwamoto, "Anal. Chem.," 31, 1062, (1959).

87. D.G. Peters and S.L. Burden, "Anal Chem", 38, 530 (1966)

88. D.J.G. Ives and G.J. Janz, "Reference Electrodes".

    D.J.G. Ives and G.J. Janz editors, pp 1-70, (1961),

    New York, (Academic Press).

89. T. Erdey-Gruz and M. Volmer, "Z. Physik Chem" 150A
    203, (1930).

90. H.H. Bauer, "J. Electroanal Chem" 16, 419 (1968).

91. J. Tafel, "Z. Physik. Chem", 50 641 (1905).

92. P.G. Allen and A. Hickling, "Trans. Faraday Soc."
    53, 1626, (1957).

93. K.J. Vetter, "Z. Physik. Chem., 194, 284, (1950).

94. K.J. Vetter, "Z.Elektrochem", 55 121, (1951)

95. K.J. Vetter, "Z.Elektrochem", 56 931, (1952)

96. P. Debye and E. Huckel, "Physik Z." $\underline{24}$, 185, 305, (1923)

97. H.A. Levy, P.A. Agron, M.A. Bredig and M.D. Danford, "Ann. N.Y. Acad. Sci" $\underline{79}$, 762, (1960)

98. Ya I. Frenkel, "Acta Physioochim, URSS", $\underline{3}$ 633,913, (1935)

99. S.E. Bresler, "Acta Physicochem, URSS, "$\underline{10}$,491, (1939)

100. M. Temkin, "Acta Physiochem, URSS, "$\underline{20}$, 411, (1945)

101. T. Førland, "J. Phys Chem", $\underline{59}$ 152, (1955)

102. T. Førland, "Norg. Tek. Vitenskapsakad, Ser. 2, No4 (1957)

103. H. Flood, T. Førland and K. Grjotheim, "The Physical Chemistry of Melts", Methuer, London (1953).

104. M. Flood, T. Førland and K. Grjotheim, "Z. Anorg Chem , $\underline{276}$, 289, (1954).

105. J.K. Wilmhurst, "J. Chem. Phys. "$\underline{39}$, 1779 (1963).

106. J.S. Fordyce and R.L. Baum, "J. Phys. Chem" $\underline{69}$, ^{5}4335, (1965)

107. J.S. Fordyce and R.L. Baum, "J. Chem. Phys" $\underline{44}$,1159 (1966)

108. J.S. Fordyce and R.L. Baum, "J. Chem Phys, $\underline{44}$, 1166, (1966)

109. J.K. Wilmshurst, "J. Chem. Phys. $\underline{39}$ 2545, (1963)

110. G. Harrington and B.R. Sundheim, "Ann. N.Y. Acad Sci", $\underline{79}$,950 (1960)

111. D.M. Gruen, "Fused Salts", ed. Sundheim, McGraw Hill, New York, 301, (1964).

112. T.J. Rowland and J.P. Bromberg, "J. Chem. Phys" $\underline{29}$,626, (1958)

113. S. Hafner and N.H. Nachtrieb, "J. Chem. Phys", $\underline{40}$,2891,(1964)

114. S. Hafner and N.M. Nachtrieb , "J. Chem. Phys" 42 631, (1965)

115. G. Alberti, S. Allulli, and L. Palazzeschi, "J. Chromatog" 31, 519, (1967)

116. R.A. Bailey and A. Steger, "J. Chromatog", 11,122, (1963)

117. S. Forcheri and A. Berlin, "Euratom Report", EUR 3160 e (1966).

118. A. Berlin, F. Menes, S. Foucheri and C. Monfrini, "J. Phys Chem; 67 2505, (1963)

119. G. Alberti, S. Allulli and G. Modugro, "J. Chromatog", 15,420, (1964)

120. G. Alberti, G. Grassini and R. Trucco, "J. Electroanal Chem, 3 283, (1962)

121. G.W. Mellors and S. Senderoff, "First Aust. Conf. Electrochem" 578, Perammon, New York (1964)

122. G.W. Mellors and S. Senderoff, J. Electrochem Soc., 111, 1355, (1964).

123. E.R. Van Artsdalen, "J. Phys Chem", 60,172 (1956)

124. E.R. Van Artsdalen and I.S. Yaffe, "J. Phy. Chem", 59, 118 (1955)

125. M. Blander and J. Braunstein, "Ann N.Y. Acad Sci", 79, 838, (1960)

126. M. Blander, "J. Phys Chem," 63, 1262, (1959)

127. M. Blander, "J. Chem. Phys", 34 432, (1961)

128. G. Pedro Smith, "Molten Salt Chemistry", ed M. Blander Interscience, New York, 427, (1964)

129. R.L. Martin and G. Winter, "J. Chem Soc", 4709 (1965)

130. M.F. Lantratow and A.F. Alabyshev,"J. Appl. Chem. U.R.S.S., "26, 235, 321, (1953).

131. M.F. Lantratov and A.F. Alabyshev, "J. Appl. Chem. U.R.S.S.", 27, 685, (1954).

132. D.M. Gruen and R.L. McBeth, "J. Phys Chem" 63,393 (1959).

133. S. Senderoff, G.W. Mellors, and R.I. Bretz, "Ann. N.Y. Acad Sci." 79, 878, (1960).

134. S. Senderoff, G.W. Mellors and R.I. Bretz, "J. Electrochem Soc", 108, 93, (1961).

135. G.W. Mellors and S. Senderoff, "J. Electrochem Soc." 112, 266, (1965).

136. M.V. Smirnov and O.A. Ryzhik, "Tr Inst. Elektrokhim, Akad, Nauk S.S.S.R. Ural'sk Filial" No. 7, 27, (1965).

137. M.V. Smirnov and O.A. Ryzhik, "Tr. Inst. Elektrokhim, Akad. Nauk S.S.S.R. Ural'sk. Filial "No. 8,43, (1966).

138. S.M. Selis, "J. Electrochem. Soc" 113 37, (1966)

139. R.B. Heslop and P.L. Robinson, "Inorganic Chemistry", Elsevier, London, 246, (1963)

140. S.H. Bauer and R.F. Porter, "Molten Salt Chemistry", ed. M. Blander, Interscience, New York, 642, (1964).

141. A.J. Edwards, "J. Chem. Soc.", 3714, (1964).

142. A.J. Edwards, R.D. Peacock and R.W.H. Small "J. Chem. Soc." 4486 (1962).

143. F.A. Cotton and G. Wilkinson, "Advanced Inorganic Chemistry", Interscience, London 921, (1967).

144. F.A. Cotton and G. Wilkinson, "Advanced Inorganic Chemistry" Interscience, London, 926, (1967).

145. L.F. Dahl, T. Chiang, P.W. Seabaugh and E.M. Larson, "Inorgan Chem", 3, 1236, (1964).

146. R.E. McCarley and B.A. Torp, "Inorg. Chem" 2,540, (1963).

147. R.E. McCarley and T.M. Brown, "Inorg. Chem", 3,1232,(1964).

148. H. Schafer and H.G. Schnering, "Angew Chem", 76, 833, (1964)

149. R. Siepmann and H. Schafer, "Naturwiss", 52,345, (1965)

150. R. Baboian, D.L. Hill and R.A. Bailey, "Canad. J. Chem".
      43, 197, (1965).

151. B.G. Rossokhin, M.V. Smirnov and N.A. Loginov,
      Electrochem of molten and solid electrolytes",
      4, 17, (1967).
      (From Trudy Inst. Elektrokhim Akad. Nauk S.S.S.R.
      Ural'skii Filial, 7 17, (1965)

152. B.G. Rossokhin, M.V. Smirnov and N.A. Loginov,
      "Electrochem of molten and solid electrolytes",
      5, 11, (1967) (From, "Trudy Inst. Elektrokhim, Akad,
      Nauk S.S.S.R. Ural' skii Filial, 8 (1966)).

153. M.V. Smirnov and Yu N. Krasnov, "Electrochem of
      molten and solid electrolytes", 1 22, (1961) (From, Trudy Ins
      Elektrokhim Akad. Nauk S.S.S.R. Ural'skii Filial," 1 (1958)).

154. N.A. Loginov and M.V. Smirnov, "Electrochem of molten
      and solid electrolytes, "2, 21, (1964) (From "Trudy Inst.
      Elektrokhim Akad Nauk S.S.S.R. Ural'skii Filial" 4, (1961))

155. I.A. Menzies, D.L. Hills, G.J. Hills, L. Young and
      J.O'M Bockris, "J. Electroanal Chem", 1 161 (1959/60)

156. G. Ervin, Jr. H.F.G. Ueltz and M.E. Washburn,
      "J. Electrochem. Soc" 106, 144, (1959).

157. M.V. Smirnov and S.F. Pal'guev, "Electrochem of
      molten and solid electrolytes", 1 127, (1961) (From "Trudy
      Inst. Elektrokhim. Akad. Nauk S.S.S.R. Ural'Skii Filial",
      1 (1958)).

158. Yu K. Delimarskii and P.V. Chernov, "Ukrain Khim Zhur.",
      32 1285, (1966).

159. R. Baboian, D.L. Hill and R.A. Bailey, "J. Electrochem
      Soc" 112, 1221, (1965).

160. V.E. Komarov, M.V. Smirnov and A.N. Baraboshkin,
"Electrochem of molten and solid electrolytes",
1, 16, (1961) (From, "Trudy Inst. Elektrokhim Akad.
Nauk S.S.S.R. Ural'skii Filial", 1 (1958))

161. V. Ya Kudyakov and M.V. Smirnov, "Electrochem of
molten and solid electrolytes, '3 15, (1966) (From "Trudy
Inst. Elektrokhim. Akad. Nauk S.S.S.R. Uralskii Filial",
6 (1965)).

162. V. Ya Kudyakov and M.V. Smirnov, "Eletrokhim",
1, 143, (1965).

163. T. Sakarura, "J. Electrochem Soc. Japan", 35 75, (1967).

164. G.W. Mellors and S. Senderoff, "J. Electrochem Soc",
113, 60, (1966).

165. D.L. Manning and G. Mamantov, "J. Electr anal Chem"
6, 328 (1963)

166. J. Dartnell, K.E. Johnson and L.L. Shrier,
"J. Less-Common Metals", 6 85, (1964).

167. V.F. Pimenov and Ya V. Baimakov, "Electrokhim",
4 1357, (1968).

168. Y. Saeki, T. Suzuki and M. Otani, "Denki - Kagaku",
35, 193, (1967).

169. Y. Saeki and T. Suzuki, "J. Less-Common Metals",
9, 362, (1965).

170. S. Senderoff and G.W. Mellors, "J. Electrochem Soc",
113, 66, (1966).

171. T. Suzuki," Electrochim Acta; 15, 127, (1970).

172. T. Suzuki, "Electrochim. Acta, 15 303, (1970)

173. S. Senderoff, G.W. Mellors and W.J. Reinhart,
"J. Electrochem. Soc" 112, 840, (1965).

174. S.M. Selis, "J. Phys. Chem. 72 1442 (1968)

175. M.V. Smirnov and O.A. Ryzhik, "Electrochem of molten and solid electrolytes", 3, 9, (1966) (From "Trudy Inst. Elektrokhim Akad Nauk S.S.S.R. Ural skii Filial", 6 (1965)).

176. S. Senderoff and G.W. Mellors, "J. Electrochem Soc", 114, 556, (1967).

177. S. Senderoff and G.W. Mellors, "J. Electrochem Soc", 114, 586, (1967).

178. E. Schmidt, H. Pfander and H. Siegenthaler, "Electrochim Acta", 10, 429, (1965).

179. J.O.M. Bockris and A. Damjanovic, "Modern Aspects of Electrochemistry No. 3, Ed. J.O.M. Bockris and D.E. Conway, Butterworths, London, 224, (1964).

180. N.S. Wrench, Thesis, London University (1967).

181. E.R. Van Artsdalen and I.S. Yaffe, "J. Phys Chem", 59 118, (1955).

182. E. Scheil and Stadelmaier "Z. Metallk", 43,227, (1952).

183. R.A. Osteryoung and F.C. Anson "Anal Chem" 36,975, (1964)

184. C.J. Smithells, "Metals Reference Book", Vol II Butterworths, London 697, (1962).

185. D. Inman, Thesis, University of London (1956).

186. J. Lumsden, "Thermodynamics of Molten Salt Mixtures, London, Academic Press, 7, (1966).

187. E.A. Ukshe and N.G. Bukun, "Elektrokhim" 5 1421, (1969).

188. D.Inman, B. Jones and S.H. White, "J. Inorg. Nucl. Chem." 32, 927, (1970).

189. S. Ahland and E. Larson, "Acta Chem Scand" 8, 354, (195).

190. K. Broderson, G. Thiele and H.G. Schnering, "Zeit anorg. Chem:" <u>337</u> 120 (1965)

191. R.D. Caton and H. Freund, "Anal Chem" <u>36</u>, 15, (1964).

S Y M B O L S

a = activity

C_∞ = concentration of species at an infinite distance from the electrode surface.

(Cx,t) = concentration of species at a distance "x" perpendicular to the electrode surface, and at time "t" after onset of electrolysis.

C^o = bulk concentration of species.

D = diffusion coefficient.

E = electrode potential or energy.

E^o = standard electrode potential.

f = activity coefficient, infinite dilution standard state.

i = current or current density.

F = 1 Faraday.

i^o = exchange current density.

i = current or current density.

i_r = limiting reaction current density.

k_f = forward formal chemical rate constant.

k_b = reverse formal chemical rate constant.

K = equilibrium constant = k_f/k_b

K_a = equilibrium constant for a linear adsorption isotherm.

K^o_{fh} = forward formal rate constant for charge-transfer.

k^o_{bh} = reverse formal rate constant for charge-transfer.

N = ionic or mole fraction.

n = number of electrons.

q (x,t) = flux at perpendicular distance "x" from the
electrode surface at time "t".

T = temperature in degrees absolute.

t = time for onset of process.

w = weight percentage.

x = perpendicular distance from the electrode surface.

z = co-ordination number or charge.

α = charge transfer coefficient.

Γ = molar surface excess concentration.

δ = diffusion layer thickness.

η = overvoltage

ν = stoichiometric number.

ρ = density i.e. g, cm^{-3}

τ = transition time.

A C K N O W L E D G E M E N T S